GIA modelling of Greenland using an ice history from the last glacial cycle to present day with lateral varying viscosity profiles on a spherical Earth

Master Thesis

Nils Jérôme Jean-Pierre Faure

TU Delft

GIA modelling of Greenland using an ice history from the last glacial cycle to present day with lateral varying viscosity profiles on a spherical Earth

Master thesis

by

Nils Jérôme Jean-Pierre Faure

to obtain the degree of Master of Science
at the Delft University of Technology,
to be defended publicly on Friday April 22nd, 2022 at 9:30.

Project duration:	5th of July 2021 to 28th of March 2022	
Student Number:	4654528	
Thesis committee	Prof. dr. L.L.A. (Bert) Vermeersen	TU Delft, chair
	Dr. R.E.M. (Riccardo) Riva	TU Delft, examiner
	Dr. Ir. W. (Wouter) van der Wal	TU Delft, (main) supervisor
	PhD candidate J.M. (Jesse) Reusen	TU Delft, supervisor

An electronic version of this thesis is available at: https://repository.tudelft.nl/.

TU Delft

Cover image made by student.

Acknowledgements

Firstly, I would like to thank my main supervisor Wouter van der Wal and daily supervisor Jesse Reussen, as they provided guidance, help and advice, which if not given, would have made this Master Thesis much harder and less productive. Through their help, I have learned a lot about Glacial Isostatic Adjustment and Earth modelling.

Secondly, I would like to thank Caroline van Calcar for her advice and for the base GIA model I was able to use for this Master Thesis which she shared with me through Jesse Reusen, along with Bas Blank too for the GIA model. I would also like to thank Gydo Kempenaar, whose discussions with me, about GIA where particularly insightful. I would also like to thank all the researchers's and engineer's scientific papers which I have used in this Master Thesis.

Thirdly, I would like to thank my mother and my partner for helping me proof read and format the final version of this report, as well as the family members and friends who have supported me through this Master Thesis.

Lastly, I would like to thank the lecturers and professors, who have taught me Aerospace Engineering since the start of the Bachelor, in September 2017, and who have awakened and deepened my interest in this study.

Nils J.J. Faure
March 2022

Abstract

Glacial Isostatic Adjustment (GIA) is a process which focuses on the deformations of the Earth due to changing ice sheets. It is an important study in Climate Sciences, gravimetric studies and Earth modelling. Studying GIA allows to contribute to a better understanding of the Earth's composition, thanks to the testing of multiple Earth models, as well as a broader understanding of the Earth's ice age cycles. Last, studying GIA is useful in our understanding of present day climate change, as GIA has an impact on the dynamic gravity signal, with which the ice losses are estimated. Modern day GIA, with present day elastic uplifts, primarily takes place in Antarctica and Greenland. GIA studies are fewer in Greenland, hence the focus of this research.

In GIA research, spherical Earth models have been used for half a century. However, 3D Earth models distinguish themselves by using a 3D varying viscosity profile. The reason for this recent interest is that little is known with precision about the Earth's mantle and deeper layers structure and that such a model was more difficult to create; the inclusion of three dimensional (3D) varying viscosity profiles have not yet been widely used in GIA studies in Greenland. Hence, to this day and to our knowledge, only two papers have made use of a laterally varying viscosity in order to study GIA in Greenland. The first, Milne et al. (2018), uses a reference viscosity profile from which a 3D viscosity profile is derived. Milne et al. (2018) do not include modern day ice changes, in order to simulate the present elastic uplift. This paper by Milne et al. (2018) concluded that using laterally varying viscosity profiles had a significant impact on the present day land deflections, which varied, according to Milne et al. (2018), by multiple decameters the deflection during the Holocene. It also found that including the use of a 3D varying viscosity profile could not solve for the discrepancies found when a 1D varying viscosity profile was used with an ice history developed to fit relative sea level data (Milne et al., 2018). The second paper, uses, just as this Master Thesis, an Olivine flow viscosity model (van der Wal and Xu, 2016). While it used an ice model which was not developed specifically for Greenland, ICE-5G, and did not have a detailed ice history in the past decades, it tested a 3D varying viscosity profile for GIA modelling in Greenland. The conclusions from this paper found that the largest discrepancies with 1D viscosity model predictions for present day uplift rates are in the South and West of Greenland (van der Wal and Xu, 2016). The first novelty introduced by this Master Thesis is the use of the Olivine flow viscosity model, with a wet rheology, to study GIA in Greenland.

The second main novelty in this Master Thesis, is the use of a unified ice history from 122000 years from present till 2019 in one GIA model; while using a resolution of 10 [km], which is an improvement, compared to for instance Milne et al. (2018) or Simpson et al. (2011) or Lecavalier et al. (2014) which use resolutions ranging from 15 to 75 [km], but is found to still not be sufficient enough to properly model modern elastic and viscous deformations. To our knowledge, this has rarely, been done. In GIA modelling, for present day uplifts, what is usually done is to model the viscous uplift due to the last glacial cycle, and then simulate in a separate model the elastic uplift due to recent ice mass changes, to then add both effects together, as done in Simpson et al. (2011) or Khan et al. (2016). We think and stipulate that the major reason why these two effects were not simulated together is that the resolution needed to accurately model elastic uplifts was too high to model deflections over a long period of time such as the de-glaciation era. For the ice history up till 1914 we use the Huy3 (Lecavalier et al., 2014) ice model, a glacier ice history from 1972 to 1992 (Mouginot et al., 2019) and a detailed ice history is used from 1992 to 2019 (Simonsen et al., 2021). To support this novelty, we investigate if a convergent surface resolution can be achieved to model both viscous and elastic responses.

It is in this context that this Master Thesis aims to add to current research into GIA modelling by: the inclusion of a 3D varying viscosity models, with a unified in time ice history from 122000 years ago till 2019, with a spherical Earth model.

The following conclusions were made through analysing the final results. First, the simulations which use 3D viscosity models, react with larger amplitudes of solid Earth deflections in shorter time spans, to ice load changes. These model's deflections take longer to come to a stable equilibrium, compared to the simulations which use 1D viscosity profiles. This is true for the glaciation phase and the de-glaciation phase, especially in the South-West region of Greenland. In Greenland as a whole, the simulations using the 3D viscosity models still have a large deflection rate at present times, although the 1D viscosity profiles have shown much smaller gradients of deflections over the present times. We do not know how this difference in reaction, between the 1D and 3D viscosity profiles, changes when the ice history varies.

Second, 3D varying viscosity models, with the same ice loads as the 1D varying viscosity models, have a

pattern of deflection which is more explicitly linked to the changes in viscosity across Greenland, whereas the 1D viscosity profiles deflection rates are clearly positive in the present day on land and negative in the sea, and hence are more explicitly linked to the coastal limits of Greenland. Here, we can see that only changing the viscosity gives a large variety of results. This then brings us to stipulate our first recommendation: that further improvements to ice models, by considering a laterally varying viscosity profile instead of a 1D viscosity when performing ice reconstruction, could lead to further changes and improvements in uplift modelling in Greenland.

Last, the inability of the model to properly model elastic uplifts in recent times, is made evident by the constant under estimation of total uplift rates. This is thought to be due to the fact that the 10 [km] resolution setting is not fine enough to model elastic uplifts accurately. This was pointed out in a paper which investigated GIA in West Antarctica (Wan et al., 2021), which found that the minimum resolution needed to be 3.75 [km] in order to significantly decrease elastic modelling errors due to the resolution of the mesh. This issue is true for all simulations, irrespective of their viscosity model. The error here is clearly due to the resolution in the areas of ice mass losses, namely on the coasts of Greenland. The recommendation which follows is to investigate finer mesh sizes than 10 [km], in order to obtain a mesh which creates better modelling results in the present day uplift rates, and allows for convergence in present day total and elastic uplifts.

Contents

Tables of symbols, units, abbreviations and concepts

Table 1: Table of symbols

Symbol	Definition(s)
A^a, p, r, α, ϕ	Constants used in the determination of creep values
$\mathbf{A}$	Matrix used in the Rbf interpolation
B	Variable used for creep in Chapter 6
b	Distance of load from beam
d	grain size
E	Young's modulus in verification chapter
E	Activation energy in Chapter 6
E	Correction term in Section 2.3
e	10 to the power which follows e, for instance: $e2 = 10^2$
$\mathbf{f_{mass}}$	Vector of ice masses, used in the Rbf interpolation
$exp()$	Euler's number to the power of what is in the brackets
$E_{percentage,mean}$	Mean percentage error
f_{H2O}	Water content
I	Moment of Inertia
k	Constant equal to 1000
L	Latitude
l	Longitude in mesh chapter
l	Length of beam in verification chapter
m_{i+1}	Mass after correction method 1
m_{i+2}	Mass after correction method 1 and 2
M_{i-1}	Sum of masses before interpolation
M_{i+1}	Sum of masses after correction method 1
$\mathbf{m}$	Vector from the Earth's centre to the middle point of Greenland
P	Force in verification chapter
P	Pressure in Chapter 6
R	Specific gas constant $\mathbf{R}$ Rotation matrix in projecting Greenland
$RorR_E$	Earth volumetric radius onto the South-Pole
S_r	Correction ratio used in Section 2.3
T	Temperature when determining creep
n	Constant used to convert creep to viscosity
$\mathbf{w}$	Vector used in the Rbf interpolation
V	Activation volume
v	Viscosity
v_0	Reference viscosity
x, y, z	Cartesian coordinates
$\mathbf{Z}$	Unit vector along z axis
σ	Stress
θ, ϕ,R	Spherical coordinates

Table 2: Table of units.

Unit	Definition
cm	centimetre
g	gram
GPa	gigaPascal
Gt	gigaton (10^{12} [kg])
kg	kilogram
kJ/mol	kilo joules per mole of substance
km	kilometre
m	meter
$mGal$	milliGal (10^{-5} [m/s^2])
mm/yr	millimetre per year
m/s^2	meters per second
N	Newton
nm/s^2	nanometre per second squared
Pa	Pascal
Pas	Pascal seconds
s	second
t	ton (10^3 [kg])
yr	Gregorian calendar year
$^\circ$	degree

Table 3: Table of abbreviations.

Abbreviation	Definition
CT	Custom Timeline
DST	Detailed Short Term
FEM	Finite element model(ling)
GIA	Global Isostatic adjustment
GNET	network of GPS stations on Greenland's coasts
GNSS	Global Navigation Satellite System
GPS	Global Positioning System
GRACE	Gravity Recovery and Climate Experiment
IS	Interpolation Skips
L	Lithosphere
LT	Long Term
Rbf	Radial basis function
RT	Resolution Tangent
Stand. dev.	Standard deviation
Std	Refers to the standard model
T	Timeline
1D	1 dimensional
2D	2 dimensional
3D	3 dimensional

Table 4: Table of concepts. These concepts are used multiple times through out the thesis, and clear definitions are needed for them.

Concept	Definition
'elastic'	instantaneous deformations due to load chances on the surface
'element'	3D object created within 8 nodes
'long term'	from 122000 years ago till present
'nodes'	points which create the elements by setting coordinate boundaries
'short term'	inside the time frame of 1972 till 2019
'uplift'	displacement in the radial direction outwards relative to the Earth's core
'visco-elastic'	both elastic and viscous deformations
'viscous'	non instantaneous deformations due to load changes on the surface which typically take place on long periods of time

List of Figures

List of Tables

1 Introduction

The law of universal gravitation, as written by Newton, stipulates that bodies with a mass are attracted to each other by a force called gravity. The strength of their attraction depends on both of their masses and the distance which separates them. Hence, as a famous example, the apple falls from the tree because the Earth exerts a gravitational pull upon the apple. Furthermore, if a body is presented a force upon itself, it can be deformed. Similar to a sponge which will naturally be deformed if one presses on it.

The two mentioned principles can be applied when studying the ice variations in polar regions, namely Greenland, and the resulting deformations of the Earth's surface. When ice forms over a region, it deforms the surface, and the subsequent layers beneath it, as the force it exerts due to its gravitational acceleration is high enough, in comparison to the force the Earth exerts in resistance. However, when the ice melts, similarly to the sponge when one stops to press on it, it aims to return back to its original shape.

As mentioned before, the forming of ice deflects the ground downwards, and the melting induces a spring and damping like behaviour, leading to the ground rising again. This process is called Glacial Isostatic Adjustment or in short GIA. The assumption made here is that the Earth's layers aim to restore to a state where there is isostatic equilibrium, where the surface is in a pressure equilibrium. The search for this equilibrium, leads the layers to either compress or extend. This process might also be called Post-Glacial Rebound in other sources, studies or research. The deflections of the ground, over multiple centuries or millennia, can have long term consequences on the Earth's gravity field. Not only because it might increase or decrease the local radius of the Earth at certain spots, but because it actively displaces mass, notably in the mantle.

From above, the reader can distinguish two deformation types, which are: elastic deformation and viscous deformation. Elastic refers to the deformation that is instantaneous. This is the 'spring like' part of the deflection. The elastic deformation typically is guided by the Young's modulus of the layers beneath the loads. The lithopshere is a layer that is often assumed to purely deform elastically, as its viscosity is so high. The viscous deformation refers to the deflection which takes a longer time to act, and thus the one which is not instantaneous. As the name suggests, it depends on the viscosity characteristics of the materials, and in this case: of the layers beneath the Earth's surface. As mentioned, the lithosphere, has an extremely large viscosity, hence its elastic behaviour. However, layers which range until 70 [km] to about the bottom of the lower mantle, at about 3000 [km] depth, have viscous properties which allow them to impact the deflections in the GIA phenomenon. Contrary to the elastic deflection which is instantaneous, the viscous deflection can take place over multiple thousands of years, depending on the load changes on the surface and the viscous characteristics of the layers at different depths and locations (Simpson et al., 2011).

Modelling GIA is crucial for multiple reasons. On an Earth modelling perspective, it provides insights in its composition, as displacements in GIA models are often compared and validated against real life measurements. For instance, there are a series of GPS stations over Greenland's coasts which track daily changes in deflection (Khan et al., 2016). Moreover, modelling GIA presents advantages in possible contributions to climate sciences, as GIA has notable effects on sea level rise (Martinec et al., 2018). The deflections due to ice melts are not limited in space by the location of the former ice sheets: the sea floor near former or melting glaciers is also partially affected by these deflections. Lastly, GIA is also less directly linked to current ice melts due to climate change, as we know that there exists a feedback loop between GIA and ice changes (van Calcar et al., 2021). Correcting the dynamic gravity field measurements by GRACE, using modelled and more refined GIA gravity rates, in order to obtain better estimations of ice melts, is also important in our understanding of climate change, as GIA uplift rates can be converted to gravity rates and subtracted from GRACE measurements in order to obtain gravity rates due to ice mass loss. Hence, with better ice mass loss estimates, we gain a better understanding of climate change.

However, there are clear uncertainties in the steps which are taken to model this phenomenon, especially in Greenland. Greenland is an extremely attractive region for GIA modelling, as all of its ice from the last ice age has not melted, contrary to the Fennoscandia plate for instance, and it is one of the major land areas, with Antarctica, which sees due to climate change, ice melting. However, the main reason why Greenland is chosen for this study is the fact that it is not studied as extensively as other regions of strong GIA signals. GIA in Europe and North America, have extensively been studied in depth with the help of a large network of GPS

stations, as pointed out in Whitehouse (2018). Antarctica has already had numerous recent research projects involving GIA.

Firstly, as for all GIA models, there are modelling uncertainties in the ice heights, that is the mass of ice variation before humans started measuring it. This uncertainty increases as one goes further in the past. For instance the uncertainty in the ice heights prior to 20000 to 25000 years ago, which is the period of the ice maximum on Earth during the ice age, is extremely high. Moreover, the uncertainty in the de-glaciation period is less but still present. Only the history in the past 30 to 50 years, and especially since 1973 - this was the launch of the Skylab altimetry mission[1] - can be assumed to be sufficient. This is mainly because there are few measurements in time of ice sheets. The second major uncertainty is on the composition of the layers beneath Greenland, and in the Earth in general. For instance we know that the temperature profile in the mantle and lithosphere, varies across the glove, which in turn varies the viscosity laterally (Hirth and Kohlstedt, 2003). However, at this stage of research, this variation pattern is uncertain, and the values in the pattern are even more so. Also, viscosity of a layer or element in a mesh is often assumed constant through out time, but viscosity is known to vary as the loads on it varies. These two large uncertainties, in ice heights and viscosity profiles, are the main driving ones, which research into GIA modelling tries to address. Uncertainty in a temporally varying viscosity profile is, at this stage, not a main priority. More accurate and more precise GIA models can be used to then find new estimations of the viscosity and in the ice height history.

This first superficial look at the background of Glacial Isostatic adjustment, leads to consider the topic of this Master Thesis: utilising a spherical Earth finite element model, in Abaqus 6.14, in order to develop a GIA model which synthesis ice histories from the glacial cycle till now, that is from 122000 years from present till 2019 (Lecavalier et al., 2014), while testing 3D varying viscosity profiles. This research has already partially been conducted in Greenland in two major research projects, with the particularity that neither used modern ice changes to predict associated present day uplift rates. The first paper inputs in the research model a 3D viscosity profile which makes use of a reference viscosity, from which other viscosities are found (Milne et al., 2018). The principle conclusion of this paper is that using laterally varying viscosity profiles impacts significantly modern deflection rates, and created a difference with the 1D viscosity profile results of various tens of meters in the Holocene (Milne et al., 2018). The second main conclusion of this paper was that using a 3D varying viscosity profile did not remove the deflection errors when a 1D viscosity profile was used with a fitted ice history (Milne et al., 2018), namely the discrepancies in the North-West and South regions of Greenland which were presented in Lecavalier et al. (2014). Milne et al. (2018) then accordingly concluded to limitations in the Huy3 (Lecavalier et al., 2014) model. The other paper, van der Wal and Xu (2016), makes use of an Olivine flow viscosity model, with a wet rheology for its 3D viscosity profile generation. The main conclusion from this paper is that the largest discrepancies between the 1D and 3D model estimates of uplift rates and deflections today are located in the South and West of Greenland.

As demonstrated research in implementing a 3D viscosity profile in Greenland for GIA research is in a preliminary state, making this master thesis topic more interesting. Adding on, there is evidence, demonstrated through this Master Thesis, that there are both ice variations in the 'short term', that is in the last half century, as well as in the 'long term', that is the past 500, 1000 and 10000 years. Thus, considering these small de-glaciation and re-glaciation processes, it becomes more pertinent to test the 3D viscosity profiles, which display regions of lower viscosity. Lower viscosity typically reacts quicker in time to surface load changes than higher viscosity, given the same layer depth. Hence, with this Master Thesis we hope to bring further contributions to the study of GIA in Greenland. This is done through the following objectives.

Synthesising the 'short term' and 'long term' ice histories, in order to have a GIA model which combines both viscous and elastic deformations from the ice maximum from the last glacial maximum till now, is one of the main objectives of this Master Thesis. 'Short term' here defines the ice history since 1914, and 'long term' defines the ice history till 1914. The ice history prior to the global ice maximum, about 25 thousand years before present, is also considered, although this one is more uncertain. The ice history used until 1914 (Lecavalier et al., 2014) is one which specifically was developed for Greenland, when the comparable research of van der Wal and Xu (2016) used the global ice history ICE-5G, which is not necessarily focused on Greenland ice history. Lastly, combining ice histories also means simulating both the elastic present responses and the viscous responses for 'long term' ice history variation, in present day uplift rates. This is, as far as this subject is understood, a rare endeavour. The method usually chosen is to simulate the modern elastic uplifts separately from the GIA model, and then super impose them, as for instance shown in Khan et al. (2016) or Simpson et al. (2011).

[1] link: http://www.altimetry.info/missions/

In using an ice history and GIA model which aims to be used to simulate both the modern day viscous and elastic uplifts accurately, we can formulate two of the three main research questions of this thesis: **'How can an ice history be designed and built, which represents the ice thickness differences from 122000 years ago till now and which is also pertinent for a GIA model?'** and **'How can we design a spatial resolution which accurately models modern day uplifts rates, given the use of a unified ice history since 122000 years ago till now?'**. From the first main question, these sub-questions can be formulated: 'What are the main limitations in the use of a unified ice history?' and 'What are models which can be assembled together to make a unified ice mass history?'. For the second main research questions, these are the sub-questions we will address: 'Assuming a unified ice history, can a convergent resolution be obtained for both the modern day viscous and elastic response? if not, why so?' and 'What are the limiting factors in developing a mesh which aims to be accurate both for viscous and elastic responses, in the long and short term?'.

This Master Thesis also aims to test and compare two types of viscosity profiles in the first 420 [km] depth of the Earth, namely a 3 dimensional and a 1 dimensional. As ice models mostly reconstruct ice histories from relative sea level data using 1D viscosity models, using a 3D viscosity profile in the GIA simulation will prove interesting in seeing the accuracy when using a 3D viscosity profile on an ice history reconstructed with a 1D viscosity profile. This brings us to our other third main research question: **'What are the effects of including a 3D varying viscosity in a GIA model in Greenland which uses a unified ice history from 122000 years from present till present day, on deflections throughout the simulations and on present day uplift rates?'**. These are the related sub-questions: 'How does the inclusion of a 3D varying viscosity affect accuracy of the model for modern day uplifts with respect to modern day uplift rate measurements?' and 'Which areas of Greenland are the most affected by the inclusion of a 3D varying viscosity?'.

All of these studies will be performed on a (3D) spherical Earth model, when most models until now model GIA on a flat plate model or on a 1D Earth spherical model. The advantage of a spherical model is that deflections across the entire globe also impact deflections on Greenland, while the flat plate models usually only simulate the regions of interest and therefore do not take into account all of the globe region's. We use an adaptive mesh, which is finer over Greenland and coarser on the rest of the sphere. Furthermore, using a spherical Earth, instead of a flat Earth, not only allows to model all of the Earth's regions, but also to simulate GIA more accurately. A deforming sphere does not have the same physical characteristics and relations as a deforming plate, and this therefore has already proven to be a major advancement towards a more accurate model, as demonstrated in Spada et al. (2011).

This project aims to be a strong basis for future research on improving the synthesising of a unified ice history of Greenland, on gaining more knowledge on viscosity estimates used for Greenland, and on researching the best configuration of mesh points in Greenland, in the objective to find more accurate GIA deflection results, both viscous and elastic, for this region.

Fulfilling these objectives and aims requires a clear structure, which is laid out here. Firstly, we design a first draft model. This involves designing the mesh and geometry of the model, designing the timeline used with the according input loads and associated grid interpolation schemes. This is quickly followed by a first round of verification and validation in order to assess the model, a first full simulation will be run, which will be considered our draft model, followed by a second round of verification and validation.

Secondly, a series of more in depth parametric studies are conducted in order to improve the draft model. The spatial resolution, temporal resolution, quality of the interpolated ice loads, and inclusion of the time ramp in between steps, are all aspects which are changed in a controlled manner in order to test what are the best configurations of the settings, with regards to criteria such as: sensitivity, time taken and accuracy. Following this chapter we present the effect and results of including two 3D viscosity profiles on the initial draft model: a lower bound and upper bound model.

Lastly, we present the final results of models which vary according to their viscosity profile. Two models have a 1D viscosity, 1e21 [Pas] and 1e22 [Pas] at depths from 70 to 420 [km], while two, consisting of an upper and lower bound model, have a 3D viscosity until 420 [km] depth. These results are then analysed by comparing the simulated uplifts to GPS station uplifts, but also to the deflection over the last 10000 years.

2
Design of the model basis

In this chapter we design the draft model which will be modified and improved in some aspects in further chapters, especially with respect to Earth properties, the mesh and the timeline. We start this chapter by designing the geometry of the Earth FEM model. Furthermore, we then detail the ice and viscosity model used. Moreover, we present the investigation performed into the interpolation of the ice loads, for all ice histories, from 122000 years ago till now, in order to convert them from the given grids to our designed grid. Lastly, we present the design of the timeline and the design of the Earth's FEM model layers.

2.1. Building the mesh layout

An essential part of the model, which we can control to an extent, is the mesh layout and thus the finite element modelling. In this chapter, the design of the surface mesh is defined and discussed. The meshing and the creation of the layers, and therefore of elements, is presented in later sections, notably in Section 2.5 and Section 4.3.

2.1.1. Spherical Earth Model used

The model used to generate the mesh is the model which will be used to simulate the Glacial Isostatic Adjustment in Greenland. It is useful to emphasise that this model is relatively new and is state of the art. It includes options for removing spherical harmonics degrees 0 and 1 and self-gravity inclusion. This section focuses on explaining the part of the model which creates the mesh, and in Section 2.2 a section is dedicated to explain more about the functioning of the 3D Earth model.

The model was created by Caroline van Calcar (van Calcar, 2020) and Bas Blank (Blank et al., 2021), following the method of Wu (2004). It was originally developed to study the GIA effect in the Amundsen Sea Embayment (Blank et al., 2021) and Antarctica as a whole (van Calcar, 2020). Hence, a function had already been added to create a region of finer mesh over the region of interest. The program, with the help of Python commands, first creates a sphere with a set radius, and a set number of layers. Once it has created the nodes, it creates the elements. The nodes are spaced by a certain amount which can be indicated, both in the direction radial or tangent to the surface. Furthermore, it then changes the elements by replacing in the finer region, the number of nodes and the distances between them, using the input finer region mesh spacing. Finally, it assigns to each layer of elements the corresponding elastic, density and viscous characteristics.

2.1.2. Designing regions

Designing the different regions of the surface mesh, refers to the fact that there will be a varying mesh mesh size. In order to design these varying mesh size regions, their number, location and size need to be determined.

Number of regions

When designing the regions on the surface of the Earth we first need to know how many regions we will have. For this, we refer to the given Earth spherical model which has two regions: one coarse and one fine.

As we focus on Greenland, the choice for two regions seems straight forward. However, there is the possibility to have an additional finer region, or multiple other ones, in regions which are known to have higher uplift rates. However, at this stage, it would require significant more time to implement, and it would therefore not fit in the 7 month long Master Thesis. Nevertheless, the possibility for such a mesh configuration to exist is addressed in Appendix C.

Location of regions

In the given Earth spherical model, the finer mesh region is located on the South Pole. However, although we wish to have this finer mesh region over Greenland, it will be a matter of rotating data points to fit over the South Pole. This is further discussed in Subsection 2.1.4.

We now thus have a finer mesh region over the South Pole, where Greenland will be located, and a so called 'global' region for the rest of the globe.

Size of regions

Greenland has an odd shape, ideally we would need an elliptical grid, as discussed in Appendix C. However, for simplicity, we will now adapt the circular finer region defined in the given model to Greenland.

The largest distance of Greenland is actually in the North South axis, when the largest angular distance is the East West direction. Greenland is 22 [°] of latitudes high, and 49 [°] in longitudes wide. However, because longitudes converge the further North or South one travels, the longitudinal angular distance is not represented in the physical distance. This apparent analysis mistake is actually due to the fact that Greenland is far up North, so the longitudes converge closely together, in terms of physical distance, over Greenland.

The middle point of Greenland is the coordinate 71 [°] latitude with 312.5 [°] longitude, according to Table C.1. The size of Greenland is about 2466 [km] tall on 1774 [km] wide. If this is is translated onto the South Pole, the finer region circle would have a radius of about 10 [°] with the centre of the Earth. What is meant here is that the 10 [°] of radius is an angle between the North-South axis and the radius of the Earth which ”draws” the limit of the finer region on the spherical Earth. However, we wish to make the surrounding region of Greenland fine too, to better account for deformations. Thus, we can double this radius, to give a finer region radius of 20 [°].

Below, Figure 2.1 displays this finer region, along with Greenland and parts of the coarser region.

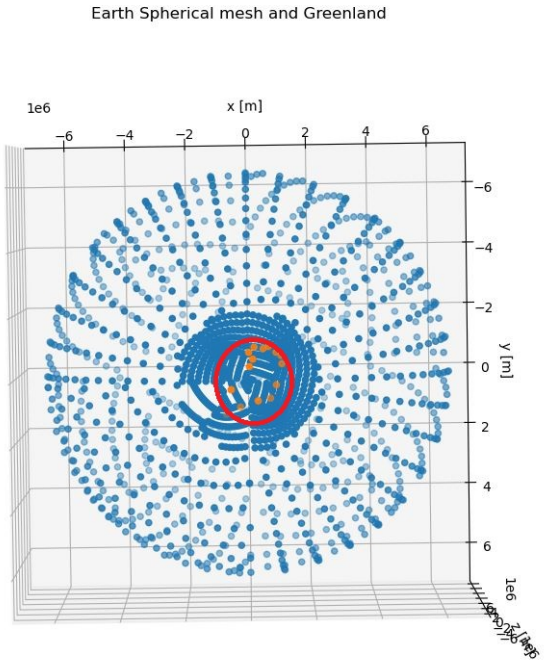

Figure 2.1: Greenland (orange) rotated on the South Pole, with the surface mesh. Only every 30 element of the mesh is plotted on the graph, hence the apparent lack of points in the bottom left of the finer region. This is only apparent. The hidden axis is the z axis, i.e. the North-South axis. The red circle limits the Greenland ’tight’ region explained below.

Figure 2.1 demonstrates and proves what has been stated: that Greenland’s height in the North-South axis is larger than its width. Furthermore, through Figure 2.1, the reader can appreciate that there is a ’buffer’ region between Greenland and the coarser region. This was done with the intent to increase accuracy in Greenland by already simulating with a similar mesh the deflections around it.

The Greenland ’tight’ region

We discuss in this subsection and the previous subsection the different regions for the mesh. However, it is worth noting that when interpolating and loading the ice masses for the ice history since 1914, that this will not be done over the entirety of the finer mesh region. This is done because viscous deformations over Greenland due to recent ice mass changes are assumed minimal (Simpson et al., 2011). Hence, just loading since 1914, to simulate the elastic deformations due to recent ice mass changes, is only required over Greenland, i.e. the ’tight’ region. We will interpolate and load this data over the smaller region called the Greenland ’tight’ region. This region is delimited by the red circle in Figure 2.1.

This region is define as a circle on a sphere, which has as a limiting coordinate: the North most vertical coordinate of Greenland. In other words, when Greenland is rotated to the South Pole, this Greenland 'tight' region stops on the North most point of Greenland on the sphere, corresponding to a maximum z value of approximately -6243447.94 [m], assuming z is the North-South axis through the Earth's centre, with North being positive and South negative.

2.1.3. Designing the mesh size

Designing the mesh size is the next logical step. The reader should keep in mind that the one presented here is purely based on literature and is an estimate for a convenient mesh size, as further on, through parametric studies, this mesh size will be varied in order to find a more efficient one, mostly in terms of accuracy, but also regarding the computation time.

Global mesh setting

For this we use the mesh size found in literature as a target mesh size (Lecavalier et al., 2014). In this paper, where the researchers create the Huy3 ice model which we use for the 'long term' ice history, they find the optimal viscosity solution by running ice models over a resolution of 0.7 [°]. Hence, because we are here designing the region outside of the finer region, we round the 0.7 [°] up to 1 [°] - important to note again for the reader, that when building the mesh model, the Earth is assumed a perfect sphere and that 1[°] represents roughly 100 [km] in any direction at the equator - and then roughly get a resolution setting of 100 by 100 [km] for the global mesh. The only reason why it is acceptable to have such a coarse resolution is that the region outside of the finer region will not be a region of study. Considering that 75 [km] was used for the region of interest in Huy3, we assume that 100 [km] is sufficient, given high computation times, for the region outside of the finer one. Lastly, the 100 by 100 [km] is an improvement compared to the given model which had 200 by 200 [km] mesh size for outside of the finer region. It is also significantly smaller than the GRACE resolution, which is of about 300-400 [km] (Ramillien et al., 2016). This presents an advantage because we can then have more points than needed if we are to compare GRACE data to gravity rates from this model.

Mesh dimensions - finer region

The shape of each mesh element is determined by 8 nodes, where 4 nodes lay on the surface, which then neglects the curvature of the surface within the finer region, and is more complex at its outside boundaries with the 'global' mesh.

When determining the size of the mesh, we should keep in mind a very plausible application of this thesis: that one could link the modelled solid Earth deformations uplifts to the change in gravity rate, as measured by GRACE, over Greenland. Thus, our mesh should be finer than GRACE's resolution. GRACE's resolution is situated around 300 [km] (Leroux and Pellarin, 2016), and getting gravity field measurements below 25 [km] (Hirt et al., 2013) is deemed for now not possible. So when modelling the uplift, we can assign a ratio of 144 mesh points to 1 gravity field measurement, yielding a mesh of 25 by 25 [km]; roughly 0.25 [°] in latitude at the South Pole. This ratio is high, that is: in order to take into account Greenland's coasts lines which would determine the ocean loading if this model were to be used later on with loads from the ocean, and the fact that the defined area is non-squared when the mesh is roughly. A high resolution is also needed for both recent ice history changes, which use precise satellite measurements, and when low viscosity values are present, as these will deflect more. Using lower resolution will affect the deflection results, which could even in turn even affect the extracted gravity rates on a large scale, if one wishes to compare results with GRACE.

2.1.4. Converting and rotating coordinates

In order to clear any uncertainties, and to allow for reproducibility, it is important to define the coordinate systems used and the methods used to translate, convert and rotate them.

Before defining the rotating tools, i.e. the matrices, it is useful to present the definition of the spherical and Cartesian coordinate systems used in this thesis, and to also present the conversion tools used between both.

Furthermore, when converting from Cartesian to spherical coordinates and using Abaqus, one can distinguish three areas. The first is the conversion from spherical coordinates, in the form of latitudes and longitudes, to the Cartesian system. An important distinction here is that unlike regular spherical coordinates, latitudes start at the equator when co-latitudes start at the North Pole. Furthermore, one can also distinguish the conversion from Cartesian to spherical coordinates. Lastly, because we are using Abaqus, laying out how the conversion between our Cartesian system and Abaqus's Cartesian system of coordinates becomes important.

Cartesian coordinates
We can first define the Cartesian system. The z axis runs along the North and South Pole, and the y and x axis are situated on a plane which is perpendicular to the North-South axis, and at equidistant from the North and South pole.

Spherical coordinates
We can thus also define the spherical coordinate system. It is made of the radius, which is in most cases the volumetric radius of the Earth, 6371 [km], the longitude and the latitude. The latitude, as defined geographically - this latitude is actually often called the co-latitude, if it starts at the North Pole - is defined as from the equator, so the plane which is perpendicular to the North-South axis and at equidistant from each pole. The longitude is defined from the Greenwich meridian. This is the definition in the given data sets. However, in spherical coordinates, the latitude is the angle between the positive z unit vector, centre of the sphere to North pole, and the vector linking a point on the surface to the centre of the sphere.

From latitudes and longitudes to Cartesian
When we refer here to longitudes and latitudes, we refer to geographical latitudes, with the 0 latitude being at the equator of the Earth. Equation 2.1, Equation 2.2 and Equation 2.3 present this conversion.

$$x = R \cdot \cos L \cdot \cos l \tag{2.1}$$

$$y = R \cdot \cos L \cdot \sin l \tag{2.2}$$

$$z = R \cdot \sin L \tag{2.3}$$

Where R is the radius of the point, which is assumed as 6371 [km], or at a certain depth: 6371 [km] minus the depth in kilometres. L is the latitude in radians, as measured from the equator, and l is the longitude in radians. x, y and z are the new coordinates in the Cartesian system.

From Cartesian to spherical
Already note that here we discuss spherical coordinates and not latitudes or longitudes. This is because we actually use co-latitudes, so the latitude starting at 0 at the North Pole. This system is therefore shifted 90 degrees up and inverted compared to classical geographical latitudes. Equation 2.4, Equation 2.5 and Equation 2.6 are the three equations which convert coordinates from Cartesian to spherical.

$$R = \sqrt{x^2 + y^2 + z^2} \tag{2.4}$$

R stands for the radius at that point, so about 6371 [km] at the surface of the sphere, if not exactly equal to that. x, y and z are the Cartesian coordinates.

$$\theta = \arccos \frac{z}{R} \tag{2.5}$$

$$\phi = \arctan \frac{y}{R} \tag{2.6}$$

θ is the longitude and ϕ the co-latitude from the North Pole. Note that the results from Equation 2.6 span -180 to 180 [°], when these should in fact span 0 to 360 [°]. To remedy this, we can simply add 360 [°] to all values between -180 and 0 [°].

This conversion is used after the interpolation of the data, when the data files are written in a spherical coordinate grid, for the simulation software to read. This conversion is also used in reading, analysing and plotting the output results from the simulation.

From Cartesian to Abaqus Cartesian
This conversion is no mathematical one, as both systems are three dimensional Cartesian systems with the Earth's centre as centre point; coordinate in x, y and z of 0, 0 and 0. However, the Cartesian system presented

in this thesis is not the same as the one in DASSAULT's Abaqus software. In Abaqus, our x axis, is called the z axis, our y axis, is called the x axis, and our z axis, is called the y axis. This is demonstrated in Figure 2.2. For anyone who wishes to work with Abaqus in the future, this is extremely important, as a lot of debugging or coding time can be lost if this is not taken into account.

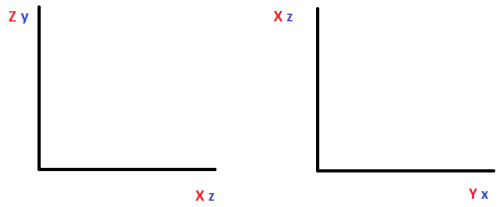

Figure 2.2: Conversion of the axis from our Cartesian system to the one which Abaqus uses. Convention: the capital red letters are our Cartesian system when the smaller blue letters are Abaqus's Cartesian system.

Rotation of coordinates

During interpolation of ice masses, we need to rotate the given data coordinates, in latitudes and longitudes, to the South Pole. We perform this task by first converting these latitudes and longitudes, as explained above, to Cartesian coordinates, and then rotate these coordinates for them to fit the South Pole. For this rotation, we find the rotation matrix which we need multiply with the original x, y and z coordinates, and it is interpreted as the rotation matrix to align the middle point of Greenland, calculated from the maximum and minimum longitudes and latitudes, from Table C.1, with the South Pole, defined as 90 [°] South from the equator. Equation 2.7 is the equation used to find the rotation matrix.

$$\mathbf{R} \cdot \mathbf{m} = -\mathbf{Z} \cdot R_E \tag{2.7}$$

Where $\mathbf{R}$ is the rotation matrix, $\mathbf{m}$ is the middle of Greenland's Cartesian vector, $\mathbf{Z}$ is the unit vector along our z Cartesian axis and R_E is the Earth's volumetric radius. The 'middle of Greenland vector' is the vector which goes from the Earth's centre to the surface of Greenland, in a middle point with respect to the latitude and longitude extremities of Greenland. The middle longitude of Greenland is assumed at 312.5 [°] and the middle latitude is at 71 [°], as already mentioned. Using the equation above, we can find the rotation matrix which will project the centre of Greenland onto the most South point on the sphere. Figure 2.3 displays this rotation matrix and Figure 2.4 displays the inverse of this matrix. Figure 2.4 is used to extract the results in the output deflections after the end of the simulations, in order to analyse them.

$$\begin{bmatrix} 0.11202227 & 0.96905765 & 0.21995066 \\ 0.96905765 & -0.05754085 & -0.24003402 \\ -0.21995066 & 0.24003402 & -0.94551858 \end{bmatrix}$$

Figure 2.3: Rotation matrix to project Greenland's centre onto the South Pole.

$$\begin{bmatrix} 0.11202227 & 0.96905765 & -0.21995066 \\ 0.96905765 & -0.05754085 & 0.24003402 \\ 0.21995066 & -0.24003402 & -0.94551858 \end{bmatrix}$$

Figure 2.4: Inverse rotation matrix to project Greenland's centre onto the South Pole.

2.1.5. Further possibilities

There are obvious improvements possible to this design for the mesh layout. The two main ones are that a more detailed mesh could be used, and that more control could be had on the Abaqus software when it makes the mesh with the target values. The first is addressed in Chapter 4 and the second in Appendix C. The ideal

scenario, would be to create nodal points outside of the Abaqus software, and input them in the simulation so that the software only needs to create the elements in between the nodal points.

2.2. Data sets and models used in the study

In order to model the uplift, we need to know the loads at different epochs, i.e. we need to know the ice masses at each epoch. This section just presents the data sets, models and constants used in this research, by describing their provenance and by describing their structure. If the reader wishes to know more about the time steps, they can refer themselves to Section 2.4. If they wish to know more about the interpolation of the data on the grids, they can refer themselves to Section 2.3. Finally, if they wish to know how the Earth characteristics values for certain layers withing the 3D Earth model were obtained, they can refer themselves to Section 2.5 and Chapter 6.

2.2.1. Earth spherical model

As mentioned numerous times already, the model is built and modified in the Abaqus software, by DASSAULT systems. In order to ease the process of modifying and improving the model, the simulation is planned and constructed through Python scripts, which input commands to Abaqus.

It was slightly modified by Jesse Reusen, before it was obtained for this Master Thesis. All of the next sections and chapters, with also Section 2.1, detail the changes made to the original given model and how these changes were implemented. Some Earth parameters in this model, like the viscosity or Young modulus at certain depths, were directly taken from Spada et al. (2011).

This Earth Spherical model, is a state of the art model. It allows the user to input ice heights, and simulate the according deflections. The user of this model can freely specify the number and the size of the time steps, by simply editing a list. He or she can also, by editing a file, freely specify the depths, density, Young's modulus and viscosity of the layers. The user can also change the size of the sphere, and can specify or not whether the core is liquid or solid.

The Python scripts are easy to work with. Hence, if the ice heights are included in matrix form, latitudes versus longitudes, the user can choose to include aspects such as ocean loads, self-gravity and rotational effects, by simply switching these variables 'on' or 'off'. Furthermore, if the user also wants to change the magnitudes of the loads, this can easily be done in the script too.

As it will be detailed in the next chapters, numerous additions will be made to this model. The most important one is perhaps the option to have a 3D varying viscosity profile, instead of the 1D varying one. We specify a 3D varying viscosity in the first 420 [km] by specifying the creep until that depth. This modification was done by adding some scripting lines from a newer version of the model, still edited by Caroline van Calcar, and by manually changing in the Abaqus portal, the visco-elastic properties to user defined creep properties. Although this is a manual and non-atomatic method, it is a simple and convenient one to use. Including a 3D varying viscosity to the model is considered a corner stone of this Master Thesis. Modelling of this 3D viscosity profile is explained in a following section, as well as in Chapter 6.

2.2.2. 'Long term' ice history & 'Short term' ice history

In this subsection, we present and justify the use of the chosen 'long term' and 'short term' ice model data. It is important to do so, as it allows the reader to gain clarity in some of the choices made in this Master Thesis, as well as allow for greater traceability and understanding of the results.

'Long term' ice history: choice and justifications

The 'long term' ice history was provided by Dr.Wouter van der Wal and Dr.Glenn Milne. It consists of files which have in them the longitudes and latitudes of points, and the associated ice mass at those points. This ice model was developed by Lecavalier et al. (2014), and is called Huy3.

This ice model is first chosen because of the methodology used. The model develops a tailored made ice history, to fit present day relative sea levels, ice extent and elevations in Greenland. It uses the ICE-5G model, while removing the Greenland component, and replacing it with the one developed by the researchers. In order to obtain the best fit given the ice reconstruction models used, 243 Earth viscosity structures were used and tested. Figure 2.5 presents the flow for the method used to generate the ice model. This is considered an advantage of this model, as it is believed that with this high number of viscosity combinations tested, an accurate ice model reconstruction was achieved.

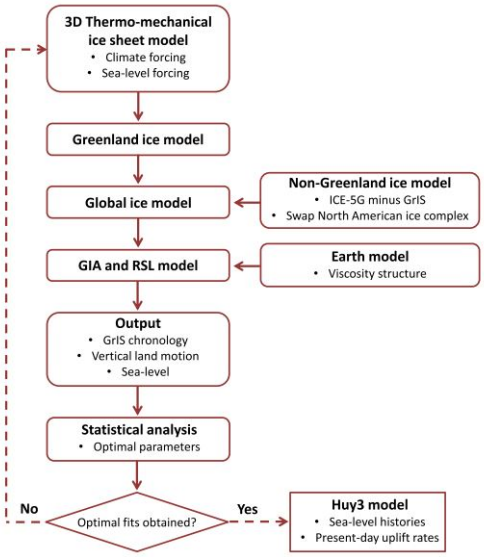

Figure 2.5: This flow diagram is the high level methodology used in order to find the best Huy3 ice model model. It was directly taken from the Huy3 paper (Lecavalier et al., 2014).

The main disadvantage which is explained in the paper by Lecavalier et al. (2014), is that the existence of a laterally varying viscosity was not used. This means that to find the best fitting ice data to the model, it used a 1D varying viscosity: 0.5e21 [Pa] in the upper mantle and 2e21 [Pas] in the lower mantle (Lecavalier et al., 2014). As we will use this ice history in part with a 3D varying viscosity profile in the final runs, this is expected to create an inaccuracy in the simulated uplifts.

'Short term' ice history: choice and justifications

The 'short term' ice history, as presented later, is first divided into the history from 1972 to 1992, not including the year 1992, which is from Mouginot et al. (2019), and which gives the ice mass change per year of about 260 glaciers on the coasts of Greenland. The actual research extends till 2018, but because it is coarse, it is only used till 1992.

The ice history from 1972 to 1992 is an ice reconstruction, as this ice history was not then directly measured by altimetry or gravimetry missions. This ice history presents the ice mass changes of Greenland through the history of the glaciers. In total, it reconstructs 260 glaciers's ice history. However, unlike for the ice data from 1992 to 2019, the method to reconstruct the ice history to the 1980s is coarse: it uses a single Digital Elevation Model (DEM), due to the lack of satellite data, this DEM is used to reconstruct the ice history, in which aerial photos were input. Moreover, in the 1980s, this model uses a 30 [m] spacing in the DEM. Furthermore, the surface mass balance used in the methodology has a spatial resolution of 1 [km] (Mouginot et al., 2019) which is an advantage as it turns out to be much finer than the final outcome, which is the history of 260 glaciers.

Hence, it is chosen for these reasons. *Note: the reader should also realise that the ice history between 1972 and 1992 has little interest to us. The first reason is that, as pointed in Mouginot et al. (2019), Greenland almost has a perfect balance over these twenty years: it only loses a bit more than 4 +/- 38 [Gt] from 1972 to 1990. Furthermore, viscous uplift rates due to the ice mass loss since 1866 are known to be negligible (Simpson et al., 2011) for most of Greenland; although this is arguable for GNSS station's location such as KUAQ as these uplifts may be heavily impacted by recent ice changes (Khan et al., 2016). Hence, this means that there are only the elastic uplifts left, and because 1972 to 1992 is not a time span of interest for this Master Thesis, we do not need an extremely detailed ice history then as we do not need a high accuracy.*

Concerning the ice mass data sets used from 1992 to 2019 (Simonsen et al., 2021), it is useful there to lay out the main characteristics of the associated research in order to justify the choice for this ice history. The ice history from 1992 to 2019 is a very detailed ice history - the resolution is discussed later but reaches 5 [km] spacing (Simonsen et al., 2021) - which gives the ice mass changes per year on a defined latitude longitude grid.

Firstly, the ice history from 1992 to 2019 is actually a synthesis of 4 satellite atlimetry missions: ERS-1,

ERS-2, ENVISAT and CryoSat-2. It is also the 'longest possible record of Gr-Is wide elevation', as stated by the authors of the paper (Simonsen et al., 2021). These two facts are a clear advantage as we are here presented with an ice model which has multiple sources of data, hence probably improving accuracy, and is the longest ice history of Greenland measured for the whole of the ice sheet.

Furthermore, using radar altimetry data proves to be an advantage, as altimetry can have a very fine resolution, compared to gravimetric data: 25 [km] (Simonsen et al., 2021) versus 300 to 400 [km]. This is very useful for 'short term' ice changes. Adding on, radar altimetry is also less sensitive to GIA signals, when compared with gravimetric studies. For instance 1 [mm] change in elevation due to GIA creates a stronger signal in dynamic gravity measurements than in altimetry measurements. Thus, we acknowledge that using radar altimetry to develop this ice history is a non-negligible advantage.

As mentioned, thanks to the altimetry data and a 'modified C3S-processing chain' (Simonsen et al., 2021), this ice model has a benefit which is its high resolution. Although it varies, the ice changes have a resolution of about 0.01 to 0.1 [°] in both latitude and longitude, which translates roughly to 5 [km] (Simonsen et al., 2021). This is extremely useful if one wishes to use this data in a GIA model with sub 5 [km] resolution in Greenland, especially for elastic uplift modelling, as demonstrated in West Antarctica (Wan et al., 2021).

The paper makes uses of other different recent ice sheet data sets, by cross calibrating its estimates, space and time wise, with previously made Greenland mass balances. To do so, it uses a machine learning algorithm which uses various ice sheet variables for calibration. This novel technique, which is explained to increase accuracy in Simonsen et al. (2021), is one of the reasons why this ice history was chosen.

Thereafter, a last advantage of this ice data is that the ice mass is smoothened for every 5 years, for the RS-1, ERS-2, and ENVISAT satellite data, and every 2 years for the CryoSat-2 and Sentinel-3 satellite data. This means that the ice history does not include climatic changes and changes due to seasons (Simonsen et al., 2021).

Lastly, the overall ice mass balance for Greenland is one of the most recently published. The assumption here is that more recent research in this field had the possibility to use more of the previous made research to verify and validate its results, but also to use previous research in the actual methodology.

Summary of the ice data

The summary of the data sets discussed above is presented here. We present the number of time steps given, the format of the files, the variables given and the number of time steps used out of these files.

	Long term
number of time steps used	22 - 37 (for the simulation inputs) and all for the time ramp
used format	R [m],longitude [°],latitude [deg], ice height [m]
number of time steps given	68: 15 from 122 to 32 thousand years from present, 15 from 32 to 17 thousand years from present, 35 from 17 thousand years from present till 2014
given format	longitude [°],latitude [°], ice mass[Gt]
	Short term 1972-1991
number of time steps used	2 - 4
used format	R [m],longitude [°],latitude [°], ice height [m]
number of time steps given by the data file	20
given format	excel table
	Short term 1992-2019
number of time steps used	12 - 15
used format	R [m],longitude [°],latitude [°], ice height [m]
number of time steps given by the data file	27
given format	NC file: grid of of ice mass changes per year [Gt/yr]

2.2.3. 3D varying viscosity profiles

The model used to find the 3D varying viscosity profiles, is actually one which calculates creep values at certain element points. The viscosity can then be converted to by using those creep values. The theory behind this model is discussed below. However, here, we should also discuss the motivation behind choosing this model, and the relevancy of its use in our research into GIA modelling in Greenland. This model was provided by the main supervisor, Dr. Ir. W. (Wouter) van der Wal, and is based on an Olivine flow assuming a wet rheology (Hirth and Kohlstedt, 2003).

This 3D viscosity profile has the advantage of not using a reference viscosity. Unlike the 3D viscosity model in Milne et al. (2018), an original viscosity is not used to then scale the others accordingly. On the contrary, our 3D viscosity model makes use of physical properties of the mantle, such as the temperature profile at various depths and the pressure at those depths, to then convert these properties into diffusion and dislocation creep. The temperature profile was calculated with global seismology models and with temperature derivatives from different mantle compositions (van der Wal and Xu, 2016). Our viscosity model replicates more the behaviour of a physical system, instead of using a reference viscosity. The user is then free to specify the water content or the grain size in order to obtain different viscosity profiles. This is done in Chapter 6.

This advantage also leads us to the main disadvantage of this model. Because the user is free to choose any grain size or water content, this can lead this model to have very large variations and also unrealistic scenarios for the Earth's creep and viscosity values. However, if a reference viscosity is used, just as in Milne et al. (2018), these anomalies would be less present , and overall the viscosity values would remain within reasonable ranges.

Due to the fact that the use of this 3D viscosity model is new, in the sense that it has only been tried once, to our knowledge, for GIA modelling in Greenland, in van der Wal and Xu (2016), and has never been used for a study which had a unified ice history, we deem it novel to use it in this Master Thesis.

The following method to generate the 3D viscosity profiles, as detailed in Equation 2.2, is used. The inputs for water content and grain size are presented in Chapter 6. Table 2.1 presents the constants used in the generation of the 3D varying viscosity profiles.

Table 2.1: Wet diffusion and dislocation creep constants used in Equation 2.8 (Hirth and Kohlstedt, 2003), assuming a constant level of COH. For the specific energy (E), the value of 335 [kj/mol] is used, for the stress exponent (n), the value of 3.5 is used, for the constant multiplied by the melting ratio (α), 30 is picked, and for the specific energy of the wet dislocation (E): 480 [kj/mol] is chosen. These constants *are not* chosen but are directly taken from Hirth and Kohlstedt (2003).

	Wet diffusion	**Wet dislocation**
A^a	1e06	90
n	1	3.5 +/- 0.3
p	3	0
r^b	1	1.2
α	30	30 - 45
$E^{\cdot}$ **[**kJ/mol**]**	335 +/- 75	480 +/- 40
$V^{\cdot}$ **[**$10^{-6}m^3/mol$**]**	4	11

Method for the generation of a 3D viscosity/creep profile

It is at this stage a relevant stage in this report to explain how the 3D viscosity profile is generated, for a purpose of reproducibility and coherence with the results to come. The viscosity profile is actually in fact a creep profile, in which the dislocation and diffusion creep are defined. For this the model uses the temperature profile WINTERC-G (Fullea et al., 2021). Then by defining a grain size and water content, the model given calculates the diffusion and dislocation creep. The model follows an Olivine flow law. It is a wet model, meaning that we assume water to be present, where both the diffusion and dislocation are assumed mostly wet. Equation 2.8 shows the equation used in converting the temperature profile to the dislocation and diffusion creeps (Hirth and Kohlstedt, 2003). Although this specific methodology and constants used are old, as it dates back to 2003, it has the advantage of being a verified and tested model.

$$B = A^a \cdot d^{-p} \cdot {f_{H2O}}^r \cdot \exp(\alpha\phi) \exp\left(-\frac{E^{\cdot} + P \cdot V^{\cdot}}{R \cdot T}\right) \tag{2.8}$$

Where A^a is a constant, d is the grain size, p is the grain size exponent, f_{H2O} is the water fugacity, also called the water content, r is the exponent of the water content , ϕ is the melt fraction by default set to 0, and α is a constant, $E^{\cdot}$ is the activation energy, $V\cdot$ is the activation volume, R is the gas constant and T is the temperature (Hirth and Kohlstedt, 2003), from the temperature profile partially shown in Appendix D. Finally, P, is the pressure at each layer, calculated in the model. Table 2.1 gives the values of these variables for the dislocation and diffusion creep. B is either dislocation or diffusion creep, depending on the constants inserted in the equation, which are presented in Table 2.1. The relation between the above mentioned variables and the dislocation and diffusion creep can be explained as done now. The larger grain size induces deflections more with dislocation creep, whereas dislocation creep is less present with smaller grain size (Ivins et al., 2021), see Figure 2.6 for a graphical illustration of this. The effect is opposite with the wetness of the rocks, i.e. the water content. A wetter mantle will deform more by diffusion creep, and a drier mantle will deflect more by dislocation creep.

Figure 2.6: Differential stresses as a function of temperature profile, with grain sizes, 10 [μm] (a) and 1 [mm] (b). The light contour lines are the values for delimiting the strain rates. The thick lines are to determine the regions of diffusion creep, Low Temperature plasticity, dislocation creep and GBS (grain boundary sliding). This graph was created in the context of an Antarctic upper mantle rheology study (Ivins et al., 2021).

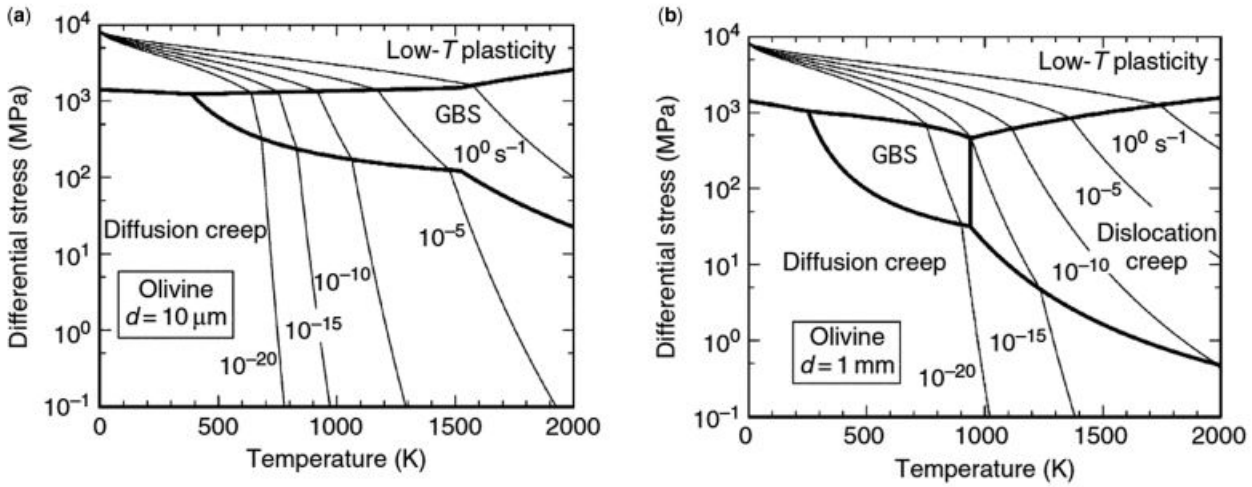

Lastly, we can also present how the creep values generated are converted to viscosity values, in order for us to create the 3D viscosity varying profiles. This is shown through Equation 2.9 (Blank et al., 2021).

$$v = \frac{1}{3 \cdot (B_{diff} + B_{disl} \cdot \sigma^{n-1})} \tag{2.9}$$

Where v is the viscosity value [Pas], B_{diff} is the diffusion creep value, B_{disl} is the dislocation creep, σ is the stress applied, for this procedure we assume a loading stress of 0.1 [MPa], and n's value is from Table 2.1 while being the stress exponent (Hirth and Kohlstedt, 2003).

2.2.4. Other parameters

Constants such as the density of ice, or the radius of the Earth, were all present in the spherical Earth model handed over, except for the density of water, and were heavily inspired by Spada et al. (2011). Table 2.3 shows these constants. In Subsection 2.5.1, we define the layers and their respective physical characteristics.

Table 2.3: Constants used.

Constant	Value	unit
Earth's volumetric radius	6371	km
Earth's gravitational constant	6.67E-11	$m^3 kg^{-1} s^{-2}$
Kilo anum	31557600000	s
Density of water	1000	kg/m^3
Density of ice	931	kg/m^3

2.3. Building the physical data interpolation scheme for mesh conversion

As mentioned in Section 2.1, we need to interpolate the ice data formulated or given, because the mesh setting in the ice data is different from the mesh setting developed in this Master thesis for the GIA model.

When building the interpolation scheme, we start by first discussing the general configuration of the interpolation scheme, that is the structure, the module and function used and the interpolation methods, and then define the specificity in each interpolation which is carried out. That is, the specificity for interpolating the 'long term' ice mass history and the 'short term' ice mass history. These specificities will depend on the physical properties of these ice histories, and degree of detail we wish to have when interpolating them over Greenland and the rest of the globe, i.e. the three regions defined in Section 2.1.

2.3.1. General set up

First, discussing the structure of the code, through a pseudo code is primordial so that the reader understands which part of the code we refer to in the explanation. We here have a brief overview of the code for the interpolation scheme, in a pseudo code format.

1. **Reading physical data values.** Here we just read and format the original ice heights.
2. **Defining regions for each type of mesh size.** This part consists of defining if we are going to interpolate over the finer, global or 'tight' region. This is in order to know which data from the original data do we pick for the interpolation. An important aspect to note is that if we interpolate, for instance over the finer region, we only use original data which is within this finer region.
3. **Reading new mesh points from the mesh model.** In this step we read over which points we will interpolate, again either the 'tight', finer or global region.
4. **Over a first loop define the interpolation technique.** This is for the 'short term' ice history interpolation, as we get to choose to what interpolation technique we use. **If we interpolate the 'long term' ice history: interpolate the global mesh using Radial Basin Function linear interpolation.**
5. **Over a second loop define whether the global or the finer mesh region is interpolated (or whether the 'tight' region is interpolated for the 'short term' ice history interpolation).** we repeat the second step.
6. **Interpolate, correct, save interpolation results.** After interpolation we apply various correction schemes to get the closest as possible, if not achieve, total mass conservation. The results are saved in text files.
7. **Optional: Perform statistical analysis of the results.** We might perform some quick statistical checks in order to make that for instance the total mass is conserved, or if certain corrections have been applied correctly.

2.3.2. Investigation of the interpolation techniques

We will first present the interpolation techniques available for 3D interpolation, and we will present how the chosen interpolation methods, for the interpolation investigation, function. The choice was made to only consider 3D interpolation methods as they better reflect the global trends, when a longitude latitude grid does not take into account physical distances between points.

When presenting the interpolation techniques used, we can define the modules used, the interpolation functions investigated and at last the interpolation methods. This way, we ensure maximum traceability.

Module used

When finding a module, in Python, to use, we directly come up with Scipy. It has the advantage of being compatible with numpy arrays, which is by experience the fastest module to work with arrays as it is written in the C language. Scipy also has the advantage of possessing a wide variety of interpolation modules, in multiple dimensions, using different mathematical techniques to do so. It allows interpolations over a sphere, a gridded data or simply in 3 dimensions. The choice was made to choose Python, as it is a language well mastered by the author, and it combines flexibility, ease of access and use, and a large amount of information/documentation available online.

Interpolation functions

For 3D interpolation in scipy, two functions are of particular interest: griddata and Rbf[1], standing for Radial basis function. The first interpolates the data by assuming it is in a grid, when the second uses a radial basis function. The Rbf's different settings will be tested, in order to get the most accurate results when modelling uplift, while the griddata function will only be used on the ice history from 1972 to 1992, as explained later on.

Spherical interpolation techniques, that is explicitly indicated by the choice of function that we are interpolating over a sphere, was not chosen because the format needed of the data to be input in the interpolation was complicated and tedious to work with. Namely the data needed to be structured: it needed to be either ordered into a grid, in some functions the points needed to be equidistant apart, and the computational memory needed to perform these interpolations was often not possessed. It did not seem to offer significant advantages over the Rbf 3D interpolation functions, apart from the fact that it was made to interpolate over spherical surfaces.

Rbf: why do we choose it? and how does it work?

As pointed out previously, there is an interest for 3 dimensional interpolations, as 2 dimensional methods only take latitudes and longitudes into account. Hence, 2 dimensional interpolation methods do not take into account: physical distances which separates points and overlapping at the poles. Thus, we can not have overlaps along the poles. For this we use the above mentioned Rbf. Rbf has the main advantage to not have to work with points which are on a organised grid. Above, we hint at the fact that spherical interpolators were not chosen due to this aspect. Furthermore, the Rbf interpolation function has the advantage to consider all the points given in the data set. This means that to interpolate one point, all the originally given points are used. In order to still favour points closer to the one which is to be interpolated, the Rbf method uses a weighed sum. Lastly, the Rbf function is relatively fast, especially compared to the spherical interpolation techniques, and is simple to use. The next paragraphs detail how the Rbf function achieved these interpolations.

Firstly, the algorithm calculates the distance between all the points within the un-interpolated data set. We can see the list of types of interpolations which the "Rbf" method can work with in the scipy module[2]. The equation for each technique given in Figure 2.7, are the equations used for each method to calculate the distance between the points. We can give the variable $\omega(r, \epsilon)$ for these equations. Where r is the Euclidean norm between the points equal to $\|x_i - x_j\|$ where i and j represent any index in the data set, and ϵ is the average distance between the points in the given data set.

[1] https://docs.scipy.org/doc/scipy/reference/generated/scipy.interpolate.Rbf.html
[2] https://docs.scipy.org/doc/scipy/reference/generated/scipy.interpolate.Rbf.html

```
'multiquadric': sqrt((r/self.epsilon)**2 + 1)
'inverse': 1.0/sqrt((r/self.epsilon)**2 + 1)
'gaussian': exp(-(r/self.epsilon)**2)
'linear': r
'cubic': r**3
'quintic': r**5
'thin_plate': r**2 * log(r)
```

Figure 2.7: Functions to calculate the norm of the distance between points on the sphere. The "self.epsilon" refers to the variability of the distance between the points, its default is the average distance between points.

After having calculated all the distances between all the points, it stores these distances in a matrix, $\mathbf{A}$ as seen in Equation 2.10, which has dimensions n by n. The diagonal row from position (0,0) to (n,n) is then 0. Each value of ice mass is then listed in the vector $\mathbf{f_{mass}}$, which has dimensions n by 1. The algorithm then solves for the vector $\mathbf{w}$, which has dimensions n by 1. Once the algorithm is in possession of this weighted vector, it can compute the value of any point given, by using Equation 2.11, where i are the indices of the original data, spanning from 1 to n, where $P(x_{new})$ is the new interpolated value and x_{new} are the coordinates where we wish to obtain the interpolation.

$$\mathbf{A} \cdot \mathbf{w} = \mathbf{f_{mass}} \tag{2.10}$$

$$P(x_{new}) = \sum_{1}^{n} w_i \cdot \omega(\|x_{new} - x_i\|, \epsilon) \tag{2.11}$$

2.3.3. Use of the interpolation methods

In the investigation, it is important to note that this investigation is done before any form of data correction, concerning the ice mass.

'Long term' ice history interpolation

The 'long term' interpolation is the only interpolation which is is done over the entire globe. This way we can define two regions of interpolation. The first one, which is the global mesh, and the second which is the finer mesh. As pointed out earlier in the thesis, the finer region is the one which encompasses Greenland. See Section 2.1 if a quick reminder is needed.

The data of the finer region are interpolated with all methods of interpolation. Furthermore, we decide to skip 9/10th of values both in the pre-interpolation and post-interpolation data. This is so that the ratio in size of the data sets stays the same, as it was originally thought that all points in the original data could be included. However, the main reason why a majority of the points are skipped, is to increase computational speeds, because this investigation is run on the student's computer and not on the TU Delft server. Hence, a majority of the points need to be skipped at this stage. In the final interpolations, where the interpolation will be run on the TU Delft server, an analysis will be carried out in order to know how many values should be skipped, to allow for high accuracy results, while saving computation time.

Concerning the global mesh, because the data is of low importance, we by default assign it the same interpolation method as the finer region data interpolation.

'Short term' ice history interpolation

There are multiple specificities when interpolating the 'short term' ice history and these are laid out here.

Firstly, the area which is interpolated in the 'short term' ice history region is the area directly around Greenland, i.e. the 'tight' region. This is due to the fact that the data available from 1972 to 1992 for the loss of mass of Greenland, is extremely coarse: only 260 points unevenly distributed over Greenland's coasts. So we can then not interpolate the history over the entire finer mesh region, which is much larger in area than Greenland. Furthermore, the ice history from 1992 to 2019 does not cover the entirety of the finer region.

Secondly, when interpolating data prior to 1992, due to the unevenness of the data points, the radial basis function 3 dimensional interpolation does not work as it tries to solve singular matrices. Thus, what is done, is

to project these data points on a latitude longitude grid over Greenland of 16 by 16 points to get roughly 260 points, then perform a 'nearest' grid interpolation, using the scipy griddata function, correct this interpolation for total mass using the functions described in Subsection 2.3.5, convert these latitude and longitudes into Cartesian coordinates, and then finally rotate the ice load points, after having converted them to Cartesian coordinates, using the rotation matrix described in Subsection 2.1.4. From there on, the interpolation is done as usual. The major limitation with this procedure is the use of the 'nearest' grid interpolation technique, as we obtain at certain spots non-zero ice heights over the seas. An option which should be considered in future research is to perform this nearest grid interpolation but on a 3D interpolating function. However, as explained at the start of the paragraph it is this far a necessary step. More investigations into this problem should be carried out in future research.

Lastly, in the investigation process, every 49/50 values is skipped both in the original data sets and in the interpolated coordinates. This is done to keep the ratio in lengths constant between the pre and post interpolated data, but most importantly, and to decrease run time, as this investigation is performed on the student's computer and not on the University's server. Performing 3 dimensional interpolations on data sets of for instance 200000 points in length - this is very roughly the size of the data set for the ice history between 1992 and 2019 - means to store and use a matrix of 200000 by 200000 points during the Rbf calculations. For a standard laptop, this is most likely unfeasible. In the final interpolations, for the models from Subsection 3.2.1, all the interpolated coordinates will be used, while a much smaller percentage than now will be skipped in the original data sets.

2.3.4. Investigation results

The results of this interpolation study for the 'long term' and 'short term' are here presented. For the 'long term' interpolation results, we present a choice of interpolator for all data files, when for the 'short term' ice history we present a choice per year. However, it should be taken into account that in Chapter 4 we add a change to the 'short term' interpolation selection, based on parametric studies on the quality of the interpolations of the ice heights and their corresponding effect on uplifts results.

'Long term' ice history results

We should start by investigating the most desirable interpolation methods, before applying corrections, to the 'long term' ice histories. We thus compare the mean and the data range, which is the difference between the maximum and minimum ice mass in the data set, consistency kept between the pre and post interpolated data sets, while also visually comparing the mapping of the loads before and after interpolation. Table 2.4 shows the actual statistical characteristics. We decided, for the 'long term' ice history interpolation investigation to leave out the gaussian method of Rbf interpolation. This is because the new range of values for the ice height was too high relative to the original one.

Table 2.4: Results of each type of interpolation, in comparison with the original data.

		Mean [Gt]	Data range [Gt]
Rbf	**cubic**	981.5032455	3796.5795
	linear	979.73954	3532.04275
	multi-quadric	980.4774	3763.5125
	inverse multi-quadric	979.837	3637.3074
	quintic	985.1481	3999.8536
	thin plate	980.3680	3674.5509
	Original data	**694.7695**	**3443.1**

The first aspect we notice from Table 2.4 is that the mean for the finer region ice mass for each interpolation method, is larger to the original mean. This is thought to be due to portions of the new data grid points being skipped, and a larger portion being skipped over areas which do not have ice. In fact, in the Abaqus model, the ratio of inland to sea points is higher than in the original data, hence the disparity in mean values. In the actual final interpolation scheme for the models from Subsection 3.2.1 onward, the new data points coordinates are

all used, so this will not be an issue.

Furthermore, we notice that in terms of data range preservation, the linear method is the one which performs best. Although, in terms of keeping an average over the interpolation the method is not optimal, the data range is largely preserved, compared to other methods. Other methods display larger outliers. As we wish to have as little correction to do as possible, we therefore choose the Rbf linear interpolation method.

In order, to further proof to the reader the accuracy of this interpolation method, we can plot the maps of the data ice masses prior and after the interpolation, as done in Figure 2.8, without any total mass correction technique applied.

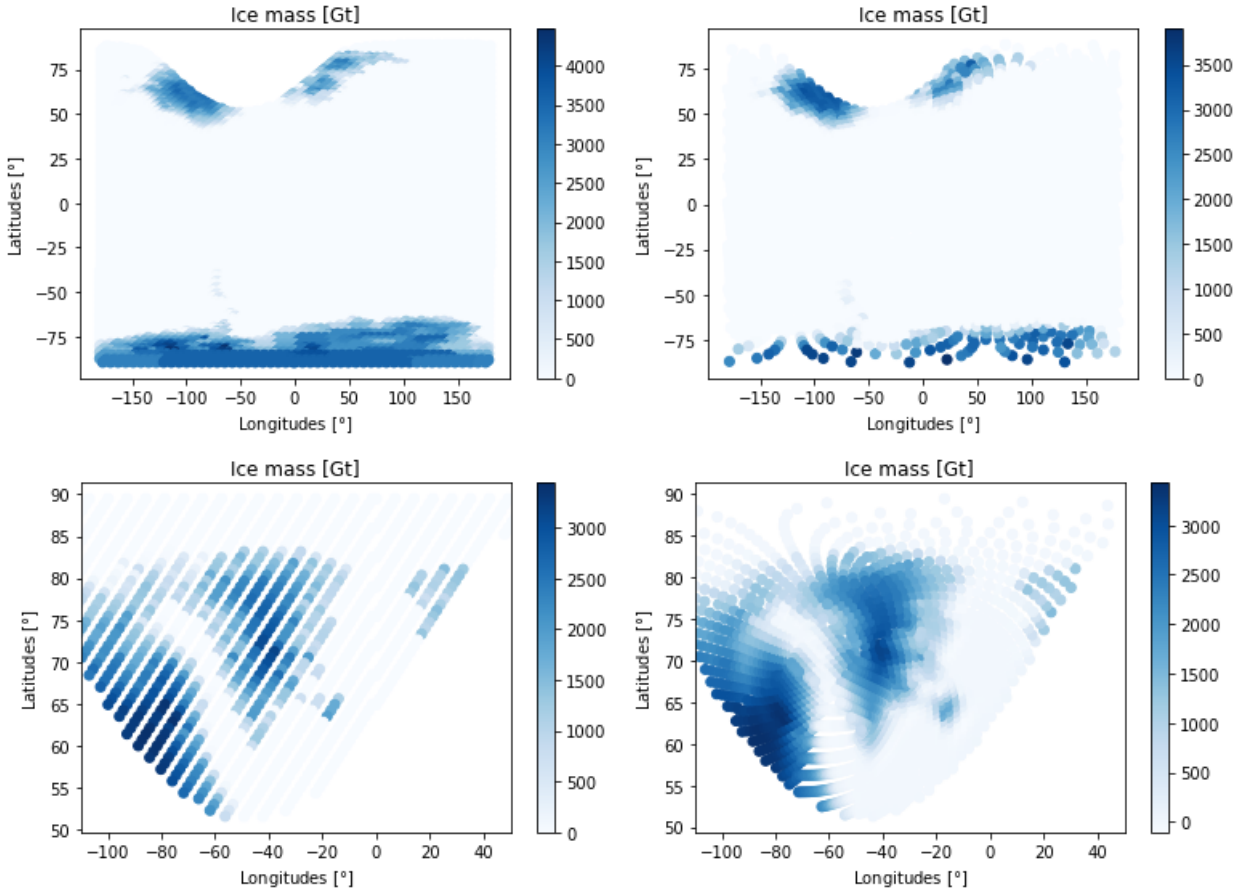

Figure 2.8: Data ice masses prior to interpolation outside of the finer region (top left), from Huy3 model at 25000 years ago (Lecavalier et al., 2014), and after interpolation (top right), prior interpolation for the finer region (bottom left) and after interpolation for the finer region (bottom right).

Above, in Figure 2.8, it can be seen that with the linear Rbf method, we not only keep a similar range of ice masses, but that the pattern of ice mass is also kept: there are no 'new' regions of ice mass, and no regions of ice mass have disappeared.

'Short term' ice history results

For this investigation into the interpolation techniques, we already apply the correction techniques, as applying them significantly changes the interpolation method choice, as noted from the variation between Table E.1 and Table E.3. The complete list of interpolation methods used for each year since 1972, can be found in Appendix E, with the final choices in interpolators per year for the 'short term' ice history presented in Table E.1 and Table E.3.

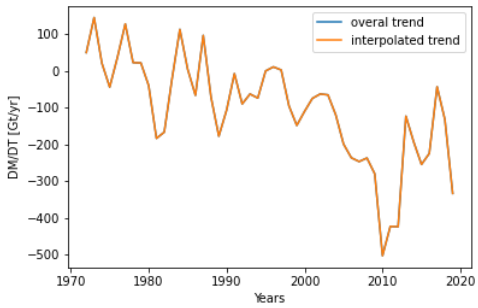

Figure 2.9: Rate of loss, dm/dt [Gt/yr], of the ice across the Greenland tight region. The result from the interpolation after total mass correction is also shown, to show clear mass conservation.

As it can be seen in Appendix E, we choose a varying set of interpolation methods, as the grades assigned are overall lower, thus better. We can now display on a map, as done above for the 'long term' ice history, through an example, how the interpolation changes the short term ice history. This is to check that the interpolation does not create new patterns in the data, and does not significantly alter the range. We can pick as an example the interpolated data at the year 1984, both at the glacier interpolation step using griddata and after while using Rbf, and at the year 1992, prior and after interpolation, during the investigation, i.e. not the final interpolated data used for the simulations. *Note: In Appendix E, we choose the interpolation technique after the correction methods have been applied. The graphs shown below are without any correction method applied. They are shown to display only the validity of the interpolation methods.*

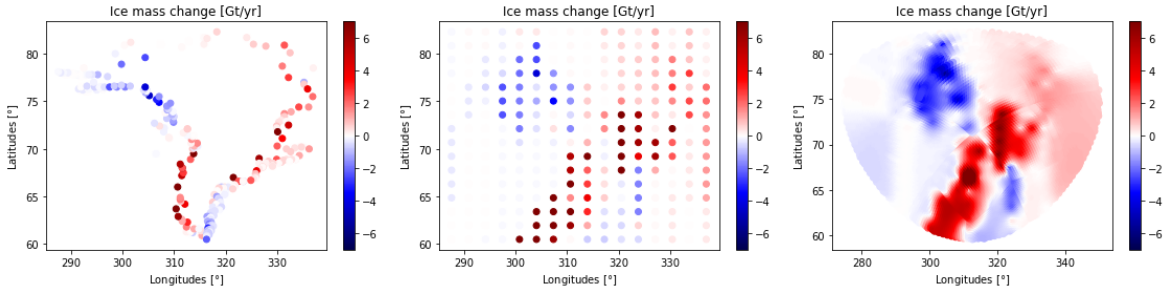

Figure 2.10: Interpolation process at the year 1984, using linear Rbf and nearest griddata method. Pre-interpolation data (left), followed by the interpolated data after the grid interpolation from the glaciers (middle), and final interpolated data using Rbf (right).

In Figure 2.10, we can notice a major limitation of our interpolation method from 1972 to 1992: the inability to interpolate directly from the glaciers to the input grid for the model, leads to inaccuracies in the final interpolated data, due to the 'in between' step of griddata interpolation. As mentioned earlier in this chapter, the griddata interpolation method from scipy is not 3 dimensional. Therefore, the 3D pattern is not properly taken into account. Although in Figure 2.10 the general pattern is respected we can see large errors, notably in the South-West region.

However, these errors are relative, as we expect in the simulation to see mostly, if not nearly only, elastic effects from 1972 to 2019, as pointed out in (Simpson et al., 2011) which estimates that the viscous effect from 1866 to 2005 is predicted to be only of -0.24 to 0.24 [mm/yr] due to the ice changes in this period. Hence, as the interesting period to analyse is from 1992, because the detailed ice history is used and there are large ice losses since then, these errors in ice history are not that significant. Furthermore, the ice history prior to 1992 is not varying as much as after 1992. We can consider for now our interpolation validated, although it could largely be improved.

From 1992 onward, as shown in Figure 2.11, we do not perform the intermediate step of griddata nearest interpolation, as the given satellite data has a very high resolution. Thus, we can directly show the pre and post interpolation data, for the chosen interpolation method. It can be seen that the pattern and the range is mostly kept, which then validates our interpolation method from 1992 onward.

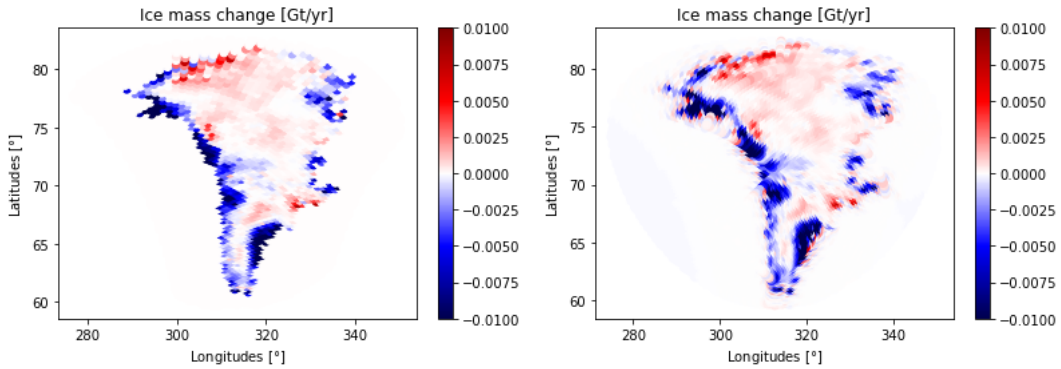

Figure 2.11: Pre-interpolation data (left) and after interpolation data (right) for the year 1992, during the interpolation investigation.

All the new data was included here in the graphs, while in Appendix E 49/50 of the results are skipped in order to give the grades. Also, the reader should realise that in Figure 2.10 and Figure 2.11, no total mass correction methods were used, as the purpose here was to show the viability and limitations of the interpolation methods used.

2.3.5. Post interpolation corrections

These corrections are only valid for the mass related interpolations, i.e. the ice histories. They were not tested on any other type of physical characteristics. There are two sets of corrections, which both aim to conserve the total mass of the data, as mass conservation is a key requirement.

The issue we face with the used scipy interpolators is that the total conservation of ice mass, change or state, is not respected. The total ice mass after interpolation decreases or increases due to the change in grid size between the post and pre-interpolation data. This issue arises due to the fact that we interpolate ice masses and not ice heights. As the interpolation function interpolates the ice mass at certain points, if the number of points on the new grid is much larger than on the original grid, then the total mass will be roughly scaled proportionally to the change in grid size.

It is advised for future work to interpolate ice heights and not ice masses. We can take a simple example to illustrate this. Suppose we have an area of 1 $[m^2]$ which has an ice height of 10 $[m]$. If we ask an interpolation scheme to find the ice heights, for the two areas which constitute this 1 $[m^2]$, both of 0.5 $[m^2]$, the algorithm will most likely find an ice height of 10 $[m]$ for both smaller areas. Then, the total ice volume is the same, prior and after the interpolation. However, if the same is asked when the input is an ice mass, say 10 $[kg]$, then the interpolating function will roughly interpolate twice 10 $[kg]$, and the total ice mass will be 20 $[kg]$, hence twice the original ice mass. With this example it becomes clear that in the future, interpolating ice heights instead of ice masses should be carried out.

Method 1: correcting for size

We first correct the interpolated ice mass data by size. As illustrated above, this is needed because we interpolate ice masses and not ice heights. This is a simple correction and is done as follows: we times the interpolated data by the ratio of pre-interpolation data size over the post-interpolation data size. The data size is the number of data points. Equation 2.12 perfectly shows this.

$$m_{i+1} = m_i \cdot S_r \tag{2.12}$$

Where m_i is an interpolated data mass point and m_{i+1} is the mass point after correction. S_r is the ratio of size of the original data over the size of the new grid. For instance, if we go from a grid with 25 points to a grid with 50 points, S_r will be a value of 0.5. However, this correction technique is not yet enough to fulfil the goal of mass conservation, and is only a first order correction. Further work is needed in order to properly correct the data, namely: the 'fine tuning' technique explained below, and the 'optimising' scheme explain in Chapter 4 when converting the ice masses to ice heights right before the loads are input in the model.

Method 2: fine tuning

Moreover, after the first correction method, we still are left with a difference in total mass. To solve such a problem, we assume that the error in mass per point is proportional to the size of the ice mass interpolated at that point. In other words, if the interpolated value at coordinate (x_1,y_1) is z_1 but at another coordinate, (x_2,y_2), the interpolated value is greater such that $z_2 > z_1$, then coordinate (x_2,y_2) will receive a higher correction than the first coordinate.

The correction is performed such that all of the excess for the entire grid or deficient mass is solved for, in order to allow for conversion of mass change. Equation 2.13 is the equation which describes this method.

$$m_{i+2} = E + m_{i+1} \tag{2.13}$$

Where E is the correction term added to m_{i+1} to find the new mass point m_{i+2}. E is the product of a ratio, determined by the share of the absolute value of m_{i+1} over the entire sum of absolute masses, and the error in total ice mass. The procedure to find E is displayed in Equation 2.14.

$$E = \frac{m_{i+1,abs}}{M_{i+1,abs}} \cdot (M_{i+1} - M_{i-1}) \tag{2.14}$$

Where $M_{i+1,abs}$ is sum of the absolute masses in the data after the method 1 correction, M_{i+1} is sum of the masses in the data after the method 1 correction and M_{i-1} is the sum of the masses in the data before the interpolation.

After having sampled these two corrections, the data is ready to be used in the simulation. Figure 2.12 gives an example of how data is corrected given the two methods, applied in the order explained here: first applying method 1 and then applying method 2 to the data already corrected with method 1. The data is fictitious hence the generality of the graph. We do not display method 3, as the results given by this method are, as shown and pointed out in Appendix E, clearly less accurate.

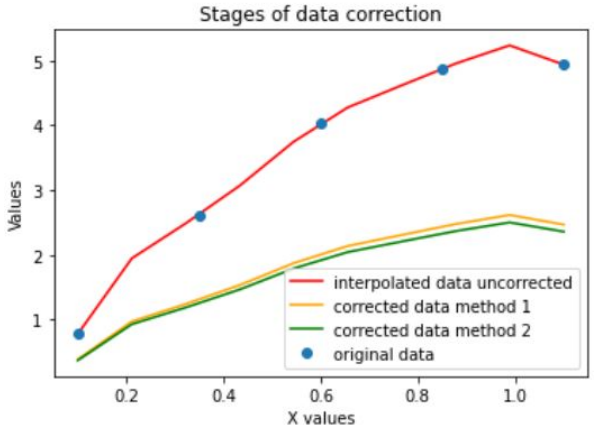

Figure 2.12: Example data corrected with method 1 and then method 2, one after the other on the *same* set. The data is three dimensional, ranging from 0.1 to 1.1 in 5 steps prior to interpolation and in 10 steps for the interpolated data.

It is worthy to note that this 'method 2' of fine tuning to get to total mass conservation, is also applicable if we had performed the interpolation with ice heights, instead of ice masses. As shown in Figure 2.12, this 'method 2' provides small correction compared to the 'method 1' technique, but would still be needed if we had interpolated ice heights. For instance, in the finer region, the 'method 2' correction provides between 40 and 60% change to the total sum after the 'method 1' correction, when the 'method 1' correction provides between 70 and 95% after the interpolation.

Furthermore, as explained in Subsection 2.3.7, in order to provide the last step towards near total mass conservation, Chapter 4 provides technique to optimally convert ice masses to ice heights, by choosing a more accurate area per mesh point. This area 'optimisation' is the last step towards near total mass conservation.

Method 3: fine tuning, constant approach

An approach which is not used further on, but which is referred to in this section is the so called 'method 3' or constant approach. Instead of using a proportional correction as in method 2, we here apply the same

technique but apply the same correction value to every data point, without any regard for the ice mass at that point. Equation 2.15 is the equation which describes this correction method.

$$m_{i+2} = \frac{(M_{i+1} - M_{i-1})}{n} + m_{i+1} \tag{2.15}$$

Where n is the size of the data after the method 1 correction. Method 3 of correction entails that because there is no way to properly know how the error in total mass is distributed, the same error should be assumed everywhere, in the region interpolated upon. The obvious flaw with this way of distributing the error is that the model will apply ice masses on top of surfaces such as the sea more than if it had not been used.

2.3.6. Mapping loads

In Section F.1, we explore two Abaqus based methods to map the loads: 'XYZ' and grid format. The grid format is the one already used in the Abaqus model given described in Section 2.2. We chose the 'XYZ' format because it produces minimal differences with the grid format method, and because it is consequently faster: about 2 to 3 times faster on simulation times. Section F.1 presents a short investigation which demonstrates these claims.

2.3.7. Areas of possible errors in the actual interpolation

We should now address possible areas in which there can be mistakes. Namely the effect of ignoring certain values in order to increase the speed of the interpolation, or the errors in interpolation linked to the spherical Earth assumptions, or even the errors in interpolations, as we do not take into account the deformations and assume a smooth surface.

Errors due to skips in the given data
Due to skips in the original data, some errors in ice height approximation can occur, which result in potential errors in deflection approximation. Appendix F explores a theoretical case of interpolation, and concludes that skipping 5/6th of values is a first good basis for the interpolation schemes. Furthermore, in Chapter 4, it is investigated how skipping ice mass values in the original data affects the end deflection results.

Errors due to spherical Earth assumption
In the given model, we assume during interpolation that the Earth is spherical. In fact, the Earth is elliptical in the sense that it has flattening, by a factor of 0.003353[3]. This value insinuates that the difference between the equatorial and polar radius over the sum of these two is 0.003353. According to the same source, the polar radius is thus 6356.752 [km] and the equatorial radius is 6378.137 [km].

This does not lead to a modelling error, as we are always consistent with the radius we choose during interpolation: 6371 [km], which is the volumetric radius of the Earth, but to a physical inaccuracy where some loads might be further or closer apart than in reality.

To solve for this error, we would need to change the geometry of the model in order to fit the Earth's elliptical curvature, and obtain ice load data which we know was created on a slightly flattened Earth. The assumption of a spherical Earth could be improved in further research.

Errors due to deformations
As pointed out earlier, the values are interpolated in three dimensions assuming a spherical Earth. Aside from the possible errors mentioned in the last part, we can theorise here an additional error, of the modelling nature.

We perform the interpolations before the simulation, i.e. the data is already interpolated before the actual simulation for all time steps. However, in between time steps, the Earth spherical model is deformed according to the ice loading and unloading. This means that the nodal point's coordinates, which were used prior to the simulation to interpolate on, are moving vertically and horizontally. The issue then becomes clear. We interpolated in a Cartesian coordinate system, assuming constant radius in the spherical coordinates, but the radius per node, according to the deformation, will change every time steps. Not only the radius, but also the longitude and latitude of each node will change.

So what does this mean in a modelling perspective? In principle, not much, for two primary reasons. The first is that when Abaqus will find the closest element to the coordinate of the load, to assign the load to that element, it is impossible that two loads end up on the same element. This is because horizontal displacement rate is

[3] This is according to the NASA fact sheet of Earth. link: https://nssdc.gsfc.nasa.gov/planetary/factsheet/earthfact.html

of the maximum magnitude of 2 [mm/yr] (Wake et al., 2016). So if this is propagated over 122000 years, the maximum horizontal displacement is 224 [m]. Hence, much smaller than the minimum size of the elements, which is of 25 [km] across or 10 [km] further on in the research.

Furthermore, as we know the vertical displacement due to GIA to not be equal or greater than the magnitude of 1 [km], and because the displacement is in the radial direction: the vertical displacement may only create negligible errors. As the loads are project to the nearest element and 1 [km] is far smaller than the minimum mesh size of 10 [km] used in following chapters, we can conclude that this vertical deformation only creates a minimal error. This is partially addressed in Section F.1.

Error in conversion between ice masses to ice heights
All the way before we save the interpolated and corrected data, we perform a conversion from ice masses to ice heights, by simply dividing the ice mass values by the density of ice, and further dividing by the area of an element. The model given works with ice heights, hence the conversion. However, an error here can occur, as the mesh which we commanded Abaqus to make may have different dimensions than instructed for each element. This issue is explored in detail in Chapter 4, where several parametric studies are investigated, namely this one, which aims to find a way of accounting for a varying area. Lastly, this potential error is a larger issue when a finer resolution in the finer region is set.

2.4. Building the timeline

In this chapter, we will design the time line for the simulation of the uplift. The time steps will be made according to the available data for the loads, i.e the previously discussed 'long term' and 'short term' ice history. Refer to Section 2.2, for details on the ice files for both 'long term' and 'short term'.

However, three main issues arise from this structure. Firstly, the 'long term' ice history stops in 1914 while the 'short term' ice history starts in 1972. The Huy3 step at 2014 is not considered here. Hence, we need to derive the ice loads at the year 1972 to then apply the ice changes. Secondly, the ice history is given per year from 1972 to 2019. These are too many computational steps, and the time line needs to be designed in order to include all of the data without having an iteration at each year. These two first issues only concern Greenland, i.e. the Greenland 'tight' region. 1914 is a crucial year as it is the end of the data given in the ice model from Lecavalier et al. (2014). These three issues will be the main focus of this chapter.

2.4.1. Determining the ice history for the globe: 122000 years ago until 1914.

Firstly, we need to design a time step from 122000 years ago till 1914.*Note that when we state X number of years ago, 2014 is the benchmark*. These requirements were formulated based on the availability of the ice model data, the large uncertainty prior to the last glacial maximum and the obvious increase in simulation time if more steps are included:

1. **There should be one or two time step between 122000 years ago and the ice maximum of the last ice age.** Similarly to discussed in Chapter 4, in the section performing a timeline parameter study, the ice history is not known prior to 25000 years ago with as high accuracy as during the de-glaciation era. This is because the Huy3 ice model is an inverted model, so the further back we go the lesser the accuracy due to lesser available data points. Moreover, the ice history prior to 25000 years ago, which the last glacial maximum, may not effect the deflection results a lot since it has been so long since then. Due to this, a minimum number of time steps is considered prior to the ice maximum, in order to reduce the overall simulation computation time.
2. **From the global ice maximum, 25000 years ago, steps of 2000 years should be taken until 10000 years ago.** The gradient of the graph from 25000 to 10000 years ago in the global ice trend is mostly steep, hence the short step size. It reality this will be done until 11000 years ago as there is not a full number of steps of 2000 years in a 15000 years long period.
3. **That from 11000 years ago till 1000 years ago it should be in 10 steps: so 1000 years time steps.** From 10000 years ago the gradient decreases, so properly modelling this 'asymptotic' behaviour of the trend is crucial. See Figure 7.3, if a deeper understanding for this ice history is needed, with regards to climate events. This figure was not shown here, as it is assumed more useful in the discussion section in Chapter 7.
4. **That the given ice histories from a 1000 years ago until 1914 should all be used.** There are only two files after this point, one at 500 years ago and one 100 years before present.

The ice maximum in the last ice age is located at 25000 years before present. Figure 2.13 displays this.

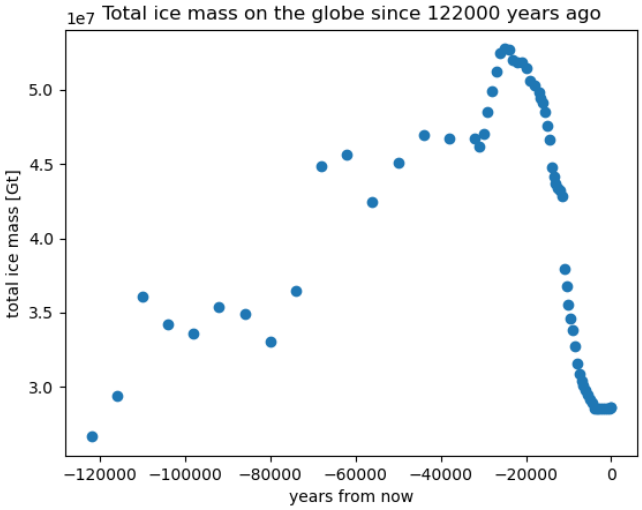

Figure 2.13: Global ice mass history, from 122000 years ago to 2019. The maximum is at 25000 years before present, with a value of about 53000000 [Gt].

Looking at Figure 2.13, the maximum is at 25000 years before present, therefore the first time step should span, according to the previous mentioned requirements from 122000 years ago till 25000 years ago. However, there is an issue with this formulation, as it does not take into account the Greenland specific ice mass trend. Figure 2.14 shows this trend.

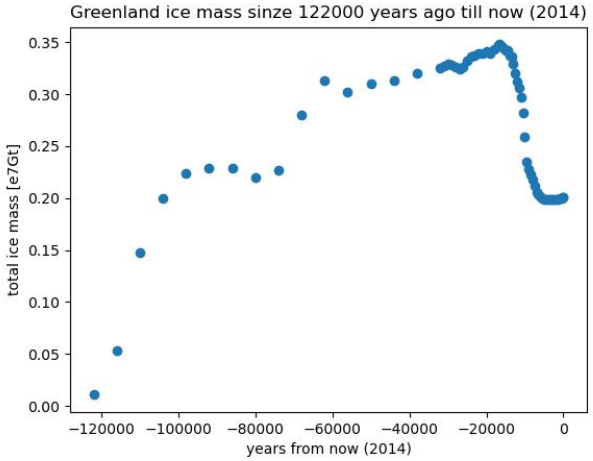

Figure 2.14: History of the ice mass on Greenland, defined within the boundaries of the Greenland 'tight' region, since 122000 years before present. The maximum is at 16500 years before present, with a value of about 3478666.15 [Gt].

We first notice that Greenland's ice mass maximum is after 25000 years ago, about 17000 years ago, so in that respect we do not need to take into account Greenland's maximum in designing the time line. However, Greenland's ice mass clearly increases and has inflection points in its trend. If we were to start at 122000 years ago and use the time ramp from Appendix G, then Greenland's ice mass until 25000 years ago would not be accounted for, as the time ramp from Appendix G is a scaling method of the already existing mass, which is practically 0 at 122000 years ago in Greenland.

In the two apparent step functions which Greenland undergoes from 122000 years ago till 25000 years ago, the first one ends at 80000 years ago, and the second at 16500 years ago. Thus, in order to represent the load in the simulation more accurately, and therefore to get more accurate deflections, we need to add a time step at 80000 years ago.

Adding only one time step about 8000 years ago is sufficient because: it is about 'half way' between 122000

years ago and 25000 years ago, the ice uncertainty between 122000 years ago and 25000 years is large, the improvement of the ice loads through a ramp might not be relevant, and the glaciation phase prior to the ice maximum has only a small effect nowadays so adding more steps would not change results significantly. This last point is further proven in Chapter 4, where adding more time steps before 25000 years ago does not change modern day deflections significantly.

2.4.2. Solving the 'missing' history issue: 1914-1972

The issue is the following: we have the ice history in 1914 and we have the changes in ice history from 1972 onward for Greenland, as Greenland is the centre of this study. However, we do not have the state of the ice history in 1972. Therefore, it needs to be derived and the following method is proposed.

For this we formulate two options; either we take into account Greenland as a whole over the previous time steps leading up to 1914, and apply the found trend to all of the points on the mesh grid to get the history at 1972, or we find a trend for each mesh point for the time steps leading up to 1914, and apply these trends to the respective points. The ice data sets would be taken from 25000 years ago onward. This is discussed further on. Furthermore, we have reasons, at this stage, to believe that the general approach may already be a better option, as we know, from Kjeldsen et al. (2015), that the ice history varies much less between 1900 and 1983 than between 1983 and 2003.

The advantage of the first option is that the computational power needed is relatively low, and that it takes into account Greenland as a whole. Its disadvantage is that it does not take into account regional specificities of Greenland. The second method has exactly the opposite advantages and disadvantages. The choice is therefore made to account the Greenland 'tight' region as whole, as we are predicting individual points and accounting for it in a unified trend is a complicated process which would require additional research.

The physical reality of this choice is questionable, and as mentioned, definitely requires more investigation. However, we can point to the fact that ice history in this time frame does not, in reality, matter significantly in the final simulation. This is because, as pointed out in (Simpson et al., 2011), the modern day deflection rates due to the ice changes for the past 100 years, are low: between -0.24 and 0.24 $[mm/yr]$. Furthermore, the ice mass balance in the period 1900 to 1983, varies about four times less as from 1983 to 2003 as demonstrated in Kjeldsen et al. (2015). Thus, regional variations then matter less in this time frame.

Time stamps taken

All the time steps from 25 thousand years before present onward are taken. This was done in order to take into the entire de-glaciation phase until now. The ice file at 2014 was not taken, as the melting of ice in the year 1990 and onward was thought to bias the data, when in fact large ice melts had not happened till then, as demonstrated by Figure 2.13.

It could be argued that less time steps could be taken into account in order to obtain a more accurate extrapolation. However, as these time steps values are not known exactly, we assume that taking all these time steps yields a satisfying result, as demonstrated in Figure 2.15.

Curve fitting

For Greenland's general trend, we will test a variety of polynomial fitting, ranging from degree 1 to degree 9. The polynomial chosen will be the one which has the highest correlation R^2 between 0.99 and 1.0. We wish to have a certain standard for the data, thus a minimum of 0.99 is wanted.

Results

Results are presented in Figure 2.15, which contains both a global trend to see how the prediction fits in, and how it fits with respect to an expected trend, by subtracting ice mass changes from 1972 to 2014 from the ice history in 2014 ice history in the Huy3 model.

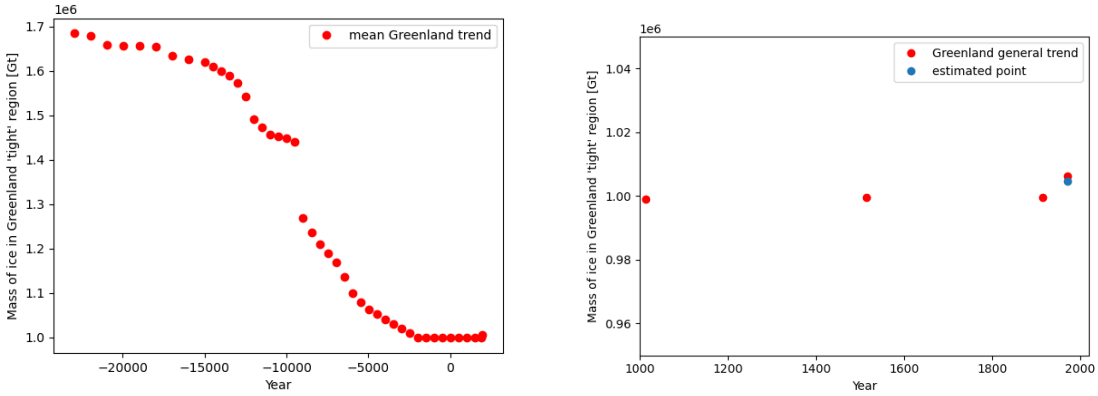

Figure 2.15: Estimation of the ice mass of the Greenland region (Greenland 'tight' region) from 25000 years ago to 1972 (left), and the total ice mass in Greenland using the extrapolation between the 'long term' ice histories, and by subtracting the short term ice losses (right).

We see in the right graph of Figure 2.15 that if we subtract the total ice mass loss between 1972 and 2014, which we know from the models presented in Section 2.2, from the ice history in 2014, we get the 'estimated point' in the above graph. This is done to verify the point which we extrapolated: 'Greenland general trend' point at 1972 from Figure 2.15. We can conclude that our method to find the 'missing' history is correct enough for now. The point does not fit properly on the curve and has an error of 0.15%. This is a small error, and thus allows us to conclude that we do not need to use the ice history at 2014 from Lecavalier et al. (2014), but that we will use the 1972 extrapolated file, resulting from the method developed in this section, and from there subtract the ice mass loss per year to get the final history nowadays. This method is also convenient as the ice history nowadays is hard to know, and the uncertainty is high. This way, we do not need to use this history for the time step at the year 2014.

The creation of the 1972 ice history file in the extrapolated scheme will then be implemented by multiplying the 1914 ice history in the 'tight' region by 1.006.

2.4.3. Determining the time step: 1972-2019

When determining the time step, for what was designated as the 'short term' ice history, we need to make two different designs: first for the time span 1972 to 1992, and a second for the time span of 1992 to 2019. This is due to the difference in type of data available between the two time periods. The focus on the data on Greenland will be the driving factor in the design.

Time step: 1972-1992

The history of ice mass changes in Greenland for the time span 1972 to 1992 is given by the history of glaciers. As explained in Section 2.3, this is coarser data than the one we wish to interpolate.

The time period of 1972 to 1992 is also further away from the current day, so getting a yearly update of the uplift may not be needed. Furthermore, we still wish to limit the amount of computing power used for this propagation. Lastly, considering that the time step before 1972, is one of about 58 years, as from 1914 to 1972 it is one time step, we can consider a time step of 10 years.

Time step: 1992-2019

From 1992 onward the ice load data of Greenland is more detailed than the mesh size we wish to interpolate on. This was extensively discussed in Section 2.3. Unlike the data from 1972 to 1992, we can therefore, in theory, have a time step of one year. However, having that many time steps, although doable considering that there are more than 26 time steps prior to the 1992 bench mark, is a considerable amount. Furthermore, taking a larger time step than one year, could also have a correction effect on the found uplift average per year. Hence, considering the previously presented information, we can develop a time step of 5 years from 1992 to 2007 and then time steps of 2 years until 2019. This way we believe will be able to develop a relatively accurate average uplift per year. This is more investigated in Chapter 4.

2.4.4. Determining the ice history of the globe outside of the Greenland 'tight' region from 1914 to 2019

For this history, we will assume that the state of the globe outside of the Greenland 'tight' region is constant: the ice history does not change outside of this region until the end of the simulation. This is not accurate, but from a modelling perspective what we wish is the uplift in Greenland due to ice melts in Greenland, and we therefore assume that ice melts outside of Greenland do not affect the uplift in Greenland from 1914 onwards as the time gap between 1914 and 2019 is too small.

2.4.5. Time line structure summary

Below is the summary of the time line.

1. $122e3$ years ago till $80e3$ years ago: time step of 42000 years, 1 time step
2. $80e3$ years ago till $25e3$ years ago: time step of 55000 years, 1 time step
3. $25e3$ years ago till $11e3$ years ago: time step of a 2000 years, 7 time steps
4. $11e3$ years ago till $1e3$ years ago: time step of 1000 years, 11 time steps
5. $1e3$ years ago till $5e2$ years ago: time step of 500 years, 1 time step
6. $5e2$ years ago till $1e2$ years go: time step of 400 years, 1 time step
7. $1e2$ years go till 1972: time step of 54 years, 1 time step
8. 1972 till 1992: time step of 10 years, 2 time steps
9. 1992 till 2007: time step of 3 years, 5 time steps
10. 2007 till 2019: time step of 2 years, 6 time steps

2.5. Building the layers of the spherical Earth model

As shown in Section 2.1, the mesh layout for the uplift model has already been determined. However, the characteristics of the layers themselves have yet not been properly analysed and designed. This chapter aims to do so.

2.5.1. Layer definitions

In defining the layers, we should define the number of layers and their properties.

Number of layers and associated depth
The model given had 6 Earth layers ranging from depths of 3480 [km] to the surface at 6371 [km]. However, we choose to add to this 2 layers one at 150 [km] and one at 300 [km].

The initial motivation to add these layers was the fact that the incomplete viscosity model - this is the same model which gave the creep values for the elements of the fine layers - had calculated values at 150 and 300 [km]. What is meant by incomplete is that only certain values were in possession and not the computation algorithm. With the complete viscosity/ creep model used instead, this reason seemed obsolete. However, the use for two additional layers between 70 [km] depth and 420 [km] seemed useful. 420 [km] depth is about the depth of the transition zone between the upper and lower mantle. We know that the upper mantle has a more immediate effect on surface deflections as it is closer to the surface. Because we wish to also model the deflections due to recent ice losses, adding two additional layers will hopefully increase the accuracy of the results. The setting for the number of layers, and the placement of layers is further discussed in Section 4.3.

Physical properties of layers
In the physical properties of the layers, we can distinguish two types of properties: the three dimensional varying ones, and the ones which stay constant per layer. The first refers to the viscosity profile for the 3D Earth models, in the top four layers, and the second is the rest, i.e. the viscosity of the other layers, the viscosity for the 1D Earth models, all of the elastic properties and layer density. Table 2.5 presents the properties of the layers. These were given in the original given spherical Earth model, formulated by Caroline van Calcar and Bas Blank, and are taken from (Spada et al., 2011). We simulate the core by employing an elastic foundation at the boundary between the core and the lower mantle. The stiffness of this foundation is guided by the density and gravity of this core, as performed in Wu (2004). Inside of this shell, there is a liquid inviscid core, as performed in Wu (2004) and Spada et al. (2011).

Table 2.5: Properties of the layers for the standard set up, all taken from Spada et al. (2011), except for the viscosity of the lithosphere, which was given in the original model discussed in Section 2.2. The layer boundaries are the radial distance between the layer upper and lower bound from the centre of the spherical Earth (Spada et al., 2011).

Layer properties			
Layer boundaries [km]	**Density [kg/m^3]**	**Shear modulus [Pa]**	**Viscosity [Pas]**
0 - 3480	10681	1E-20	0
3480 - 5200	4978	2.28E+11	2.00E+21
5200 - 5701	4978	2.28E+11	2.00E+21
5701 - 5951	3871	1.05E+11	1.00E+21
5951 - 6071	3438	7.04E+10	1.00E+21
6071 - 6221	3438	7.04E+10	1.00E+21
6221 - 6301	3438	7.04E+10	1.00E+21
6301 - 6371	3037	5.06E+10	1.00E+44

2.5.2. Coarse layers

As the resolution of deeper layers has a smaller effect on the uplift at the surface, some of them are made coarser. Their number, as well as their coarseness is explored in this section. More on the configurations of layers is presented and explored in Section 4.3.

Number of coarse layers

As shown in Subsection 2.5.1, there are seven layers. We would like to have the separation between the coarse and finer layers. For this, we can thus define the limit between the coarse and fine layers to be at 420 [km] depths. This is an arbitrary choice. This means that the top four layers will have a fine mesh, when the bottom three will have a coarse one.

The choice for the depths of 420 [km] results from two aspects. The first is that, as mentioned, deeper layers' resolution have a smaller influence on the uplifts than shallower layers' resolution. Hence, as it will be seen in this section's results, increasing the number of nodes considerably increases computation times. Considering that final simulations, especially with 3D viscosity profiles, will have large run times with a magnitude in days, we do not feel that it is appropriate to have the same resolution in the upper mantle as in the asthenosphere.

This choice of division between fine and coarse layers could be investigated for this model. However, we do not believe that including more fine layers in the model to be crucial for the deflection accuracy, as proven with the results below.

Coarseness of coarse layers

In the spherical Earth model provided, it is possible to set the ratio by how much the coarse layers are effectively coarser compared to the surface regions.

To determine by how much the 3 bottom coarse layers need to be coarser, as ratio to the top mesh, we should run a visco-elastic response, to determine how much the deflection varies in function of the coarseness of of the coarser layers. The ratio settings are 4, 3, 2 and 1. A ratio setting of 1 means that the target resolution for the coarse and fine layers is the same. However, if the ratio setting is 2 it means that the resolution in the coarse layers is 2 times less than in the fine layers.

For this parametric study, we will, as done in the time ramp short study presented in Appendix G, analyse the statistical properties of the results. We decide, if the deflection results vary by less than 1% from the non-coarse layer simulation, that we keep that setting, given that there is a significant improvement on the run time. For instance, if we find that the 2 times coarser setting have deflections within 1% of the non-coarse setting, we would keep the 2 times coarser settings. We present the results in Table 2.6. The final settings for these results are as follows:

- The number of coarse layers is 3.

- The ice load data is the one from the year 122000 years ago. The full data is used, no values are skipped, hence 52522 ice load values are included in the simulation.
- It is a visco-elastic step, meaning that it contains both an elastic and a viscous response.
- We only propagate for a 1000 years, hence we load the step as a step function, and not a ramp function. We believe that if for a 1000 years propagation the difference is minimal, we extrapolate the difference to also be minimal for longer periods of time.
- The mapping method is done using the 'XYZ' format.
- The hipparchos servers, from TU Delft, are used. This is also true for all other simulations in this thesis.

Table 2.6: Table showcasing the advantages in time and disadvantages in accuracy of using coarse layers, in the bottom layers of the Earth. The results are the percentage difference with respect to the case where the bottom layers have the same resolution as the top layers.

	Deflection statistics for different settings percentage change			
	ratio 1	**ratio 2**	**ratio 3**	**ratio 4**
Min	0	0.07385	0.239895	0.394416
Max	0	-0.01166	-0.0309	-0.06498
Range	0	0.071969	0.23394	0.384313
Median	0	-0.0267	-0.07521	-0.15461
Std	0	0.048208	0.131229	0.250081
Mean	0	0.088929	0.220876	0.405309
	CPU run time percentage difference			
Simulation	0	-77.8303	-83.1539	-84.5802
Total run time	0	-77.7213	-83.0403	-84.471

The difference w.r.t. the finest setting counter part, Table 2.6, presents results from which meaningful conclusions can be made.

Firstly, if the statistics of the deflections are considered, there is no notable difference between the settings, as they are all within 0.5% of each other. The proximity between the standard deviation and the mean allows to draw the conclusion that the data sets between the different settings are relatively similar. The finest setting, when the radial resolution is the same for coarse and fine layers, does not excel in that regard. Secondly, with regards to the CPU run time, the time taken for the coarsest settings is, that is with ratios of 3 or 4 times coarser than finer layers, extremely attractive when compared to the ratio settings of 1 and 2.

The choice can therefore be made to choose the bottom layers, below 420 [km] depths, to have a setting of ratio coarseness which is 3 times coarser than the fine layers. We do not choose 4 times coarser, as we still wish to obtain some higher accuracy so we do not opt for the model which has the highest potential for inaccuracy, especially considering that we only propagated for a 1000 years. Moreover, the advantage in time possessed with the setting of ratio 4 is minimal when compared with the setting of ratio 3.

3

Verification, validation & first hand results

After having developed the base model in the previous chapter, we can here proceed to multiple rounds of verification and validation, prior and after the so called 'first hand' results, which are results from the draft model. At this stage, it is important to engage in such an endeavour, in order to make sure that the parametric studies which we will conduct in the following chapters, use an already partially tested and analysed model.

3.1. Uplift model verification and validation: part 1

Before applying the 3D varying viscosity and making the parametric studies, we can already make a short verification and validation of the model. The verification is done through explaining, in the context of the model and the functions used, the results already presented so far, i.e. to show that the results vary as expected. Furthermore, the validation of the results already obtained cannot be done properly at this point, as the model is not final, so the results cannot be compared to previously made research. However, we can compare the magnitudes of the results, to check if the deflections per year, i.e the down-lift of the Earth, is comparable in magnitudes to values simulated for today's uplift.

3.1.1. Verification of load vs. deflection

First, we can analyse whether the loads correspond to the deflections, both in magnitude, with the analysis of the elastic loads, and in location, by checking that the load's magnitude locations correspond to the location of the according deflections.

Elastics deformation magnitude
When verifying the elastic deformation magnitude, we can refer ourselves to Table F.1, which displays the mean elastic deflection after, a static step of the load data from 122000 years ago of -14 [m], a maximum positive deflection of 419 [m], a minimum deflection of -7840 [m] and a median deflection of 319 [m]. The data set tested in Table F.1 had 2231 points loaded. *Note: -7840 [m] is clearly unrealistic. However, it should taken into account that in this example only 2231 nodes were loaded instead of the maximum about 52000. Hence, the ice mass is much more concentrated at certain points on the globe, and therefore can reach ice heights of multiple kilometres, explaining therefore this large unrealistic deflection. In our final simulations, and from Subsection 3.2.1 onward, all nodes will be loaded, to avoid such unrealistic scenarios.*

To verify these values, we can take the load values used in Table F.2: and check how the number of load elements used has made the elastic deformation change. The verification is as follows: if the elastic deformation has changed as expected then the elastic deformation process is partially verified. We will establish a trend with the results from 18556 load values and 2231 load values, and test it on the elastic deformation when all points are loaded. But what do we expect? Are we able to develop here what is expected from the elastic deformation, when all nodes are loaded? To determine the behaviour of deflections with respect to the number of points, we can simplify this problem in an example. Figure 3.1 already shows this problem simplified to one load point force, where P is the magnitude of the load, a is the distance on the left side of the load to the end of the beam and b is the length of the beam minus a.

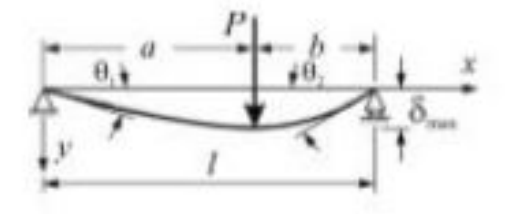

Figure 3.1: Single point load deflecting the point[a].

[a] Link: https://librarycivil.blogspot.com/2016/06/deflection-of-beams.html

Table 3.1: Example: effect of increasing the number of point loads on the deflection

In our model we load a spherical object in 3 dimensions. However, for the purpose of this example we can simplify this problem into a one dimensional beam loaded vertically. The beam is constrained by hinges at both ends. We assume that the loads are loaded as point forces.
Figure 3.1 shows an example of a single load point deflecting the beam[a].
The associated equation for the deflection, Equation 3.1 and Equation 3.1, as a function of the span, x, is:

$$y = \frac{Pbx}{6lEI} \cdot (l^2 - x^2 - b^2) \quad for \quad 0 < x <= a \tag{3.1}$$

$$y = \frac{Pb}{6lEI} \cdot (\frac{l}{b}(x-a)^3 + x(l^2 - b^2) - x^3) \quad for \quad x > b \tag{3.2}$$

E and I are the Young's modulus and moment of inertia.

We can then proceed to make a small algorithmic simulation which investigates how the statistics of the deflection vary with the number of point loads, with the point loads being equidistant apart, when the total force stays the same, just as when the total pressure or ice mass stays the same in the simulation. *Quick structural analysis reminder: in 2 load cases, we can superimpose the load cases to work out the deflections. So if we have two loads, we can make two separate problem cases and then add the deflections along the spans to know the final deflection function.*
Specifications of the load case:

- length of beam: 1 $[m]$
- total sum of forces: 10 $[N]$
- number of point loads: ranging from 1 to 99
- steps of integration: 0.01 $[m]$

From Figure 3.2, one can conclude that the relation is logarithmic. This way we know that we can fit a logarithmic function for our modelling case.

[a]This is the link to the picture and equations, link:https://librarycivil.blogspot.com/2016/06/deflection-of-beams.html.

The following figure, Figure 3.2, is the results from the example analysis presented in Equation 3.1.

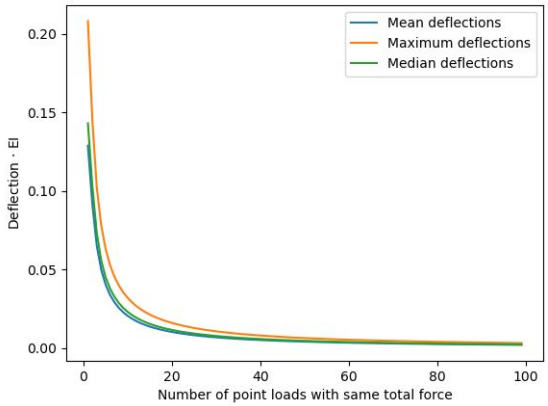

Figure 3.2: Deflection statistics as the number of loading points increases. On the y axis: the product of deflection, E modulus and moment of inertia.

The important aspect to note from Equation 3.1 and Figure 3.2, is that in the example the exponential curve tends to 0. However, in our model, the maximum amount of load points available is the maximum number of mesh, as there cannot be less than that pressure/mass due to the ice on that element. This means that there is an asymptopte at the convergent point for the deflection where all mesh are loaded. This function is thus impossible to forecast. However, we can try and predict the statistics for a number of loading points between 2231 and 18556: 11763. Table 3.2 presents the verification results. If the prediction/estimation in deflection statistics, found with a logarithmic fit matches to a degree the statistics from the simulated data, then we can

claim to a partial verification of the elastic loads.

Table 3.2: Estimated versus actual deflection when having 11763 points loaded.

	Estimation	Actual
Mean	-4.54229848	-4.60603
Median	131.0891966	143.7229
Min	-2463.545665	-2588.78
Max	100.0715556	109.3783

We see from Table 3.2 that the approximated values, using a logarithmic equation, fit the simulated values to a certain degree. The conclusion we can make is that, because we could predict to an extent our model behaviour when loading more points during elastic deformation, on the assumption that we do not extrapolate points too far from the ones used for the trend during the estimation, that our elastic deflections are partially verified.

Geographical location of loads In the previous subsection we demonstrate that the magnitudes of the elastic deflections are verified because the loads match the change in magnitudes. From those calculations, we therefore know that the loads are geographically placed where they should be, as the increase in magnitude directly affected the deflection accordingly. Thus, the location of the loads is verified.

3.1.2. Verification of characteristics of results

The first round of verification, with respect to certain characteristics of the results, can be done through the verification of the impact of the time ramp on the results.

In using the time ramps, in Appendix G, we noticed that the deflections were generally increasing in magnitude. This is because the ice masses are increased throughout the time step. Both viscous and elastic deflections depend on the load case, although elastic even more than viscous in the short time frame.

As a verification, we can multiply the minimum deflection when there is no ramp, taken from Appendix G, -1153.73 [m] by the ratio of loads at the end of the two ramp settings, 1.08415. If the ramps were applied correctly, this ratio in loads should roughly translate to the ratio in deflection.

We use for this quick verification the maximum absolute deflection, as we believe it to have the most predictable deflection behaviour. With this procedure, for our model to be verified, we should then get within close range of the end deflections for the linear and complex ramps, when multiplying -1153.73 [m] by 1.08415. Refer to Appendix G, for a reference on these values' origin. *Note: As explain in Appendix G, the difference between the linear and and the complex ramp is as follows. As the name suggests the linear ramp assumes that the ice load changes linearly with the same gradient through out the whole time step, whereas the complex time ramp assumes multiple linear ramps within one time step.*

Through the above mentioned procedure we obtain that the approximated end minimum deflection for both ramp settings is -1250.817 [m]. This is a -1.36% difference with the linear ramp, and a 2% error with the complex ramp minimum deflection. This is deemed acceptable and thus verifies our ramp integration into the model. Furthermore, it makes sense that the error is larger for the complex ramp, as it undergoes larger changes in ice loads than the linear ramp. Refer to Figure G.6.

The small difference can be attributed to fact that viscous behaviour cannot exactly be translated as we just did, and that the complex ramp changes multiple times ratios throughout the time step. *Note: as mentioned in other chapters, viscous behaviour takes time to act, and therefore the times for the loads to act on the deflection differ. Hence, as the loads are different in the different ramp scenarios, this viscous deflection is not everywhere the same, and thus induces an slight difference with the estimation.*

3.1.3. Validation through magnitudes

As suggested by the title of this validation, we are performing a partial validation through the analysis of the magnitudes of the deflection rates. For this, we are propagating it from 122000 years ago to 98000 years ago and from 98000 years ago to 80000 years ago. Table 3.3 shows the results. The aim here is to spot any

outliers, or clear mistake.

Table 3.3: Results of the deflection results which take place, with the complex ramp, between 122000 and 98000 years ago, as well as between 98000 to 80000 years ago.

	Deflections [m]	
	122k to 98k years ago	98k to 80k years ago
Min	-1255.567383	-260.78284
Max	87.60253143	278.848572
Range	1343.169914	539.631408
Median	12.55819035	-0.8800182
Std	117.2091348	37.7011108
Mean	-2.893692887	-6.6660361

In Table 3.3 the deflection rate of the minimum deflection is about -41 [mm/yr], if we exclude the elastic deformations, while the mean deflection rate can be found with the same procedure to be -0.098 [mm/yr]. The mean deflection rate, is clearly within reasonable bounds: measured GPS viscous uplift rates in Greenland today range from 3 to 22 [mm/yr] (Khan et al., 2016). The -41 [mm/yr] can be stipulated to be mostly due to the fact that the Earth did not have any ice load before we started the time step from 122000 years ago to 98000 years ago.

Again, excluding the elastic deformations, we find that the viscous deformation rate of the minimum deflection between 98000 and 80000 years ago is about -14.4 [mm/yr] and 15 [mm/yr] for the maximum. We now know that these values are within realistic limits (Khan et al., 2016). Hence, our model is now partially validated.

3.1.4. Errors spotted & future change(s)

After this first take at validation and verification, one error was found and a change in further simulations can be addressed.

An error was found in the interpolation algorithm. The elements in the Greenland 'tight' region were loaded twice. Hence the number of points of 52522. This is of course a mistake. The real number of points should be 45288. However, this error does not change the findings in the parametric study this far, as the ice mass in the Greenland 'tight' region only represents 0.3% of the Earth's total ice mass 122000 years ago. As this was the ice data mostly used for the parametric studies, we consider that this error had negligible effects.

Furthermore, for future chapters the resolution of the finer layers will be of 70 [km] in the radial direction, when it was until now 300 [km].

3.2. Non finalised model: first hand results, verification & validation part 2

With all the studies done previously, we have established a model which we run from 122000 years ago to now, 2019. We first present a set of results and comment on their validity, while also verifying them.

3.2.1. Results

In presenting results this far, we should present the uplift rates for Greenland, particularly the so called finer region, as this is the focus of this thesis. We should first present how over time, since the start of simulation, 122000 years ago, the deflection rates have varied, and then as well present a map of deflection rates since 1972 until today of this region. Figure 3.3 shows the uplift rates for this region.

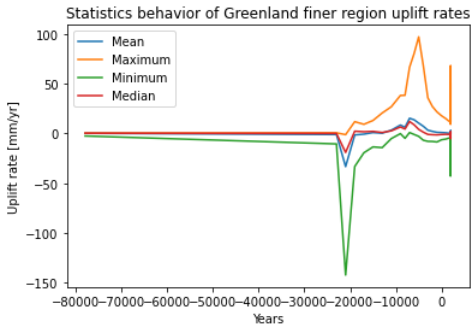

Figure 3.3: Uplift rates of the Greenland finer region, from 122000 years ago till 2019. Clarification: the graph starts at about 80000 years ago, as this is the rate graph.

We notice in Figure 3.3 that there is a minimum deflection rate at around 23000 years ago, and a maximum at around 5000 years ago. If we refer to Figure G.6, we see that these years are the ones of inflexion in the de-glaciation period: these years are the start and end of the 'semi-linear' trend of de-glaciation phase of the last ice age. Because these uplifts are directly linked to the ice loads applied, it makes sense that the maximum negative uplift is close to the maximum increase in ice mass, and the maximum positive uplift, is when the extent most of the ice has already melted. There is a slight offset between maximum/minimum ice mass and minimum/maximum uplift, due to the fact that viscous deformation takes a few hundred years, or even a few thousand years, to fully take effect. Figure 3.4 shows the mean uplift rate from 2009 to 2015.

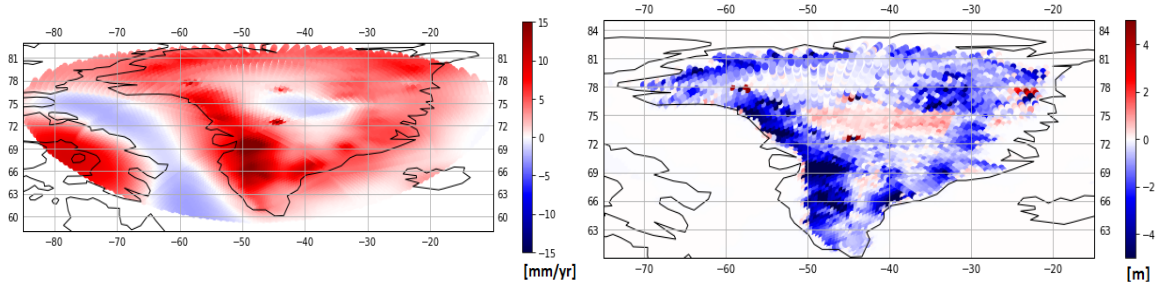

Figure 3.4: Simulated Greenland uplift rates [mm/yr] from 2009 to 2015 in the 'tight' region (left) and change in ice height in Greenland during that time period (right).

Figure 3.4's left map displays the described uplift rate from 2009 to 2015, as this is a common time range for all GPS station's measurements as described later on. We notice that the uplift in the Northern region, especially the North-East and North-West, as well as midway down the Eastern Coast, and mid way up the Western coast, have particularly high uplift rates, about 5 to 6 [mm/yr], in comparison with the rest of Greenland, which has uplift rates ranging from -5 to 2.5 [mm/yr]. It is logical that the coastal areas have a higher value for uplift rates, as these are the regions losing the most ice, due to their proximity with the sea. This is clearly seen in Figure 3.4's right graph, where deflection rate regions have a slight inverse correlation with the changes of ice regions. Hence, this is where the response to this loss of ice is highest, as also seen in Simpson et al. (2011) or Khan et al. (2016).*Note: that viscosity is not discussed as a variable, as it is constant through out the different Earth's regions. Therefore it can not be used to explain the disparities in rates. However, this will come as an argument once a detailed viscosity is included.*

3.2.2. Verification and validation part 2

This section is a continuation of Section 3.1. We want here to validate and verify the model results from Subsection 3.2.1. We do so by first verifying the original given model, then validate the results and then verify them by trying to replicate results from Khan et al. (2016).

Verification of the original model

First, in order to make sure that the model which was given is verified, we should run it, and make sure that the loads and deflections are corresponding, i.e. the relative loads and deflections are located in the same

geographical locations, and that the trend in the load is the same as the trend in the deflection. We should expect this process as we know that the elastic and viscous deformation both depend directly on the load established. The original model is ran for 1000 years, has a resolution of 200 [km] outside of the fine region, has a resolution of 30 [km] inside the fine region, and has a fine region of radius of 28 [°]. Figure 3.5 shows respectively the elastic deformation and viscous deformation due to the ice loads in the same figure.

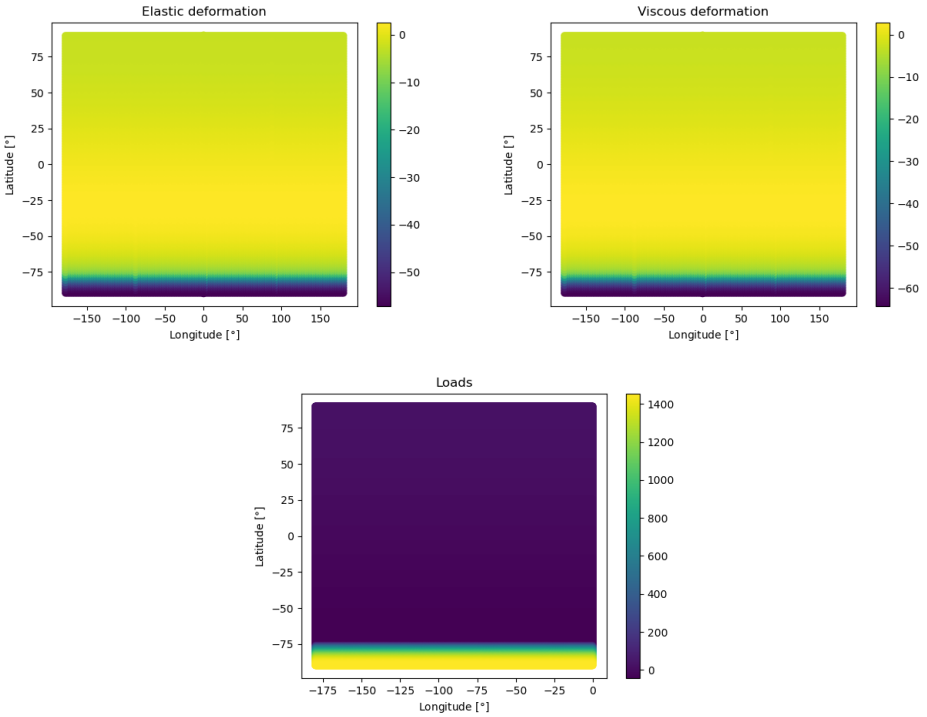

Figure 3.5: Elastic deformation [m] (top left), and viscous deformation [m] (top right), due to the loads in the third graph (bottom), which are displayed according to ice heights [m]. This viscous deformation also incorporates the elastic deformation, so it is actually a visco-elastic response. The visco-elastic response spans 1000 years.

We can see that the deflections in Figure 3.5 are direct mirrors of the loads in the same figure. This is already a first step of verification, as we then know that the model's trend behaves as expected: the positive loads induce negative deflections. Moreover, places where there is no load, have a very small deflection in the positive direction.

Furthermore, as we see that the load and deflection only really varies in the latitudes, we can plot both the pure deflection and loads versus the latitudes to compare their trends, as done in Figure 3.6. If their trends are matching and can be explained then the original given model is considered verified.

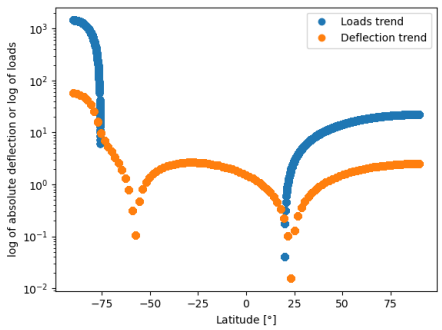

Figure 3.6: Load trend versus the absolute deflection trend. They are both in log scale base 10.

In Figure 3.6, the absolute deflection is taken the log of, so the reader should note that deflection where loads

are present should be negative. Moreover, we can note a perfect match of the trends in the area of loading. Furthermore, when no loads are present, we still see an upward deflection. To explain this we can use the comparison with a simply loaded beam, constrained around the region where no loads are present, which would still see a deflection although it is only loaded at its ends. With this present analysis, we consider the original given model verified.

Verification of interpolation scheme

Through testing the interpolation scheme, we have found two prominent mistakes. Firstly, that the nodes which were interpolated on, i.e. the new grid, were too few: we thus have now 57958 nodes, instead of the previous 45288.

Secondly, the other mistake which was found was that from 1972 onward, the loads were changed at the incorrect indices. Thus, the loads of Greenland were effectively not changed from 1972 onward. This lead our model to effectively see no elastic deformations from 1972, as we know that ice mass changes since 1972 mostly cause elastic changes and not viscous changes (Simpson et al., 2011).

These two mistakes have now been fixed.

Validation of total uplift

From Khan et al. (2016), we know that the measured uplift by the GNET network of GPS stations is of 8.69 $[mm/yr]$, from about 2007/2009 to 2015, with a maximum of 23.8 $[mm/yr]$ and a minimum of 3.1 $[mm/yr]$. When interpolating our uplift values to find the uplift at a similar time interval in the GPS coordinates - as mentioned later, not all GPS stations span exactly 2007 to 2015, there are small variations in the years spanned - we find an average uplift between 5.39 and 5.42 $[mm/yr]$, a maximum uplift at 18.40 $[mm/yr]$ and a minimum uplift at 1.84 $[mm/yr]$.

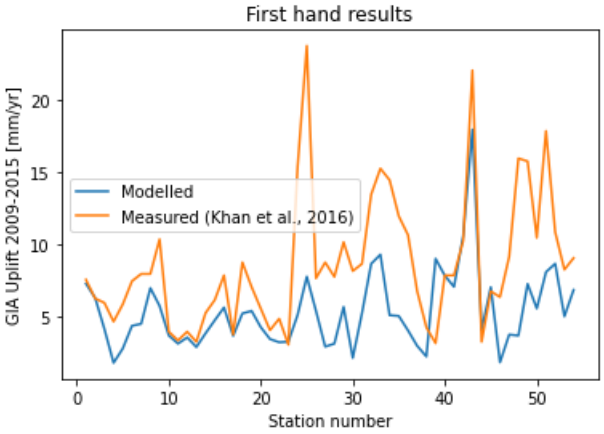

Figure 3.7: Mean uplift rate between the years 2009 to 2015, from the results in Subsection 3.2.1, at the GNET stations from (Khan et al., 2016). The mean error is situated between 3.46 and 3.51 $[mm/yr]$. For this graph and the similar graphs which will follow through out this Master Thesis, the station number refers to the GPS index indicated in the table in Appendix A.

Above, in Figure 3.7, it can be seen that the shape of the trend of the interpolated GPS uplifts, corresponds nearly exactly to the one of the measured uplifts. The Figure 3.7 shows an average error between 3.46 and 3.51 $[mm/yr]$. At some points the error, is within a 5% margin, namely at GPS stations 1, 2, 17, 40, 42 and 45: corresponding to GNSS stations BLAS, LEFN, YMER, SENU, QAQ1 and QEQE. It is worth noting that in the highest uplift region as given by the model, the uplift per year is extremely similar to the measured one.
However, in Figure 3.7, we can still notice disparities, which seem to be constant at nearly all points, except for station number 25, called KUAQ (Khan et al., 2016). The constant offsets could be due to multiple factors, namely:

- The interpolation performed to get the uplift at GPS station points is performed for a single point, when we model GIA on a grid with resolution 25 by 25 $[km]$, i.e. the resolution in the simulation is coarser than the GPS resolution, and the GIA signal is thus smoothed out b. This is likely, but might not actually highly affect the results, as for some points this interpolation yields credible results. Hence, we believe

that because the GIA signal is smoothed out, both the viscous and especially the elastic response, could be constantly under estimated at those GPS stations which see an underestimation of the uplift rate.
- The elastic characteristics of the model are not accurately portrayed, namely the lithosphere and upper mantle elastic properties, as shallower layers usually have a higher effect on the elastic deflections than the deeper layers, although *all* have an effect. This is supported by the fact that later, in item 3.2.2, the viscous response does not follow the same trend in under or over estimation as the trend in Figure 3.7. This could become one of the leading issues and will be further discussed in the final conclusions of this Master Thesis.
- The viscosity profile beneath Greenland has deep inaccuracies. This is one of the most plausible options, one which will be investigated in the next chapters relating to the parametric studies. The viscosity across Greenland varies, but does not in the current model. Thus we expect that in regions where viscosity is the most similar to the constant used one, we get better approximations.
- The layering of the mesh beneath Greenland, is not accurate. We will also investigate if changing the radial resolution in the upper mantle and lithosphere changes the results, and if yes, if the estimations are then more accurate.

Concerning the station KUAQ, where the offset is the largest, it is believed now that the error could be due to the three following scenarios:

1. The viscosity is significantly inaccurate.
2. The load is vastly underestimated at a certain epoch, or is underestimated because of the lack of resolution or satellite measurement errors.
3. The load change is not well portrayed by the current time scale.

Lastly, these results will be further improved, in the next chapters, thanks to the tests presented in Section 4.1.

Verification of total and viscous uplift: 2014

In this section, we aim to verify our model further than done previously. We therefore try to replicate the results from Huy3 (Lecavalier et al., 2014). We use this paper because the ice history is the same, although we slightly change it through interpolation. In this paper, the uplift rate at the year 2014 is presented. We therefore adapt our model to fit the Earth structure of the original paper, and try to replicate the uplift rate in 2014. The uplift rate in 2014 is presented in Figure 3.8.

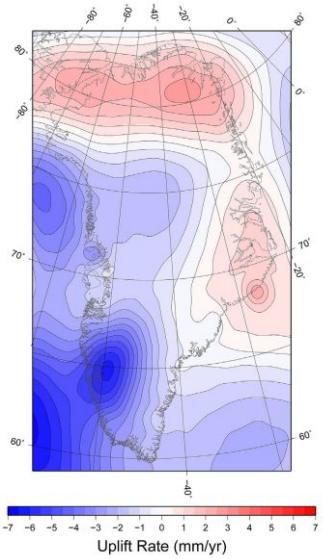

Figure 3.8: Graph taken from the Huy3 paper (Lecavalier et al., 2014), which displays the uplift rate in 2014 due to the viscous response from the ice loads.

The following changes were made to our model from Subsection 3.2.1. In order to obtain a comparable graph to Figure 3.8, presented in Figure 3.9.

- The lithosphere thickness was increased from 70 to 120 [km].
- The viscosity from 120 to 671 [km] depth was changed from 1e21 [Pas] to 5e20 [Pas].

- In order to simulate viscous uplift nowadays from the Huy3 ice history, the ice loads were not changed since 1972 until 2019. See Section 2.2, for more information on ice models.

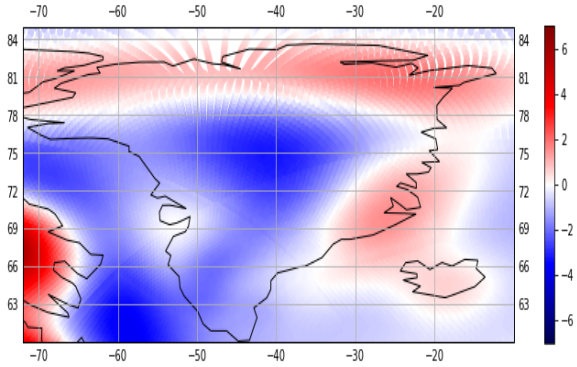

Figure 3.9: Replicating the graph in Figure 3.8, by inputting the same Earth parameters such as viscosity profile in order to verify our model. The uplift rate is in [mm/yr].

By comparing both graphs, the one from the Huy3 paper, and the one we created here to verify our model, we can point major similarities. The first is that the regions of uplift and down-lift are the same. The North and East have uplifts while the sea West of Greenland, and the central and central West parts of Greenland see down-lift. Moreover, the magnitudes of uplift and down-lift seem, generally speaking, to be the same: the down-lift magnitude is larger than the uplift magnitude. The only difference between the two is the fact that the large down-lift rate region in the South-West of Greenland in Figure 3.8, has a larger magnitude than in Figure 3.9. A suggestion for this disparity maybe be that in this model this far, we load full ice thicknesses and not ice height relative to the ice height 122000 years ago, as done from the end of Chapter 4 onward. Hence, because ice thicknesses are large in the South-West region, the uplift effect due to ice changes is not as explicit, as proportionally less ice is lost or gained. However, this difference is considered minor given that all other areas of Greenland display similar uplift rates in both graph. Hence, we consider our model to be verified.

4

Further parametric studies

This chapter is a continuation of Subsection 2.5.1, Section F.1, and Appendix G, in the sense that it follows a similar approach to those chapters in order to improve the model. Hence, as the title of the chapter suggests, this chapter contains multiple parametric studies, which all have as a goal to improve accuracy and precision of the deflections while limiting the increase in computation time. The base model on which we will conduct the studies is the one which produced the results in Subsection 3.2.1.

Depending on the type of parametric study, different methods of quantifying the differences between the set ups are used. Firstly, if we are faced with a parametric study which simulates uplift in the 'long term' ice history period, that is either from 10000 years ago till now or till 1000 years ago depending on the study, then we present the statistics: mean, maximum (max), minimum (min), and standard deviation (std), of the deflection between 10000 years ago and the deflection at the end of the simulation. We perform this analysis by using these statistical tools, in order to spot the general differences between data sets obtained by running different sets of settings. This allows us to make quick conclusions on the sensitivity of the settings. If used in a graph or table with an accompanying description, the term 'std' maybe also refer to the 'standard'/draft model from Subsection 3.2.1. We also present a graph of the mean deflection across this time span. This allows us to have a global view of the deflections, but is severely limiting by the fact that it is only one curve describing an entire region of the globe.

Secondly, for parametric studies which only simulate the deflection from 1972 onward, we only compare the deflections' statistics which were created during the entire simulation from 1972 to 2019.

Lastly, for parametric studies which have 'entire' simulation runs, that is running the simulation from 122000 years before present till 2019, we also present the uplift since 1992 at four relevant GPS stations in Greenland: ILUL, DKSG, JGBL and KUAQ. The first three stations were chosen because they all have different magnitudes of uplift rates, low, medium and high, which correspond to less than 10 [mm/yr], more than 10 [mm/yr], and more than 15 [mm/yr] (Khan et al., 2016). KUAQ was chosen because of its high uplift rate, higher than 15 [mm/yr], in a region of low ice mass loss. These four GNSS stations are situated in different locations of Greenland, with DKSG having the particularity of being in a region of high ice melting today and in the past centuries. More information on the uplift rates of the stations can be found in Appendix A. Lastly, we may also compare deflection and deflection rates using map projections. This allows us to have a quick insight into the effect of changing specific settings.

For calculations, statistics and map projections, we only use the finer region so not the entire globe. This is because we also consider areas surrounding Greenland to be important when modelling it's deflections. Only in the uplift rate colour maps, is the 'tight' region shown, as this is the region of interest when visualising uplifts.

This chapter will include parametric studies on: lithosphere geometry, radial seed resolution, tangent to the surface resolution, timeline, quality of the interpolated ice loads, and a time ramp sensitivity analysis resulting from the time ramp section in Appendix G, while Chapter 6 will focus on the implementation of a 3D varying viscosity profile. These parametric studies are explained in the first section of this chapter.

4.1. Plan for in-depth parametric studies

In formulating these parametric studies, we wished to pick ones which, aside from the simulation time, would not require excessive time of work, and which would have a high certainty of small influence on the results. In doing so, and with only two and a half/ three months to complete the thesis, five to six parametric studies were formulated.

The primary concern with the results shown in Subsection 3.2.1, is that the degree of variation of the uplift, in function of the region, is not as high as in comparable research, i.e the graphs do not show clearly higher uplifts in the known regions, such as the KUAQ glaciers (Khan et al., 2016), compared to other areas. This could be due to multiple factors such as: resolution in space, both linked to the resolution of the mesh in 3 dimensions,

resolution of the ice loads, resolution in time and the resolution in viscosity. Knowing this, we can formulate the required studies, with a motivation for each.

1. *Investigation of the thickness of the lithosphere: does dividing it into 1, 2 or 3 sections change considerably the results?* This would enable us to find out what the impact of splitting the lithosphere in the last 40/50 years is. Why 40/50 years: because the lithosphere is responsible for the elastic deformation, and as there is nearly only elastic deformation in the last 40/50 years (the viscous response is nearly only due to the last glacial cycle and not to recent ice melts), we want the most accurate results.
2. *Investigating the variation of the seed size in the radial direction.* This study would be to check if the actual 70 [km] seed size is sufficient, or if a finer one is needed. If a finer one is used, it would also come down to splitting the lithosphere. However, this test would then also test the seed size for more layers.
3. *Investigating the variation of the tangent to surface resolution.* As one, from this research, might still aim to compare simulated gravity gradient to real life measurements by GRACE, which have a 300 [km] resolution, we will only test one finer resolution than 25 [km]: a 10 [km] resolution. This is because a resolution of 25 [km] is already high enough if we are to find long-wavelength gravity signals of 300 [km] wide. Moreover, we will also investigate coarser ones, in order to check if we can potentially decrease the run time of the model, while still getting similar deflections.
4. *Investigating time steps between 25000 years ago (the global glacial maximum) and now.* Instead of just proposing alternative time steps, we could try and design a time step with regards to viscosity. The method would enable us to to find the area of Greenland with the lowest viscosity, as the lowest viscosity will have the largest displacement since the de-glaciation. We would then analyse the ice history of that Greenland's region, by setting time steps at inflection points of the ice history, given that the ice masses change at this point in Greenland. To this investigation we would also add resolution, time -wise, studies where we increase and decrease the number of time steps taken at each point throughout the last 25000 years, in order to more accurately portray the associated deformations.
5. *Investigating the effect on the deflections when the quality of the interpolated ice height values changes.* The quality of the interpolated ice loads varies when less or more of the original data is ignored. As discussed earlier in this Master Thesis, ice loads from the original data may be skipped to decrease computation time. Investigating the effect of ignoring such data is in this study carried out.
6. *Investigating the effect of the inclusion of the ramp on the end results.* This test is to investigate whether the ramp has or has not, a significant effect on the results. This test will also be accompanied by a test on whether loading full ice thicknesses or the ice height difference w.r.t. the ice height 122000 years ago, has a significant impact on the uplift results. Partial ice heights would be loaded in order to put in practice the assumption that the Earth was in isostatic equilibrium 122000 years ago. Please refer to Section 4.8, in order to find a detailed justification why loading the ice height difference w.r.t. the ice height 122000 years ago is a more accurate option than loading full ice heights.

All the parametric studies shown here will not necessarily be performed in chronological order, and will not use results from the others listed here. They will all use the settings, set for generating the first hand results displayed in Subsection 3.2.1, aside from the time ramp parametric study which will use ice height differences w.r.t the ice heights 122000 years ago. This is further explained in the last section of this chapter.

4.2. Dividing the lithosphere into layers

The first parametric test decided upon, as pointed out in Section 4.1, is to divide the lithosphere in multiple layers in order to see how much the end results change. Ideally, the lithosphere is divided in as many layers as possible. However, we need to limit them for computational space and time reasons. Thus, the main objective with this study is to see whether the results converge, meaning they do not vary significantly when the setting is changed, or not.

The study is conducted from 1972 to 2019, with ice loads only from 1972 onward. We wish to get the best approximation of the elastic and viscous deformations, as the lithosphere thickness, is an important contributor to these deformations. Hence, properly modelling the lithosphere is key for this Master Thesis. Furthermore, we limit the study in the timeline from 1972 onward as elastic deformations due to recent ice mass changes are dominant over the viscous deformations due to recent ice changes (Simpson et al., 2011), and also because we wish the best accuracy for modern changes. However, we will simulate this test using the visco-elastic function, as this is what we will use in the final simulations.

This limitation in time thus means that the model will be undeformed before the year 1972. Hence, we

expect that the deflections will be mostly negative, as the model is not loaded before this parametric study starts. This does not matter, as the point of this study is to show the sensitivity of the model to the changes in radial spatial resolution in the lithosphere, given the same recent ice loads.

We can prove this last point by showcasing that there is still an elastic uplift, which is directly related to the load removed. We do this by assuming that the deflection rate of the viscous behaviour is constant over this small time frame, and we thus compare a 'proto' elastic behaviour. This 'proto' elastic behaviour is obtained by subtracting the deflection rate between 1982 and 1992, from the deflection rates after 1992, assuming that there is a strong and dominating viscous effect between 1982 and 1992. This way we are left with an estimated elastic deformation from 1992 onward, hence the use of the word 'proto'.

Note: In this section and chapter, we will often refer to the term 'imposed' 1, 2 or 3 layers. What is meant is the minimum imposed number of mesh in a defined geological layer. We know for instance that if we imposed 1 layer of 70 [km] of the lithosphere, with a target seed size of 70 [km], there are two levels of meshes in the lithosphere. We thus state that if we imposed 2 layers, there are between 2 and 4 layers of meshes, and if we impose 3 layers, there are between 3 and 6 layers of meshes.

4.2.1. Results - dividing the lithosphere into layers

We can first present the three deflection maps. What was done here, as mentioned above, was to subtract the deflection rate between 1982 and 1992, from the rate of deflection between 1982 and 2019. This was done, because the deflection is assumed through out the whole runs to be dominated by a strong negative viscous response, as the model is only loaded from 1972 onward. The viscous rate from 1972 to 1982 is not usable as it is inseparable from the strong elastic response created by loading a model which was not loaded before hand. We know it is dominated by a negative viscous response because the mean deflection goes from -4.36 [m] to -4.59 [m] from 1982 to 2019, while if the elastic upward was dominant the mean deflection would increase as large amounts of ice are lost over this period. Because the deflection between 1972 and 1982 is mostly elastic, we chose the deflection rate between 1982 and 1992, and subtracted it from the deflection between 1982 and 2019. This procedure is supported by findings in Appendix H.

This way, it allows us to display only the deformations between 1982 and 2019 which are assumed to be due to the change in loads in that time frame, i.e. primarily the elastic deformations upward. The associated deflection maps are presented in Figure 4.1. This is a good method of evaluating the sensitivity of the lithosphere settings to modern day uplift rates, if we do not load the model prior to 1972.

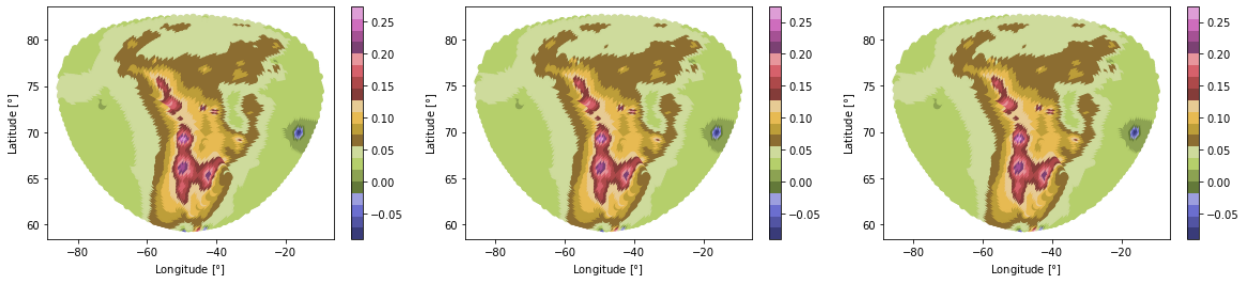

Figure 4.1: Estimated deflections between 1982 and 2019 [m] due to recent ice changes, on a latitude longitude map, for all three model lithosphere settings. We do not show from 1972 onward because the elastic deflection is too large between 1972 and 1982 due to the model being not loaded prior to 1972, and has little use in the analysis, i.e. the change in ice mass through out the years can better be approximated.

From Figure 4.1, we can see that that the deflection pattern, due to recent ice changes, is the same for all three settings. Moreover, the magnitude of deflections are also the same. Hence, we can already make a preliminary conclusion that the division of the lithosphere in more parts, in our model, does not significantly change the results. The method to obtain these graphs can be verified from that fact that largest uplifts are in areas of high ice mass loss, as shown in Appendix H. Moreover, it is interesting to note, for later conclusions, that the 'proto' elastic deformation is quite weak, reaching only a maximum of about 6 [mm/yr] in the South of Greenland. This number is to take with precaution, as it is an estimation and does not directly result from a simulation.

We can now present the statistics comparison between the different parametric settings, as done in Table 4.1. We here compare the full deflections between 1972 and 2019, in order to give another perspective on how the division of the lithosphere can impact deflections, both elastic and viscous.

Table 4.1: Percentage differences between the imposed lithosphere split options.

	End deflection		**Mean rate over years**	
	L1 to L2	**L2 to L3**	**L1 to L2**	**L2 to L3**
Mean	-0.93288	0.034457	-0.6937	0.02219006
Min	0.018036	0.003298	0.01215	0.00192202
Max	0.006276	-0.01929	0.00581	-0.0202683
Range	0.016895	0.001106	0.01164	0.00011859
Median	0.725827	-0.02311	1.11327	-0.0491185
	Run time			
	L1 to L2	**L2 to L3**		
mean magnitude	28.57143	44.44444		

On a first look, we can clearly see that forcing the lithosphere into multiple layers, has a large effect on the run time magnitude, changing it from 29% to 44%. This is because the lithosphere is the first layer to deflect when ice is loaded, so the number of elements there greatly impacts the computation time. However, the variation in final deflections is close to negligible.

From Table 4.1, we can also see that the statistics of the lithosphere imposed layering of 2 layers are extremely close to the imposed 3 layer configuration's, while having a run time which is significantly smaller. However, the imposed 1 layer configuration presents slightly different results. The reader here should keep in mind that from the next chapters and sections to come, the run time significantly increases with the 3D viscosity and the finer mesh resolution of 10 by 10 [km]. So improving the result by less than 1%, while increasing the run time by 30% can not be considered a viable option. These changes in percentages, as presented in Table 4.1, roughly equate to changes in final deflection statistics between 1 [mm] to 1 [cm]. For instance, the maximum deflection varies by 1 [mm] between all three settings, which equates approximately to 0.027 [mm/yr] difference in uplift rate. This is well below the error margins of GIA studies, as seen in Simpson et al. (2011) or Khan et al. (2016) for instance. Lastly, considering the estimated elastic deflections from Figure 4.1 and the difference in run times, we can safely state that the imposed one layer configuration is the most viable option.

4.3. Varying the radial resolution configurations

As part of the investigation into the geometry of the FEM model, we should investigate whether the radial size of the mesh, is appropriate for the model or not. With this logic, we can set up a parametric study with 3 new configurations of mesh layers until 420 [km] depth.

Important to note for the reader is that if the target resolution is for instance 100 [km], this resolution will rarely be observed. This fact is a recommendation to Abaqus users. The terms 'organised' and 'unorganised' refer to whether the target resolution fits a full number of times within the imposed layers.

4.3.1. Set up

The set up consists of 4 configuration's, with C4 being the original one used in Subsection 3.2.1. As Abaqus's arrangement of centroïd is not predictable, multiple configurations of radial seed and imposed layering were investigated, in order to find four distinct configurations.

- C1 - Unorganised with 100 [km] target resolution, with 2 initial imposed layers: effectively 7 layers above 5951 [km]
- C2 - Organised with 70 [km] target resolution, with 2 initial imposed layers: effectively 8 layers above 5951 [km]

- C3 - Organised with 70 [km] target resolution, with 4 initial imposed layers: effectively 9 layers above 5951 [km]
- C4 - Unorganised with 70 [km] target resolution, with 4 initial imposed layers: effectively 8 layers above 5951[km] (Original results, i.e. the draft model as it is sometimes called)

First, three different configurations were chosen, based on the number of layers they incorporated, as shown in Table 4.2. Furthermore, a fourth configuration was added, C2, which had the same number of layers as C4, but in a different arrangement. This was chosen to test how the arrangement of layers impacted the end results.

Table 4.2: Ranking of the radial seed configurations in function of the number of layers present in the configuration.

	ranking	
finest	C3	**9 layers**
	C2, C4	**8 layers**
coarsest	C1	**7 layers**

Below, in Figure 4.2, the configurations C1, C2, C3 and C4 are presented respectively. Through these configurations, we can see the different types of layering since the depth of 420 [km]. These variations will later on be translated into the deflection results.

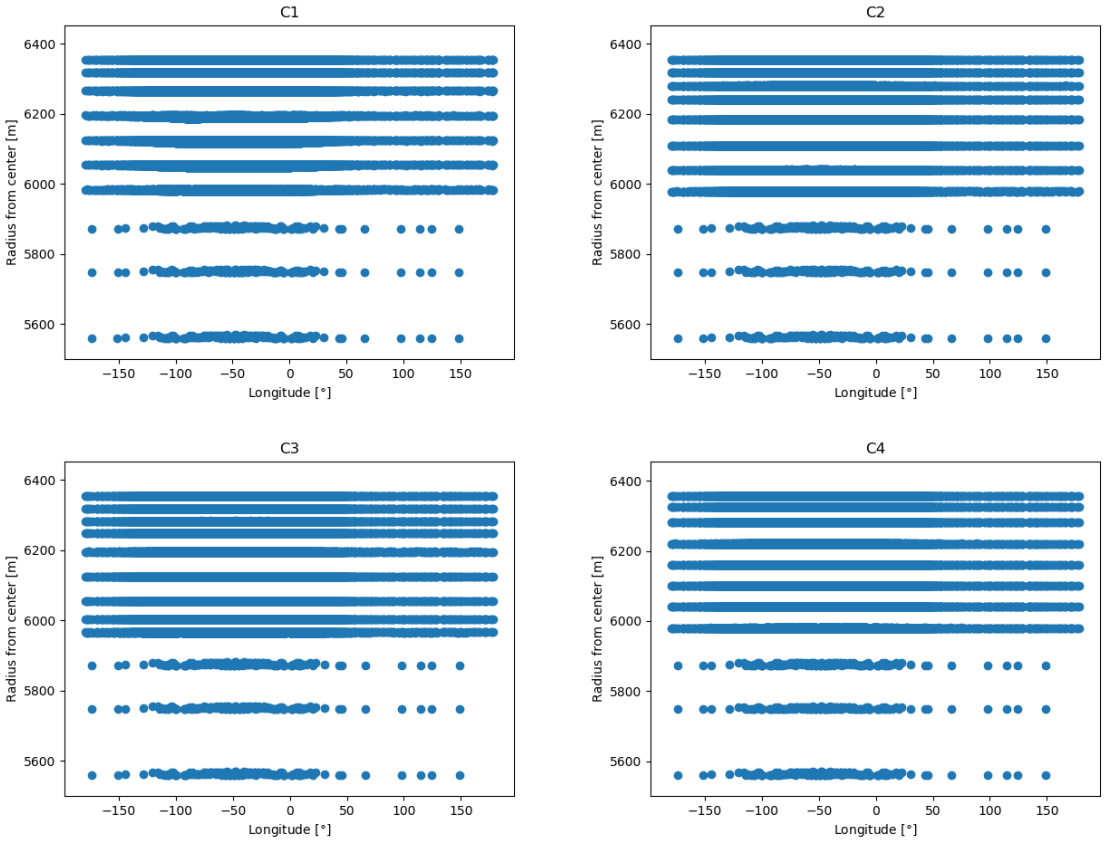

Figure 4.2: Configuration C1 (top left), C2 (top right), C3 (bottom left) and C4 (bottom right) respectively from centre to depth of the centroid of the elements over the finer region.

The position of the element centroïds presented in the graphs above, are illustrated in Table 4.3. In this table, one can clearly see the numbers of layers, and their different configurations, as well as the differences between the configurations C2 and C4.

Table 4.3: These are the values of the layer centroïds, +/- 2 [km] (as these were visually analysed), radial position with respect to the centre of the sphere before the simulation is started. These represent the layers portrayed in Figure 4.2.

	Radial distance from the model's Earth centre			
	C1	**C2**	**C3**	**C4**
Layer 1	6355	6355	6355	6355
Layer 2	6319	6324	6319	6319
Layer 3	6247	6281	6283	6281
Layer 4	6193	6221	6248	6241
Layer 5	6122	6161	6196	6181
Layer 6	6053	6100	6125	6108
Layer 7	5984	6040	6057	6040
Layer 8		5980	6004	5980
Layer 9			5968	

4.3.2. Results - varying the radial resolution configurations

We should now synthesise the results, in order to present an overview of the differences between the different set ups, as done in Table 4.4. As mentioned previously the set up C3 is the finest. We thus assume that its results are the most reliable.

Table 4.4: Final deflections with respect to the deflection 10000 years ago for all configurations.

	Deflection statistics [m]			
	C1	**C2**	**C3**	**C4**
Mean	55.52636	55.52636	54.94329	54.94367
Min	-32.0744	-32.0744	-32.1001	-32.1536
Max	327.5212	327.5212	328.6773	328.6733
Std	93.18258	93.18258	92.65652	92.65471

From Table 4.4, it can be seen that the final deflection, is actually little impacted by the seed configuration we have. What creates the largest difference in the mean and maximum deflection, seems to be at which point 'layer 2' is placed. See Table 4.3 and Table 4.2 for illustration of the placement of this layer. The largest difference between C4 and C2 is that layer 2 in C2 is at radius from the Earth's centre of 6324 [km] where C4 is at 6319 [km]. However, this large difference is not noticeable when C2 is compared to the other configurations.

The similarity between C1 and C2 results comes from the fact that they both do not have imposed layers at 150 and 300 [km] depths. The exact reason why this matters is unknown, but it can be stipulated that this imposed layering, by the geological values that it specifies, affects in a certain way the deflection behaviour. The C4 results are most similar to the C3 results, with less than 0.05% difference, while having a run time which is significantly smaller.

The behaviour of the mean deflection for all configurations is the same and overlaps for the past 10000 years of deflections. Thus, this hints at the fact that all these configurations are close to the convergence point: adding more layers or re-arranging them would not significantly change the overall deflection results for the past 10000 years.

Lastly, as stipulated at the start of this chapter, we present the results of the uplift since 1992, through the prism of four GPS stations in Greenland. Figure 4.3 displays the uplift graphs since 1992 for four configurations and four GPS stations.

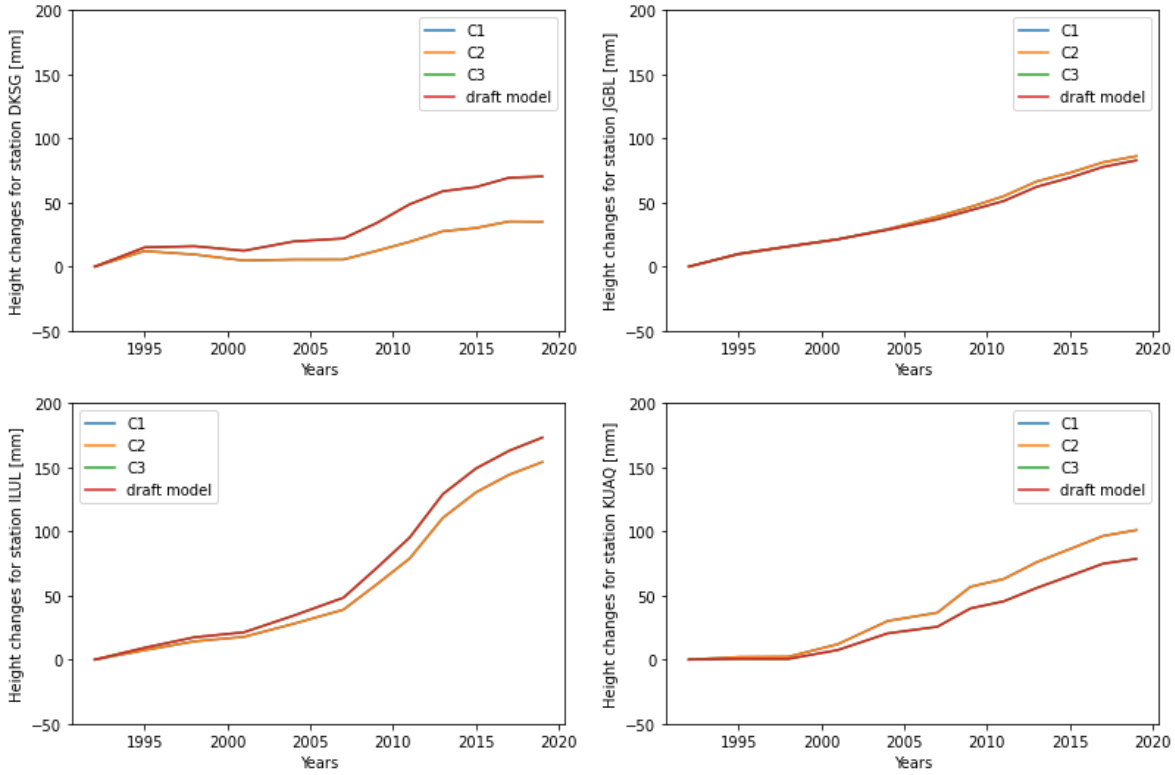

Figure 4.3: Comparison of uplifts for stations DKSG, KGBL, ILUL and KUAQ, between the four configurations of radial seed. In all graphs, configurations C3 and C4 (draft model) overlap, as well as C1 and C2.

We can conclude that the mean and maximum deflection rate per point since 1992 is more affected by this change in radial seed configuration, than the deflection statistics over the past 10000 years. Again, we find that the configuration C4 is the closest in results to the finest configuration: C3. The decision was made to choose configuration C4, as the most appropriate configuration, given its proximity with the finest setting, C3, and its lower run time.

4.4. Variation of the resolution tangent to the surface

As depicted in Section 4.1, this parametric study aims to test whether the resolution that is used: 25 by 25 [km] over Greenland is too fine or too coarse to accurately depict the uplift. In other words, because GRACE's dynamic gravity field measurements are only on a resolution of magnitude 300 to 400 [km], we would like to know if coarser or finer resolutions than 25 by 25 [km] lead to similar deflection values, and if not, what is then the most appropriate tangent to surface resolution setting. This allows us to tune our model with respect to accuracy and efficiency computation time wise. This section will therefore be a study on the surface resolution and its impact on uplift results.

4.4.1. Set up of the study

Keeping this in mind, we then test a run where the resolution over Greenland is 50 by 50 [km], effectively having about 4 times less points than the draft model, or 100 by 100 [km], therefore having about 16 times less points than the draft model, and one where the resolution is 10 by 10 [km]. Important to note is that: the resolution change is in the finer region, and not for the entire globe, and that these are settings which do not represent fully the reality of the mesh sizes; Abaqus does not fully apply the input setting for the mesh resolution. See Subsection 4.4.2 for a more in depth explanation of this phenomena, and how it is tackled in this parametric study. The important point to note is that this technique is developed and used here in order to make a more accurate investigation into the mesh size and its effect on deflections, and that this 'area correction' technique is used only in this study and in the final models: Final0 to Final3 for the final results of this Master Thesis.

- Setting of 10 by 10 [km] resolution in the finer region with the 'area correction' technique applied: 10 by

10 area corrected
- Setting of 25 by 25 [km] resolution in the finer region with the 'area correction' technique applied: 25 by 25 area corrected
- Setting of 50 by 50 [km] resolution in the finer region with the 'area correction' technique applied: 50 by 50 area corrected
- Setting of a 100 by 100 [km] resolution in the finer region with the 'area correction' technique applied: 100 by 100 area corrected

As said previously, we will test whether the results of uplifts rates, and final deflections vary with the above listed settings.

4.4.2. 'Area correction' technique

Throughout the interpolations we divided ice masses by the set mesh area, to convert from ice volume to ice height. However, the number of nodes in the finer region, or outside of it, do not reflect the theoretical amount of points. For instance, outside the finer mesh region, we should always have about 49468 points, as the mesh size is 100 by 100 [km], and the finer region is a 20 [°] width circle. See Section 2.1 for the mesh and region definition. However, we know that we have about 39500 points. So the mesh area is larger than expected. This becomes even more apparent for the 10 by 10 [km] setting, where the surface area for an element can vary by more than 50% from the setting. We can then conclude that Abaqus only uses the setting as an indication and not a hard constraint.

The question then becomes what is the set area per element. The ideal method would be to extract the surface area of each element. However, at this stage, due to time constraints and the complexity of the procedure, this was not done. Instead, as we noticed that the area of elements, in Abaqus, strongly varied along a latitude based trend, as seen in Figure 4.4 for the 10 by 10 [km] setting in Abaqus, we proceeded to extract a mean area of elements at each latitude.

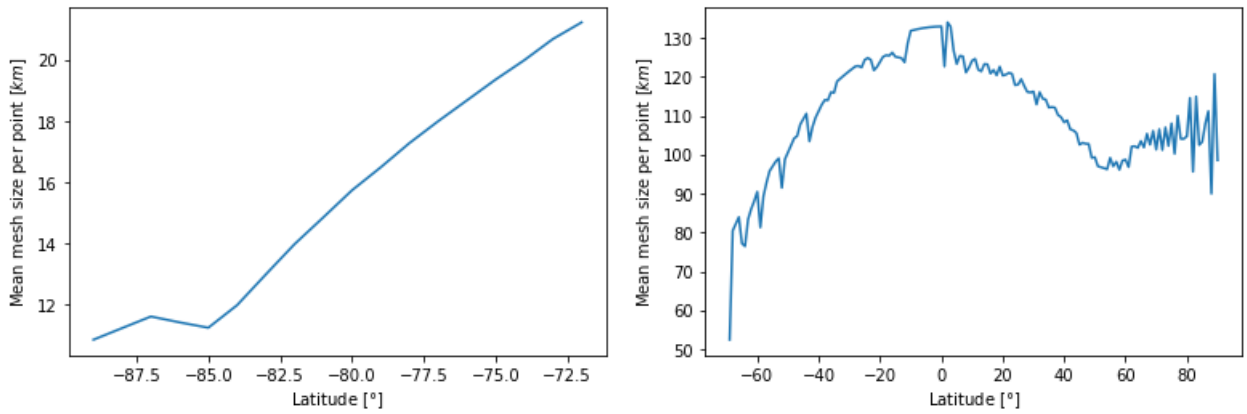

Figure 4.4: Mean mesh size at each latitude in the finer region (right) and in the coarser region (left). Note that the latitudes shown here are the ones in the model, when Greenland and the finer region are projected on the South Pole of Earth. The setting for these meshes were 10 by 10 [km].

For all four settings in this parametric study, we extracted the mean area of elements at each latitude, and converted the ice volumes, resulting from the interpolations, to ice heights with these areas. The direct effect of this area 'correction' technique is that for instance, for the 10 by 10 [km] setting, the maximum deflection goes from about -969 [m] in 2019 for the normal setting, since the start of the simulation, to about -863 [m] for the 'area corrected' setting. This is non-negligible. At the end of this section, Subsection 4.4.4 verifies the 'area correction' method.

4.4.3. Results - variation of the resolution tangent to the surface

We can then present the results through two aspects. The first is the mean uplift rate between 2009 and 2015 for all GPS stations locations, as done in Figure 4.5. View Appendix A for details on their specific locations and uplift values (Khan et al., 2016). Presenting results this way will allow to draw conclusions on the effect of

changing resolution on modern day uplifts. Furthermore, we also present a graph which displays the maximum deflection in the first time step of the model, and the associated change in ice height. Both results displays will allow us to draw conclusions on the convergence or not of the resolutions tangent to the surface.

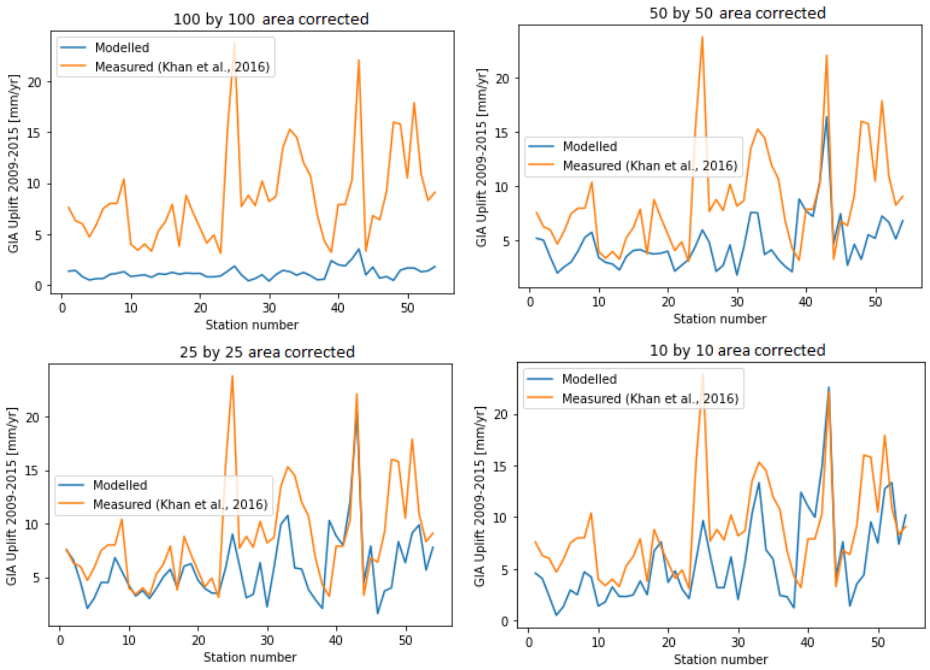

Figure 4.5: Modern day uplift rates at the GPS stations locations, see Appendix A for the precise coordinates, for the all mesh settings from this parametric study.

Through the graphs in Figure 4.5, we first notice that none of them are identical. However, we find that when we increase the resolution, they start to stabilise along a certain shape, adopted in the 25 by 25 and 10 by 10 area corrected results. Furthermore, from 25 by 25 area corrected onward, the values of uplift rates start to stabilise in a certain range of values, and the improvements are much smaller than previously, when the resolution was increased. We can then logically conclude that we are approaching a convergence point, but are not yet at one.

In Figure 4.6, we present the maximum deflection of the model, in the finer region, in the first time step with the associated change in ice height, for all four model settings. We choose the first time step, because the model is not loaded prior to it. Therefore, we are able to analyse the direct relation between loads and associated deformations.

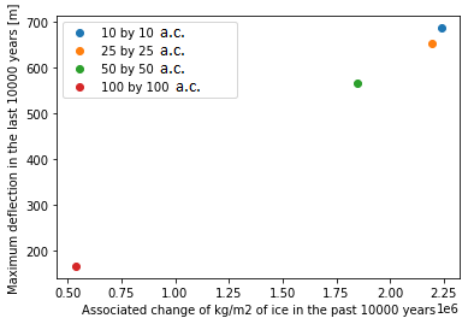

Figure 4.6: Maximum deflection points in the first time step of the simulation for the four 'area corrected' (a.c.) resolution settings.

We find, in the figure above, that the points nearly make a straight line. Deviations from that straight line are certainly due to errors in discretisation of the ice heights across the nodes, i.e. two large ice heights maybe right next to each other, but the smaller ice height has the largest deflections due to other factors. The reason why higher resolution runs yield larger deflections is solely due to the fact that with higher resolutions, a larger

variation in ice heights is possible. Thus, higher values of ice heights are present which then create larger deflection points.

In Figure 4.6, we also notice that after the resolution of 25 by 25 [km] the maximum deflection starts to converge, as the distance along the straight line linking the points becomes smaller as resolution is increased. This leads us to think that the convergence point is not far ahead of the 10 by 10 [km] setting, but that we have not yet reached it.

Considering all that has been discussed in this section, we can come to the conclusion that the 10 by 10 [km] area corrected setting is the most accurate one, as it brings our model a step closer to convergence on the 'long term' deflection scale, and because it yields significantly different results to the draft model setting of 25 by 25 [km]. We also do not chose a setting finer than 10 by 10 [km] as the increase in computation time is deemed too high, accounting for the fact that other parameters, such as viscosity or number of time steps, will already greatly increase the run time, as seen in the next sections.

4.4.4. Verification of the 'area correction' scheme

We now perform a verification of the 'area correction' scheme. This is done in order to see whether the 'area correction' technique actually improves the results, and whether it is an accurate approach. For this verification, we need to compare the results above to a benchmark model. For the benchmark, it was chosen to perform the interpolation on the 10 by 10 grid setting using ice heights and not ice masses. Interpolating ice heights has the advantage of better conserving mass. Hence, no correction scheme is applied as the total interpolated mass is kept within 3% of the original mass. We convert the original ice model data to ice heights by dividing the masses by the area found at the grid points; the area solely depends on the longitude and latitude resolution. As the resolution is constant angular wise, the spatial resolution along the longitude direction varies as longitude lines come closer together the further North or South one goes. Furthermore, interpolating ice heights is a more common practice in GIA modelling as it allows to better conserve mass. Thus, we can run this benchmark model for the first time step, and compare the output deflections in the finer region and over Greenland, with the first time step of the area corrected 10 by 10 model. We assume that if it is verified for the first time step, it will be for the rest of the model.

The area corrected scheme is verified because the differences in mean deflection is within 1.5% and the differences in maximum and minimum deflections in the finer region are of 5% to 5.9%. This is deemed acceptable, especially when considering that without this area correction technique, the difference in mean was 20.6% with the benchmark, and the maximum and minimum deflections were 21.7% and 55.7% off from the benchmark. Moreover, the mean difference in deflection between the benchmark and the area corrected scheme is of 0.88 [m], hence 1.9%. Over a period of propagation of 42000 years, we think that this statistic further verifies the area correction scheme, as most time steps, if not all except the second, are considerably shorter than that.

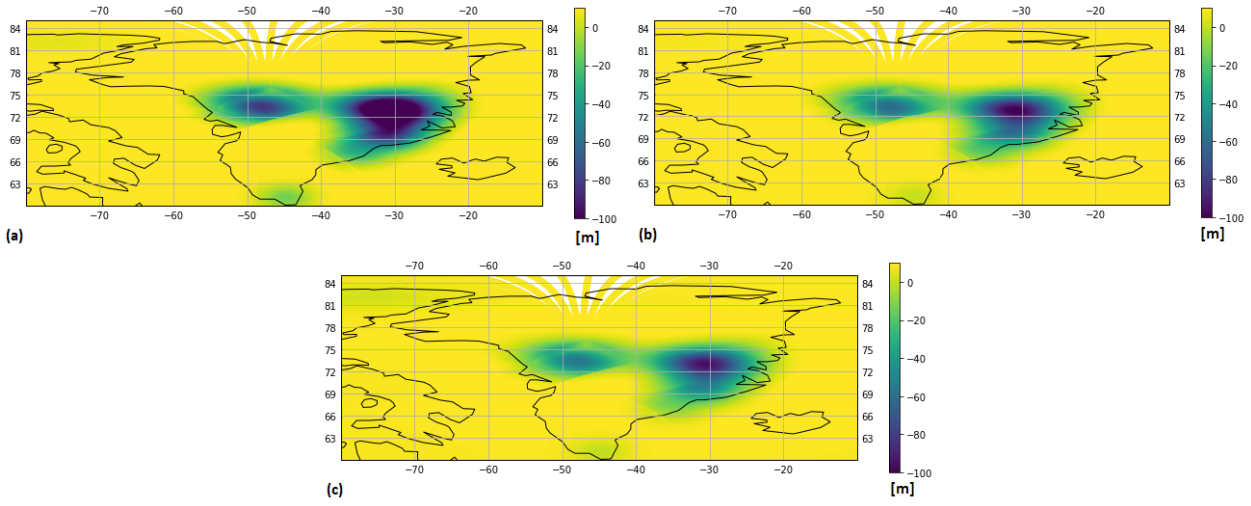

Figure 4.7: Deflection [m] on a longitude latitude grid after the first time step of 42000 years, for the 10 by 10 model (a), the 10 by 10 'area corrected' (b) and the benchmark model (c).

From the three deflection maps shown in Figure 4.7, we can see that the area corrected 10 by 10 model, yields more similar results to the benchmark model than the original non-area corrected 10 by 10 model. We can see that the magnitude and pattern between the benchmark and the 10 by 10 area corrected are extremely close. This comforts the idea that the area correction scheme is verified.

Lastly, the uplift rate between the 10 by 10 area corrected and the benchmark, that is the one in figure c from Subsection 4.4.4, differ from 0 to 0.26 [mm/yr], with a mean of 0.02 [mm/yr]. This is deemed acceptable as it is within the range of error in uplift rates in GIA modelling and measurements, as proven in Khan et al. (2016) and Simpson et al. (2011); these mentioned papers have GIA modern day uplift errors estimated between 0.1 and 0.6 [mm/yr] for the model (Khan et al., 2016) and of the magnitude 1 to 2 [mm/yr] for the measurements. Although the simulation above only performed one time step which is not in present day, we still think it is useful to compare the uncertainty between the benchmark and the area corrected 10 by 10 model through the uncertainty at present days in order to prove its verification. *Note: This error is most likely over estimated. To support this statement, the reader should here take into account that the time step tested here is very long, 42000 years, and sees a large change in ice as the model went from unloaded to fully loaded with the full ice thickness. In the final simulations, the model is only loaded with the difference w.r.t. the ice thickness 122000 years from present, most time steps are much shorter than 42000 years, and the ice mass change is never as significant as in the first time step of the benchmark or of the parametric studies model. Therefore, we can reasonably conclude that this difference in uplift rate, but also deflection, is here over estimated between the 10 by 10 area corrected and the benchmark models.*

With the above mentioned statistics comparison, the help of the graphs, and the context given to the uplift rate disparities, we can state: that the 'area correction' scheme yields better results than if not applied and that it is verified. We can also choose it because it brings the model closer to total mass conservation: a better ice mass to ice height conversion means more accuracy in total mass estimation. We can then safely use it for the final simulations of this Master Thesis.

4.5. Variation of the timeline resolution

This parametric study, aims to test the sensitivity of the time resolution taken, during different parts of the recent and 'long term' ice history. This time resolution study concerns both the resolution in terms of ice load chosen, in terms of regularity of the step function taken, and in terms of the integration of the deflections over time. This refers to when there is a transition between two time steps: the load, although a ramp is present, shifts just a bit over an instant. See Appendix G for further explanation on this. The point is that when these 'steps' are taken, it is thought to influence the uplift results.

This section aims to test the sensitivity of the model in the two specific timeline parts: de-glaciation and 'short term' history. We will therefore run the model only from 25000 to 1000 years ago or from 1972 to 2019.

4.5.1. Set up

Considering the introduction of this section, we can formulate both a set up: to test the de-glaciation timeline, and a set up to test the 'short term' ice history period, i.e. from 1972 onward.

The de-glaciation era, in the standard timeline, has three main parts. The first is from 25000 years ago to 11000 years ago, where steps of 2000 years are taken, the second is from 11000 to 1000 years ago, where steps of 1000 years are taken, and the third is the steps between 1000 and 100 years ago. This third part is not included in this study as we already use all the ice files available. For the first two parts, we consider two scenarios where the time resolution is coarser, T1C and T1E, and two where the time resolution is finer, T1B and T1D, for the respective periods. We then check the deflections between 11000 and 1000 years ago.

- T1A - from 25000 to 1000 years ago: apply standard timeline (draft model settings) - 17 steps
- T1B - from 25000 to 1000 years ago: take every 1000 years from 25000 to 11000 years ago, and take every 1000 years from 11000 to 1000 years ago - 25 steps
- T1C - from 25000 to 1000 years ago: take every 7000 years from 25000 to 11000 years ago, and take every 1000 years from 11000 to 1000 years ago - 13 steps
- T1D - from 25000 to 1000 years ago: take every 2000 years from 25000 to 1000 years ago, and take every 500 years from 11000 to 1000 years ago - 27 steps

- T1E - from 25000 to 1000 years ago: take every 2000 years from 25000 to 1000 years ago, and take every 2000 years from 11000 to 1000 years ago - 12 steps

As T1A is the nominal case (T1 is 'long term' and T2 is 'short term'), we aim to see with this study if finer settings such as T1B and T1D provide vastly different results. In that case, we would pick the one which varies the most from T1A. We also then aim to see if coarser settings provide similar results, namely T1C and T1E. T1B and T1C concern the period 25000 years ago to 11000 years ago, while T1D and T1E concern the period 11000 years ago to 1000 years ago.

For the 'short term' history, we run exactly the same settings except that now there are three parts which are tested: the one from 1972 to 1992 with T2B and T2C, where the spatially coarser ice history is used, the one from 1992 to 2007 with T2D and T2E, and the more recent period from 2007 to 2019 with T2F and T2G. We will compare percentage changes in final deflections, just as in Section 4.2, and we will only load the model from 1972 onward. T2B, T2E and T2F are finer than the original setting T2A, while T2C, T2D and T2G are coarser.

- T2A - Restart at 1972, and apply standard timeline (draft model settings) - 13 steps
- T2B - Restart at 1972, and take steps of 5 years between 1972 and 1992 - 15 steps
- T2C - Restart at 1972, and take 1 step of 20 years between 1972 and 1992 - 12 steps
- T2D - Restart at 1972, and take steps of 5 years between 1992 and 2007 - 11 steps
- T2E - Restart at 1972, and take steps of 1 year between 1992 and 2007 - 23 steps
- T2F - Restart at 1972, and take steps of 1 year between 2007 and 2019 - 19 steps
- T2G - Restart at 1972, and take steps of 3 years between 2007 and 2019 - 10 steps

4.5.2. Synthesis of results for the 'long term' timeline resolution parametric study

For the time resolution investigation in the 'long term' ice history, contrary to previous results, we here present the change in mean deflection in the finer region from 11000 years ago (before present) and 1000 years ago. Thus, it is only logical to compare the 11000 years ago to 1000 years ago period.

At this stage it is important to note that what is valuable is the magnitude of deflection statistics, rather than the absolute values of deflections in the finer region, as the simulations in this parametric study are not loaded prior to 25000 years ago. This study is a sensitivity study, to see what is the sensitivity of the model to changing the time resolution. So, just as in Section 4.2, the results are to be taken relative to each other. Table 4.5 presents the statistics of the deflections in the finer region.

Table 4.5: Deflection statistics in the finer region between the years 11000 (before present) and 1000 (before present), for all five timeline set ups.

	deflection statistics [m]				
	T1A	**T1B**	**T1C**	**T1D**	**T1E**
Mean	60.82964	58.37481	80.82958	60.9415	33.48515
Min	-78.1693	-81.5843	-75.394	-79.9274	-2.1026
Max	321.2499	322.1874	392.2585	327.0295	131.3163
Std	92.52525	92.56357	107.9052	93.38381	29.13615

T1B and T1D are assumed more accurate than T1A, as they have a finer temporal resolution, it can be seen that they both yield similar results to T1A. T1C and T1E's results are both too different in terms of statistics, varying between 25% and 50% change in results compared to the standard set up, as seen in Table 4.5, equivalent to 70 or 290 [m] respectively for the maximum deflection. As T1C and T1E are both time-wise coarser options, we do not chose them.

T1D seems at first hand more similar to T1A than T1B, as the maximum deflection is within 2 [m] of T1A's and T1B's minimum deflection. However, it should be noted that T1D has a significantly different maximum deflection to T1A, about 6 [m], through the specified time span, which may point towards the fact that it could be chosen for final simulations, while T1B only has a difference of 1 [m] with T1A's maximum deflection. Figure 4.8 presents the variation of the mean deflection for each setting over time relative to present deflections.

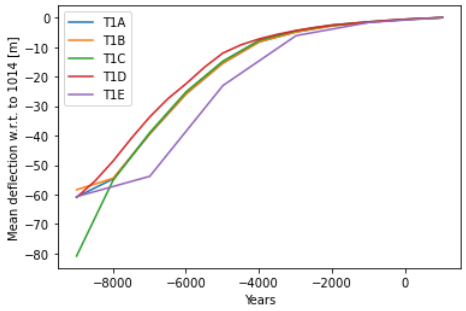

Figure 4.8: Mean deflection evolution across the fine region from 11000 years ago till 1000 years ago (before present).

What is interesting to notice here is that, as seen in Table 4.5, the draft model has more similar results to the finer timelines: T1B and T1D. Moreover, T1B is nearly identical to the standard set up, while T1D has a similar start and end point, but varies greatly across the time period. Considering that T1D is finer than T1A, and provides significantly different mean deflections in time, as well as a different maximum deflection at the end of the simulation, this timeline is to our knowledge the best option available here: both combining difference in results with the draft model, and increase in temporal resolution.

4.5.3. Synthesis of results for the 'short term' timeline resolution parametric study

When investigating the sensitivity of the model to the short term timeline resolution, that is from 1972 to 2019, the model was loaded and started from 1972. Thus, we compare statistics of deflections throughout the finer regions at the end of the model, as presented in Table 4.6.

Table 4.6: Percentage difference of the final deflections at the year 2019 years (before present), between the different timelines configurations (T2).

	Percentage difference in end deflection					
	T2A-T2B	**T2A-T2C**	**T2A-T2D**	**T2A-T2E**	**T2A-T2F**	**T2A-T2G**
Max	0.190289	0.005002	-1.6E-05	7.77E-06	0.103798	0.280362
Min	-0.27771	-0.00732	4.67E-05	-2E-05	-0.14758	-0.41983
Range	-0.2323	-0.00612	4.07E-05	-1.7E-05	-0.12319	-0.35189
Mean	-1.18984	-0.03138	0.000319	-0.0003	-0.65009	-1.74339
Median	0.622945	0.015824	1.17E-05	0.000121	0.372798	0.926567

Therefore, we can conclude the following points:

- Considering that T2B is the finest setting between T2A, T2B and T2C, the results for the T2B configurations are deemed varying enough from T2A, with a variation of the mean deflection of 1%. Although 1% may be small, the cost for such an improvement would only be two more time steps, which is a low cost. Hence, we choose the T2B configuration for the 1972 to 1992 period.
- T2E is the finest setting for the period of 1992 to 2007, and T2G is the coarsest. Given that T2A, T2D and T2E, have a low variation, about 1e-4 to 1e-5 %, the coarsest configuration, T2D, is then chosen.
- T2F is the finest setting in the 2007-2019 period, and is considered for the final simulations, because, although the difference in results is only of 0.1 to 0.7 % in deflection statistics, the 2007 to 2019 period is a highly interesting time span when comparing the uplift to modern measured one. We wish for a higher temporal accuracy in this time span. Hence, we choose the T2F configuration for the period 2007 to 2019.

With all these choices, we go from 2, 5 and 6 steps from 1972-1992, 1992-2007 and 2007-2019 respectively, to 4, 3 and 12 steps for the according time periods. This corresponds to an increase of 6 steps, so at least 2 hours computation time with the settings from Subsection 3.2.1. This increase in computation time may be greater later, as more computational time heavy settings may be chosen, resulting from these parametric studies.

4.6. Customisation of the timeline

The aim of this parametric study, is to test whether the loads chosen, based on a lower viscosity region, have a higher effect on the end results or not. The conclusion is the following: if there is a lower viscosity that means that the uplift response will be faster in time, and possibly greater especially in modern days although not necessarily. Thus, it seems natural to pick the time steps, where the load varies in function of time, of a lower viscosity region, and therefore design a new timeline. By testing such a 'custom' timeline, we can conclude after analysing the results, whether this customisation effect has a real impact or not. The point of this customisation of the timeline, of the ice history, is not to test whether the 3D viscosity has an impact or not, as the viscosity will be constant in this study, but it is to determine if key loading aspects and their choice in time have an effect on the deflection results, so that we know we have chosen the most adapted load configuration in time for when the 3D viscosity profiles are used in the final results. In sum, it is not the time resolution but the effective use of time steps which we aim to decide, which may include a larger amount of time steps used.

For this parametric study, we exclusively alter the long term ice history from the standard model in Subsection 3.2.1, as it is the one which is the most sensitive to viscous properties of the upper mantle. I.e. we customised the timeline by changing the frequency and placements of time steps prior to 1000 years ago. The 'short term' ice history does not provoke a significant viscous behaviour (Simpson et al., 2011). However, we will run the simulations from 122000 years ago to present day.

There are two customisation possible. The first is to pick the differences in inflection points between the specific low viscosity region, and the general Greenland trend, and then check at which point they differ in trend. Then, we simply add these time stamps, if not already present, to the standard timeline used in Subsection 3.2.1.

The second customisation, is a more detailed one. It is performed by effectively choosing the key points which can help to represent the ice trend in this lower viscosity region. In other words, we take into account every 'kink' in the ice trend, in order to model the ice mass trend through the input files chosen.

4.6.1. Determining the low viscosity region

In order to find this lower viscosity region, we need to formulate a list of requirements or properties of this region, to ease our choice.

- The region has no required spatial limits. This region could therefore be the whole of Greenland, in theory, if the whole of Greenland had a uniform viscosity. This requirement is necessary due to the fact that complex regions are hard to define, and we thus need to make simple 'cuts' into Greenland. The region should be simple to define. This is to allow ease in assumptions, and ease of replication of this process by other parties.
- The region needs to have an overall lower viscosity, at multiple depths, than the rest of Greenland.
- The region should have a changing load case. If the region does not have a varying ice load, then there is little point in testing these costumed timelines.
- The region, should be one which has a high uplift rate and/or shows mistakes in the uplifts rates estimated.

With the above requirements, we can derive the following region, in Figure 4.9, to be the 'low viscosity region'.

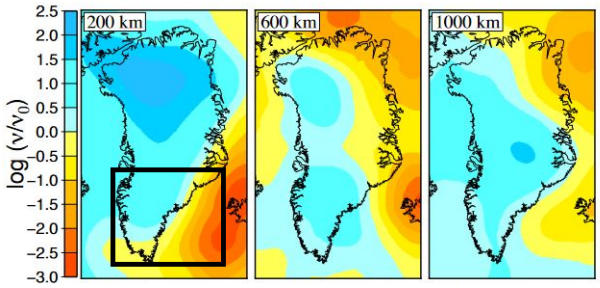

Figure 4.9: Relative viscosity map with a reference of $5 \cdot 10^{20}$ [Pas] for the upper mantle and $2 \cdot 10^{21}$ [Pas] for the lower mantle, directly taken from Milne et al. (2018). It can be seen that the lower viscosity region is below the latitude of 70 [°] (Milne et al., 2018), circled by the black box (own addition to the original figure).

It can be seen that in Figure 4.9, the region labelled, meets all the requirements. It is easily defined, has a changing ice history (Lecavalier et al., 2014), has one of the highest uplifts as shown in Subsection 3.2.1, and also has some of the highest errors as demonstrated in item 3.2.2. Hence all requirements are met and we can proceed to design the customised timelines using the customisation techniques possible, explained earlier on.

4.6.2. Customised set ups

We can therefore, as explained earlier, generate two customised timelines. They are represented in Figure 4.10, and compared to the standard model from Subsection 3.2.1, using the maximum ice heights. Showing the maximum ice height is useful as it may be linked to the maximum deflections.

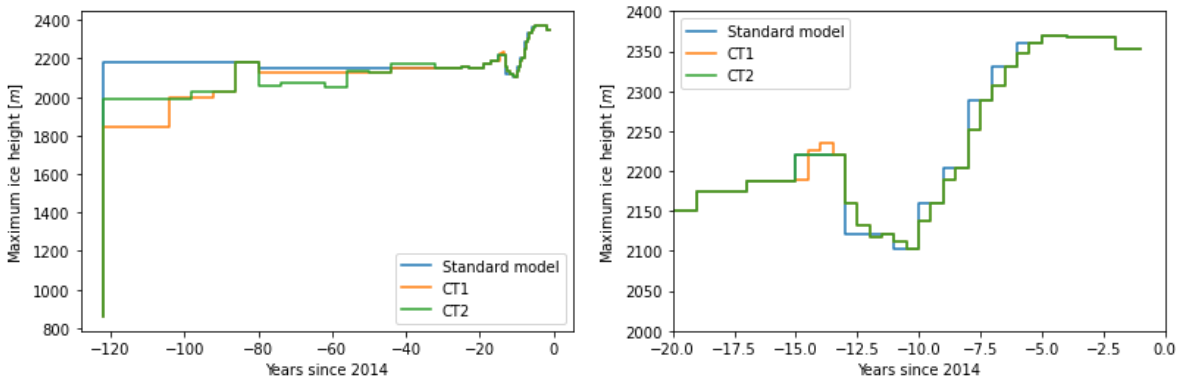

Figure 4.10: Customised timelines trend for the region of low viscosity, showcasing the maximum ice heights, with an overall overview of the 'long term' ice history (left), and of the de-glaciation era (right).

Furthermore,in the 'zoomed' in version of the timeline, where the de-glaciation era is shown, the second customised timeline, Custom 2, is more detailed than the Standard model, as this one has less points. Furthermore, in Figure 4.10, we can see that CT1 both varies in the glaciation phase, as well as the de-glaciation era. In practice the list below contains the time steps taken, in Custom 1 (CT1) relative to 2014. This timeline, as explained previously, is found by picking the points which have a difference in trend between the lower viscosity region, and the general Greenland trend.

- Time steps at: 122000, 104000, 92000, 86000, 80000, 44000, 25000 years ago
- From 25000 to 15000 years ago: steps of 2000 years
- From 15000 to 5000 years ago: steps of 500 years
- From 5000 to 1000 years ago: steps of 1000 years

For the customised timeline Custom 2 (CT2), below are listed the time steps taken. These again, correspond to the points which would be needed to accurately map the trend in ice heights, without using all points, as this is deemed counter productive.

- Time steps at: 122000, 98000, 86000, 80000, 74000, 62000, 56000, 50000, 44000, 32000, 25000 years ago
- From 25000 to 13000 years ago: steps of 2000 years
- From 13000 to 5000 years ago: steps of 500 years
- From 5000 to 1000 years ago: steps of 1000 years

4.6.3. Results - customisation of the timeline

Therefore, we can discuss the results from the different custom timelines, as shown in Figure 4.11.

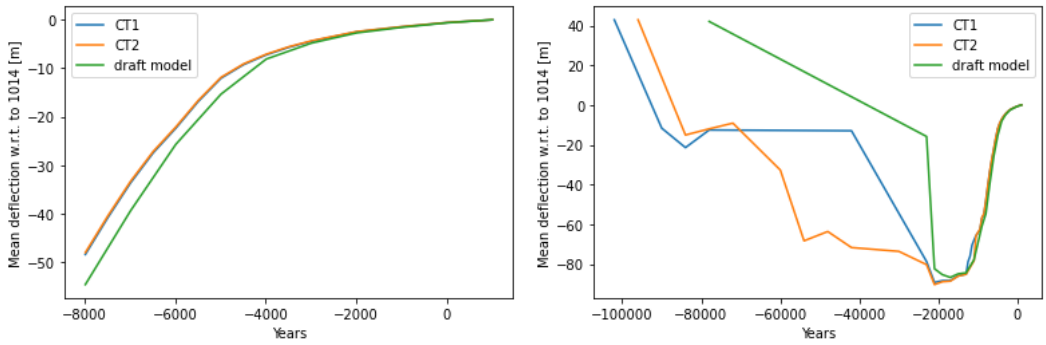

Figure 4.11: Time series of the mean deflection relative to the deflection 10000 years ago (before present) in the finer region from 10000 years ago (left) and between 104000 years ago and a 1000 years ago (right). The draft model is the same as the standard model from Subsection 3.2.1.

As defined in the previous subsection, it is worth recalling that both custom timelines, are finer than the standard set up used in Subsection 3.2.1. Furthermore, we see as a general rule that CT2, presents a higher difference in results with respect to the standard model than CT1 when looking at the right graph of Figure 4.11. However, we notice that CT1 presents still quite different results from the standard model. Both the percentage differences from CT1 and CT2, are larger than the ones from Section 4.5. Here, the variations are in multiple percentages, while the ones in TL1 rarely reach 1.5% for the finer set ups.

We can thus conclude from this specific parameter study that the custom timeline is needed, and that we should use primarily the timeline CT2, with the addition from CT1 at the time steps 104000, 92000, 15000, 14500, 14000 and 13500 years ago, as these steps are not included neither in CT2 nor the draft model. CT2 provides the most different results from the draft model, while being more detailed time-wise.

4.6.4. Discussion around time steps between 122 and 25 thousand years before present

In the custom timelines, additional time steps were added prior to 25000 years ago. However, in Figure 4.11, it can be seen that although prior to 20000 years ago the deflections are widely different, they all converge after this point, especially starting from 15000 years ago.

So a relevant question is whether these added steps are useful or not, as they add considerable time in the simulation. Looking at Figure 4.11, contrary to what was concluded earlier, it does not seem to be the case. Adding on, the ice history prior to the last glacial maximum is more uncertain, and thus using more points in time is not necessarily more accurate.

The deflections of CT1 and CT2 converge at 15000 years ago and diverge until 13000 years ago. This is because CT1 starts with steps of 500 years from 15000 years ago, when the draft model and CT2 do not. CT2 then 'jumps' to the CT1 curve, as they both have steps of 500 years from 13000 years ago. A similar phenomenon to the one described above, happens from 5000 years ago on wards, where all three curves merge, due to the fact that they have similar time steps of 1000 years. Both of these phenomena are proofs that steps prior to 25000 years ago, do not significantly matter.

4.6.5. Synthesis of a unified timeline - with section Section 4.5

Previously, we concluded to combine both the custom timelines, as they both showed different results from the standard time set up. However, the unified custom timeline does not have a resolution of 500 years between 5000 and 1000 years, before present. We know from Section 4.5, that the resolution of the set up T1D, which varied the resolution between the years 11000 and 1000 years ago, influenced the results by 0.5%.

Given this variation in results, we find it coherent to add to this unified custom timeline, a resolution of 500 years between the years 5000 and 1000 years ago, before present. Finally, it was also decided to keep the standard set up prior to 25000 years ago. The synthesised timeline prior to 1000 years ago, is then as follows:

- Time steps at: 122000, 80000, 25000 years ago
- From 25000 to 15000 years ago: steps of 2000 years
- From 15000 to 1000 years ago: steps of 500 years

With this new timeline prior to 1000 years ago, we go from 19 steps in the standard model to 35. However, this

increase in computation time is deemed acceptable considering the fact the model is now more accurate, and the gain is estimated at several percentages differences.

4.7. Quality of the interpolated ice loads

As presented in Section 2.3, we are given ice masses or ice mass changes on unique grids. However, there is a need to interpolate them in order to convert them onto our mesh grid. For this, we skip values from the given ice masses, in favour of a lower computation time. Unfortunately, skipping these values, affects the quality of the interpolated loads, and thus of the simulated deflections. Thus, in this section, the effect of skipping data in the original data set on the simulated deflections is investigated.

For this parameter study, just like the others, we will be considering the draft model, with a 25 by 25 [km] mesh setting. The simulation will be re-done with interpolated loads with 1 less skipped and 1 more skipped from the original data. The interpolation methods used here are the ones presented in Section 2.3.

4.7.1. Set up

The set up for the 'long term' term ice history files is as follows: skipping 4/5 (IS1) or 6/7 (IS2) instead of 5/6 (std draft model), and for the 'short term' ice history: skipping 8/9 (IS3) or 10/11 (IS4) instead of 9/10 (std draft model). We run the full simulation each time, so we have four distinct set ups. These ratios are presented in more detail in Table 4.7.

- IS1: skipping 4/5 of the original 'long term' ice mass values
- IS2: skipping 6/7 of the original 'long term' ice mass values
- IS3: skipping 8/9 of the original 'short term' ice mass values
- IS4: skipping 10/11 of the original 'short term' ice mass values
- std draft model (standard draft model): skipping 5/6 of the original 'long term' ice mass values, and 9/10 of the original 'short term' ice mass values

Table 4.7: Ratio of values used over values to interpolate to, i.e. the ratio of the number of ice mass values used from the old grid over the number of nodes in the new grid. 'ratio globe' and 'ratio finer' correspond to interpolations for the 'long term' ice history , where as the 'ratio tight' correspond to interpolation in the tight region for the 'short term' ice history.

	Ratio globe	Ratio finer	Ratio tight
IS1	0.61207089	0.1103912	
IS2	0.43719349	0.0788508	
IS3			2.417098
IS4			1.977626
Std draft model	0.51005907	0.0919926	2.175388

Looking at Table 4.7, it can be seen that interpolation in the 'tight' region, which are interpolations done from 1972 onward, use more values from the original data set than the interpolations prior to 1972, which are for the finer and globe regions. Thus, in theory these are more accurate. This is done on purpose, as uplifts during that period, especially elastic ones, need a high degree of accuracy as it is the period of interest for ground elevation analysis. It can also be seen that the ratio in the finer region is smaller than on the rest of the globe. This is due to the fact that the used original data has a similar distribution across the entire globe, but that our mesh grid has a larger amount of points in the finer region. This leads to theoretically worse quality loads, but this is not considered a problem as it occurs during the 'long term' ice history period, and displacements there are not that relevant if we wish to use uplifts for other studies: such as for instance the gravity rates from 1992 till now.

4.7.2. Results

We can then present the deflection results which were found when skipping a different proportion of the data for the interpolation. This is again using the 25 by 25 [km] setting. Figure 4.12 presents the results for this parametric study for the four chosen GPS stations.

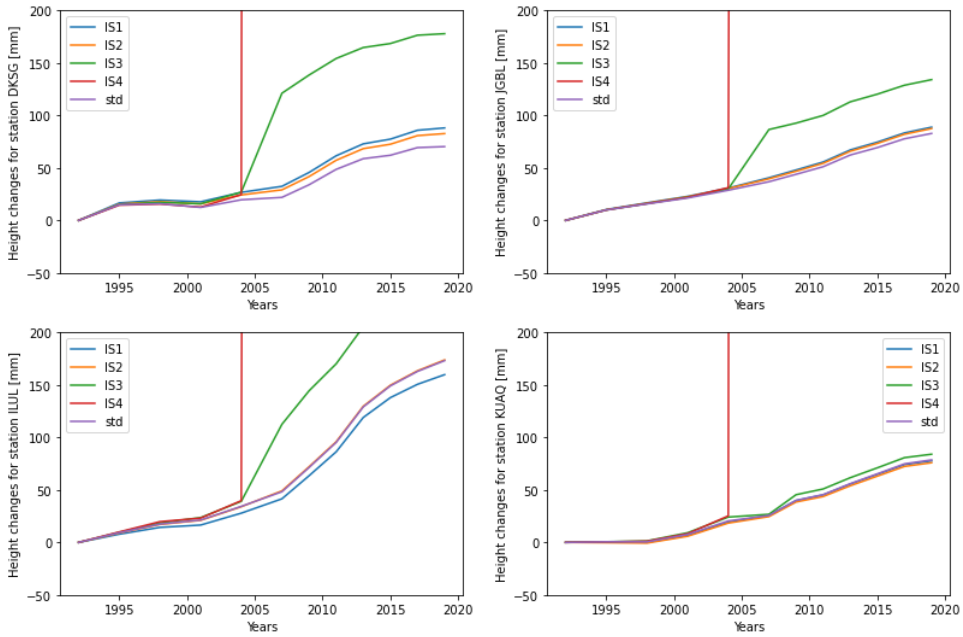

Figure 4.12: Comparison of uplifts for stations DKSG (top right), JGBL (top left), ILUL (bottom right) and KUAQ (bottom left), between the five interpolation quality settings. 'std' here refers to the standard model, also called the draft model.

In Figure 4.12, the deflection behaviour between the different settings is the same for all GNSS stations. The setting IS4 clearly creates results which are not accurate. This is thought to be because skipping too many values, when using interpolation methods such as Gaussian - hence the spike from 2004 - yields wrong load estimations. See Section 2.3 for a reminder on the interpolation settings for each year. This is also partially true for the IS3 setting, which sees vastly different results for stations DKSG, JGBL and ILUL.

For the other settings, skipping less or more values yields slightly different results, but nothing apparent. As the interpolation scheme only has to be run once, skipping less values, just as in IS2 and IS3, is considered a viable option for the final runs. Table 4.8 presents the statistics of the deflections over the past 10000 years for the four settings and the draft model. *Note: the order of convergence between IS1, standard and IS2 might not seem obvious at first hand, as the curves are not layered in this fashion in Figure 4.12. However, we believe that the order in which the curves appear has little to do with convergence. As values are skipped indiscriminately, it could be that the ice heights at the GPS stations are more similar between IS1 and IS2 than with the standard model, although IS1 skips more values than the standard model, and IS2 skips less.*

Table 4.8: Final deflection statistics for the deflection in the past 10000 years before present for the different interpolation skips settings.

	Deflection statistics [m]				
	IS1	**IS2**	**IS3**	**IS4**	**draft model**
Mean	54.87209	54.86884	54.9496	56.56128	54.94367043
Min	-30.4719	-32.3058	-32.0566	-717.189	-32.15356445
Max	330.1809	328.0709	328.6766	329.2395	328.6733246
Std	92.62416	91.7986	92.65865	96.89875	92.65470547

With respect to the deflection 10000 years before present, the behaviour is in Table 4.8 the same as in Figure 4.12. The deflection statistics in IS1, IS2, IS3 and in the draft model are similar in the finer region. IS4, once again, presents a large anomaly.. This reinforces the idea that in the years 1992 to 2019, a simple interpolation method should be used, such as: linear Rbf, which proved itself accurate in the 'long term' interpolation method. This will be applied to the model from Chapter 5.

Given that the settings IS1 and IS3 are theoretically more accurate, as a smaller proportions of the results are skipped, we can say that skipping less values does improve the deflection results, bu not significantly, as we see that IS3 does not perform well. Moreover, concerning the mean uplift rate over recent epochs, see Figure 4.12, skipping less values in the recent ice history has non-negligible effects, and this should be implemented. However, the question is how can we apply this to a 10 by 10 [km] setting grid. We should aim to have more points used from both the 'long term' and detailed 'short term' data sets in the 10 by 10 [km] setting interpolation, as this has just been proven to provide significantly enough different results since 1992, and to a lesser extent in the 'long term' history. Lastly, we should also aim to keep a similar ratio of points used to points interpolated upon. In Table 4.9 we can see the number of points per region in the original ice data.

Table 4.9: Amount of data points in the ice mass (change) data. 'DST' stands for the detailed short term history, spanning from 1992 to 2019, and 'LT' the long term history, spanning from 122000 to 1000 years before present.

	LT	**DST**
Total	131072	209664
Tight		166700
Finer	10188	
Globe	120884	42964

When interpolating the data for the 25 [km] setting, the ratios of data skipped can be found in Table 4.7. For the 10 [km] setting, if we wish to have similar ratio settings in the finer region and 'tight' region, we should skip 1/2 of the 'long term' ice history data, and 3/4 of the 'short term' ice history data, as shown in Table 4.10.

Table 4.10: Ratio of data used in the given ice (change of) masses over the amount of points in the respective regions in the surface grid mesh.

10 km resolution setting		
Globe	**Finer**	**Tight**
skip = 2	**skip = 2**	**skip = 4**
1.53017722	0.0979615	2.096855
LT	**LT**	**DST**

In this interpolation set up we use three times more points from the 'long term' ice history, and a little more than two times more points from the 'short term' ice history, compared to the draft model interpolation set up.

4.8. Time ramp & the effect of loading partial ice thicknesses

Previously to this, the time ramp was already mentioned, and is presented in Appendix G. Here, we test the effect of this time ramp on the draft model from Subsection 3.2.1. Furthermore, until now, the full ice thicknesses were loaded in the Abaqus FEM model. However, just as it will be done in Chapter 5, we test in this section, the loading of the ice height differences with respect to the ice height 122000 years ago. This is done, in order to actually take into account the assumption that the Earth was in isostatic equilibrium before the start of the simulation. *Note that the time ramp for the 'long term' ice history was made then accordingly to these new ice loads. This then means that the first time step for instance, starts at 0 ice mass, and linearly ramps to the ice heights at the year 80000 before present by the end of this step.* 'draft 2.0' is the draft model from Subsection 3.2.1, but with ice height differences w.r.t 122000 years ago loaded.

We therefore have, for this parametric study, three settings. This way, we will be able to test the effect of the ramp, and the effect of loading partial ice heights.

1. The original draft model from Subsection 3.2.1: we load full ice thicknesses and develop and include a ramp.
2. A modified original draft from Subsection 3.2.1: we load the ice heights differences with respect to 122000 years ago, and develop and include a ramp.

3. A second modified original draft from Subsection 3.2.1: we load the ice heights differences with respect to 122000 years ago, and do not include a time ramp.

This section aims to discuss both aspects and compare them, as it was found that they seem to have comparable effects in magnitude. As in previous sections and chapters, we start by presenting the modern uplift, from 1992 to 2019, at the four GPS stations: DKSG, JGBL, ILUL and KUAQ, in Figure 4.13.

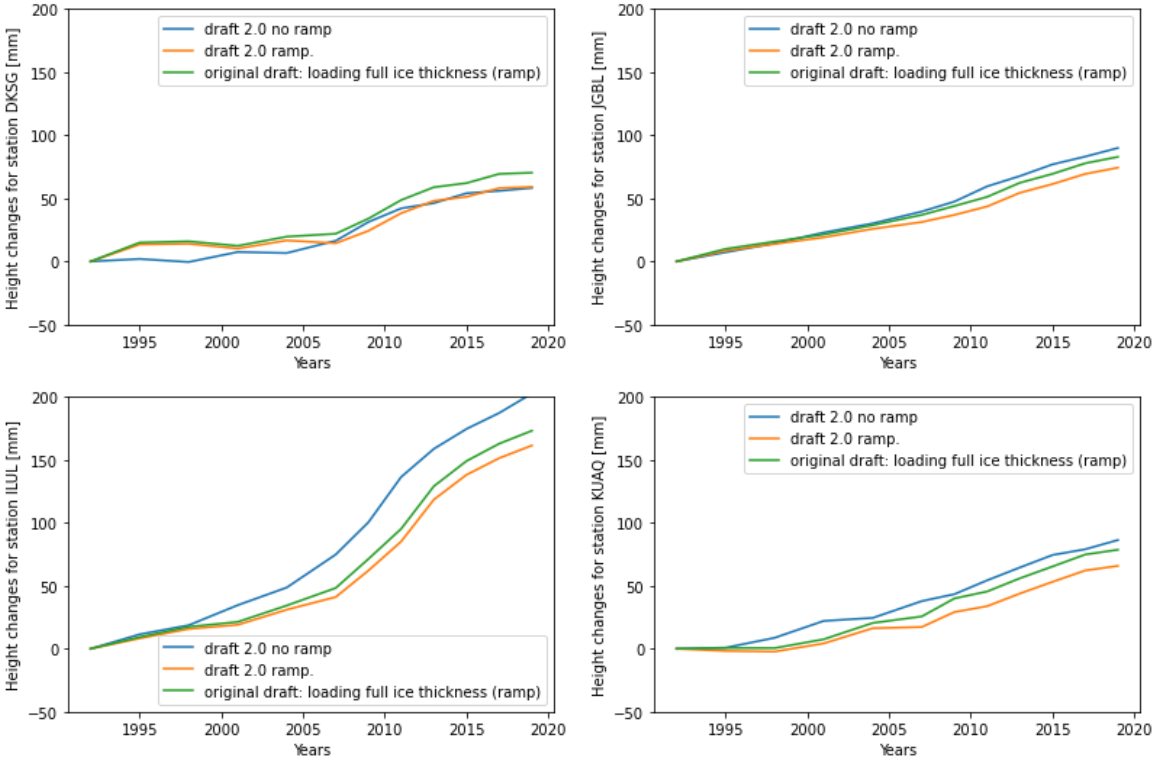

Figure 4.13: Variation of the uplift trends since 1992 at four GPS stations: DKSG (top left), JGBL (top right), ILUL (bottom left) and KUAQ (bottom right).The difference between "draft 2.0 ramp" and "original draft: loading full ice thickness (ramp)" is that the first only loads the ice thickness difference with 122000 years before present, when the latter loads the full ice thickness..

In Figure 4.13 the common point between stations ILUL, JGBL and KUAQ is that the no ramp method always over estimates the uplift compared to the other settings. This is due to the fact that the ice loads are removed later than when the time ramp is applied, as by definition the ramp can change the magnitude of loads through out a time step. However, at the DKSG station, the ramp seems to have little to no effect, as the solution converges after 2010. The main effect at the DKSG station is whether a full or partial load is applied.

Figure 4.14 shows a behaviour of the mean deflection over time for the three settings.

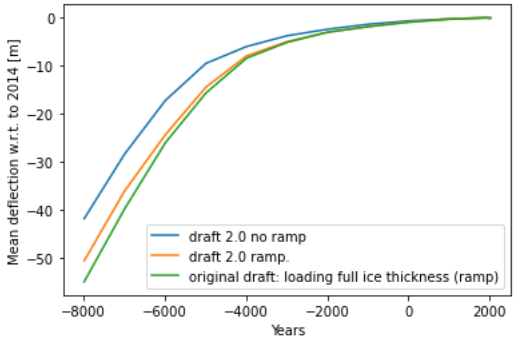

Figure 4.14: Mean deflection [m] since 10000 years before present until 2019, in the finer region.

In Figure 4.14, in becomes clear that the time ramp has a larger effect than the type of loading for the ice, whether it is partial of full ice thicknesses. Furthermore, overtime, although the ramp/no ramp solutions converge, there is a noticeable difference between them. Using a ramp is, if the ice model is trusted, objectively more accurate, as it uses the ice loads in between the time steps taken, in order to formulate ratios of the input load at the start of a time step. No ice loads are created here, unlike the ice load in 1972. Please refer to the discussion on accuracy of the time ramp in Appendix G.

5

Finalised model: standard 1D viscosity

After performing the parametric studies shown in Chapter 4, it is estimated that performing a run, where the standard draft model used so far is used with all the added changes from the parametric studies that were deemed useful, brings value to this research by including a small preliminary analysis of the results while comparing the first results to previous models. This run will be called and referred to as 'Final0'. It brings value to the research for one main reason: we will be able to assess the need for the implementation of a 3D varying viscosity profile, and what could be the profile's effect on the results. We also present here the contribution of the load changes since 1914 to modern day uplift rates.

5.1. Modifications from Subsection 3.2.1

As mentioned earlier, the changes to the draft model in Subsection 3.2.1, span a selection of changes made from the parametric studies, namely: the 10 by 10 $[km]$ setting of the surface mesh, the 'area correction' of the ice mass-height conversion, the inclusion and modification of various time steps, and the larger size of the initial population of data points used in the interpolation between the given grid and our own mesh.

Furthermore, as it was explained at the end of Chapter 4, that not the full ice thicknesses are now loaded, but only the difference with respect to the ice thicknesses 122000 years ago, at the start of the simulation. This way, the simulation is faster, and more accurate, as we put into practice the assumption that the Earth was in isostatic equilibrium at 122000 years ago, before the simulation starts. However, this creates negative ice heights, which are not a problem for Abaqus, but may seem illogical.

5.2. Results

As done previously, we can present the results of the recent uplift rates and deflection with respect to 10000 years ago, as well as the recent deflections at the locations of GPS stations.

5.2.1. GPS stations recent uplifts

The results are here compared at certain GPS locations and compared to the measured trend. The results are presented, as done previously, against the four chosen GPS stations: DKSG, JGBL, ILUL and KUAQ, in Figure 5.1.

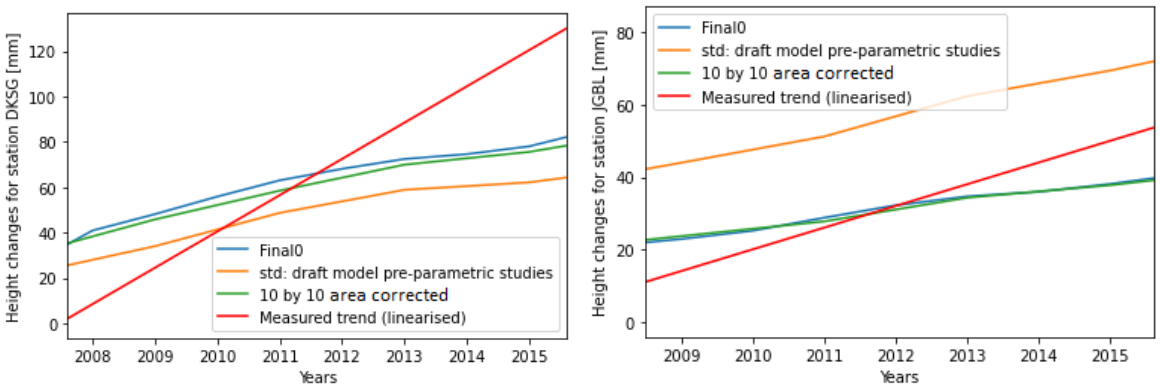

Figure 5.1: Comparison of uplifts for stations DKSG and KGB, between the modelled and the measured (above). We also the results with the 10 by 10 area corrected setting from the Chapter 4, and with the original model from Subsection 3.2.1.

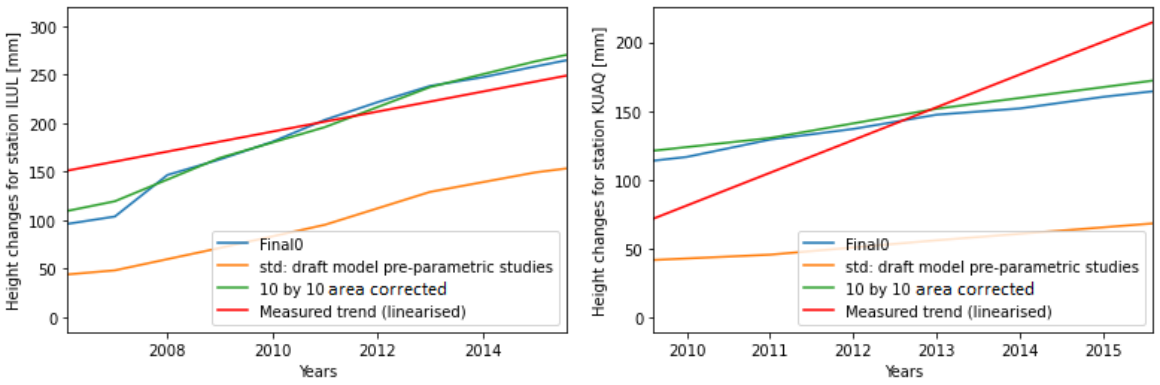

Figure 5.2: Continuation of Figure 5.1. Comparison of uplifts for stations ILUL and KUAQ, between the modelled and the measured (above). We also the results with the 10 by 10 area corrected setting from the Chapter 4, and with the original model from Subsection 3.2.1.

In the fit of all stations, with regards to the uplift rates, we find that the solutions from the simulation Final0 are not necessarily a better fit than all the ones shown previously, namely: the 10 by 10 area corrected run or the standard draft model from Subsection 3.2.1. Moreover, Figure 5.1 also demonstrates that the disparities between the modelled and measured uplift rates for all stations, are still there. In the graphs for the 4 GPS stations, it can clearly be seen that there is a more accurate fit for the GPS station JGBL, on the right of Figure 5.1. However, again, we find that the modelled uplifts lack in local accuracy.

For both of the issues mentioned in this paragraph, we can conclude that 3D varying viscosity profile is needed. This is because the uplift rate is accurate for some stations, namely the ones from 18 to 22 in Appendix A, but that for most stations, there seems to be a clear lack of uplift. As mentioned this lack of uplift, could be caused by the viscosity profile being locally, at the GPS station, different, or regionally, on the entire scale of Greenland. Moreover, another reason for this discrepancy could come from the ice history and the mesh: how the mesh translates the local changes in ice into uplifts. This last point is especially true for modern day ice changes, where the model may not be able to properly translate local changes in ice, into elastic uplifts.

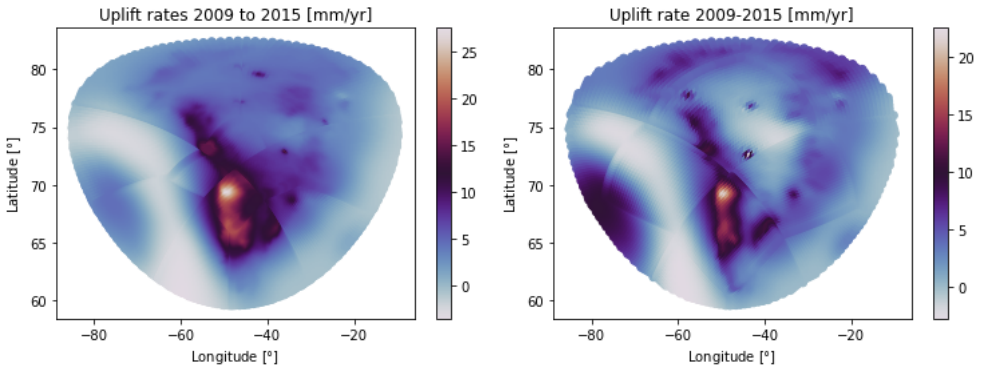

Figure 5.3: Mean uplift rates between 2009 to 2015 [mm/yr] for the Final0 model (left) and for the first hand results copied from Figure 3.4 (right), i.e. the draft model.

Figure 5.3 presents the mean uplift rates over the Greenland 'tight' region. These uplift rates can be directly compared to the first hand results in Figure 3.4, as Figure 5.3 is an improvement on Figure 3.4, thanks to the parametric studies. This way, we are able to visually assess the effect of changes on the model, decided in Chapter 4. In comparing both, it can be found that the greatest contributions that Final0 brings are that: the deflection velocities are generally higher, especially in the South and in the West of Greenland which is thought to be due to the higher resolution in Final0, and that there is a new 'high' uplift region which is on the West of Greenland at about 75 [°] latitude.

In general, this is something that can be seen in all of the results from Final0: the uplift rates are higher, and the deflections are larger too. In theory this is because the resolution is finer, and thus allows for higher loads, contrary to a coarser mesh, which has 'smoother' loads over large areas.

5.2.2. Dissociating 'short term' and 'long term' contributions to modern day uplift rates

In this subsection, we present, for Final0, the uplift rate maps when loads are not changed from 1914 onward, and compare this map to the Final0 map. We calculate the uplift rate from 1992 to 2019, as done in Chapter 7's modern day uplift results. This way we can assess the importance of the loads change since 1914 in our model by analysing their influence on final results for Final0.

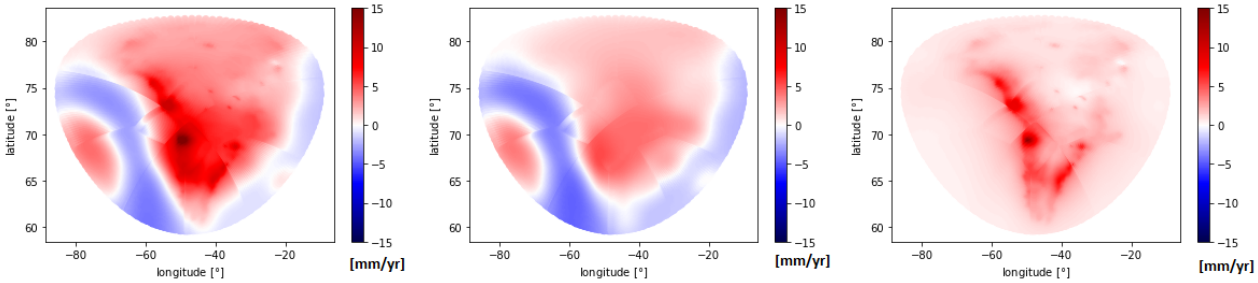

Figure 5.4: Deflection rates [mm/yr] from 1992 to 2019 for Final0 (left), for Final0 when loads from 1914 are removed (middle) and uplift rates caused by the ice changes since 1914 (right).

With Figure 5.4, we have first proven that using a unified ice history from 122000 years ago to 2019 on one GIA model is possible and useful; this is because the contribution in deflection rate from the loads change since 1914 is key for modern uplift rates. On average, the uplift rate from 1992 to 2019 due to changes in ice loads since 1914 contributes about 70% to the total uplift rates of Final0, over the same time period. The mean uplift rate for Final0 from 1992 to 2019 is 2.56 [mm/yr], when the load changes since 1914 bring a contribution with a mean of 1.80 [mm/yr].

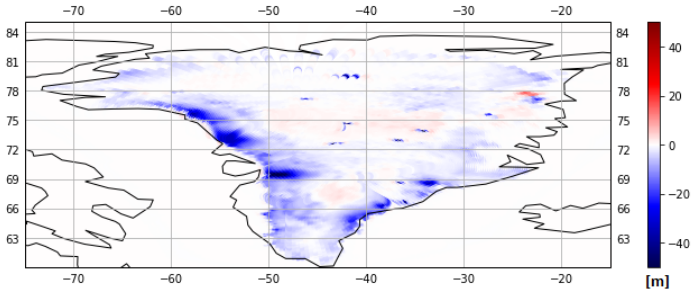

Figure 5.5: Ice height change from 1992 to 2015 [m]. This is used in all final models.

Moreover, we can conclude that the contribution in uplift from the load changes since 1914 is mostly located on the coastal regions. This is logical as the ice melts are mostly situated on the coastal regions, namely in the West (Kjeldsen et al., 2015). This and the fact the time since the loss of ice has not been high enough, point towards the fact that these modern ice change due uplift rates are mostly caused by elastic deformations; we can easily see from Figure 5.5 that the uplift rate due to ice changes since 1914, presented in the left most figure from Figure 5.4, is strongly related to the ice change from 1992 to 2019. Whether this present day elastic deformation is accurate or not is investigated in Chapter 7, along with the general accuracy of the model. However, we can already notice that the present day uplift rates due to ice load changes prior to 1914, the middle graphs in Figure 5.4, are simulated according to Final0 to be between -5 and 5 [mm/yr], which is similar to the uplift rate due to 'long term' ice changes in Simpson et al. (2011); these are between -6 and 6 [mm/yr] including deformations due to ocean loads. Hence, we can already hypothesis that the elastic deflections are underestimated as we know that the total uplift rates at various GPS stations are underestimated, as seen in Figure 5.1. Lastly, as pointed out in Chapter 4's study on surface resolution, we know that we are close but that we have not yet reached a convergence point in terms of tangent to surface resolution. Hence, this hypothesised underestimation in elastic uplift may be due to this lack of surface resolution.

5.2.3. Finer and 'tight' region 'long term' statistics

Although the deflections present are solid Earth deflection, we take into account the fact that relative sea level records can only go accurately to about 10 to 15 thousand years ago. Hence, we present the deflections over the past 10000 years. We do this because this allows expert readers to then trace back, with the help of sea level estimates, the accuracy of the results presented here.

Table 5.1: Statistics of the deflection in 2019 with respect to the deflection 10000 years ago, for the finer region.

	Deflection statistics [m]
Mean	43.17633066
Min	-58.29338455
Max	611.7326355
Std	74.61701891

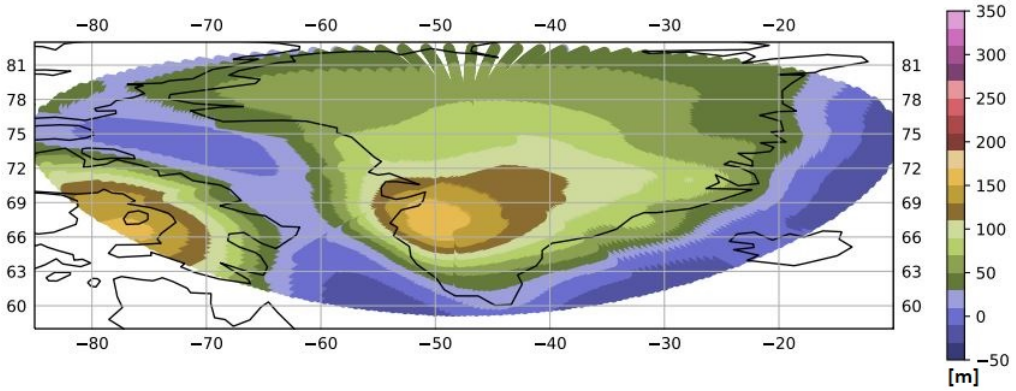

Figure 5.6: Simulated deflections [m] in the finer region from 10000 years ago till now in 2019. Plotted on a latitude longitude grid.

The deflection in the last 10000 years, is mostly positive over land, that is in the direction outward from the Earth's centre. Moreover, we find that the deflection in Greenland is equivalent to that of the region of North America directly across the sea. This is logical, as the sheet of ice of North America was exposed to the same coastal regions as the West of Greenland. The deflections in Figure 5.6 are slightly different to the ones in Table 5.1, as the figure only takes into account the 'tight' region.

6
Inclusion of the 3D viscosity

For these preliminary results, with respect to the Master Thesis question, the draft model from Subsection 3.2.1 will be used. Hence, it is the model prior to the parametric studies which is here used, while loading ice height differences w.r.t. to ice heights at 122000 years ago.

When investigating the viscosity, we aim to diversify the type of profile. As such, the previously used one dimensional viscosity, is put aside in favour of two three dimensional viscosity profiles: an 'upper bound' and a 'lower bound'. Due to the fact that a simulation runs with a three dimensional viscosity, it takes considerable more computation time; therefore only two 3D profiles were tested.

6.1. Set up

There are four model results which are compared in this study: the draft model with a 1D viscosity profile of 1e22 [Pas] in the upper mantle instead of 1e21 [Pas] as done in the draft model from Subsection 3.2.1, the draft model, the draft model with an 'upper bound' estimation of a three dimensional viscosity profile, and the draft model with a 'lower bound' estimation of a three dimensional viscosity profile. Again, note here that this version of the draft model is slightly different to the original one from Subsection 3.2.1 due to the fact that the load differences with respect to the ice heights at the start of the simulation are used. The 3D varying viscosity profile generation is shortly summarised in Section 2.2. As building the viscosity/creep model is not part of this thesis and was done by authors of Ivins et al. (2021), the model itself is not elaborated in detail in this Master Thesis. However, if more is wished to be learned by the reader on this viscosity model, it is strongly encouraged to read Ivins et al. (2021) and Fullea et al. (2021).

The following 3D varying viscosity models were obtained, using the creep generation algorithm presented in Section 2.2, for the first 420 [km] depth. The set up for the lower bound viscosity profile was a grain size of 10000 [μm] and a water content of 1000 [ppm] when the set up for the over-estimated 3D viscosity profile was a grain size of 100000 [μm] and a water content of 50 [ppm].

Although, we are aware that a grain size of 100000 [μm] is extremely high, and even unrealistic, this is done on purpose, in order to obtain a viscosity model which is either at or slightly further the boundary of realism. This way we can really study the effect of implementing a 3D varying viscosity profile in a GIA simulation over Greenland. The 'lower bound' estimated profile, or also referred to as a the wet diffusion profile, is already more realistic, and aims to be more accurate, but also different enough from the 'upper bound' so that low and high 3D viscosity profile estimations can be compared.

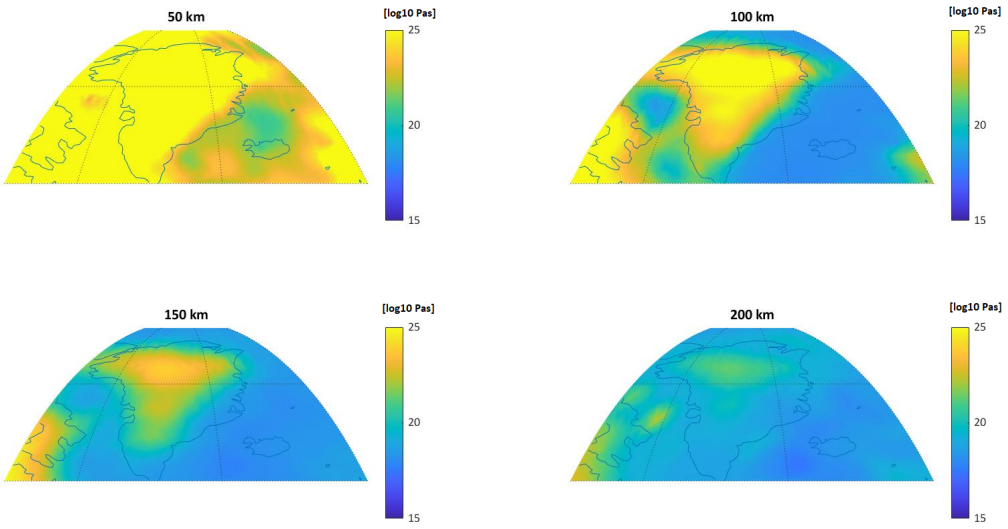

Figure 6.1: 'Lower bound' estimation of the 3D viscosity profile of Greenland [$log10Pas$].

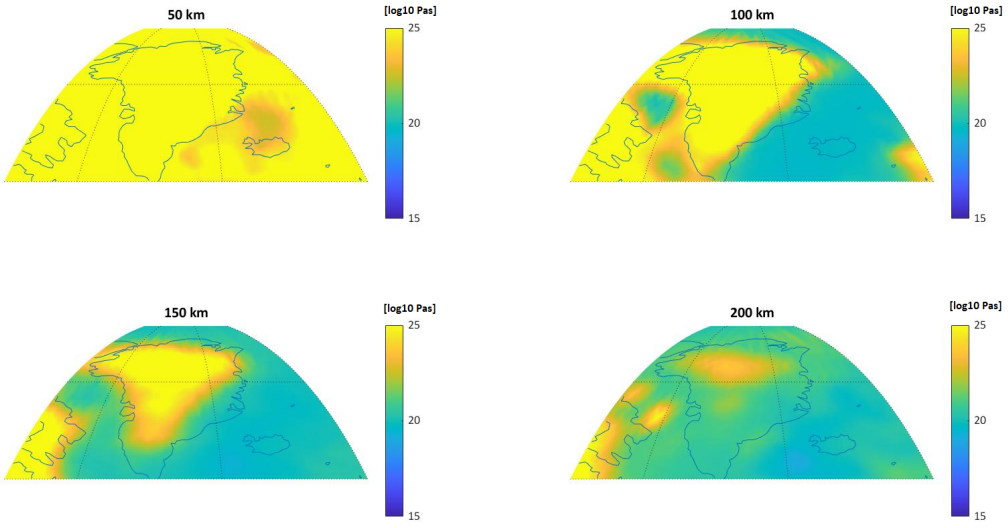

Figure 6.2: Continuation of Figure 6.1. The 'upper bound' estimation of the viscosity profile.

In order to develop the values of the viscosity maps, we used Khan et al. (2016) as a reference, which provided accurate results with a 1D viscosity profile and a 1D model. This study had viscosities in the upper mantle, which is mostly represented by the viscosity profile at a depth of 200 and 150 [km], between 2e20 and 5e20 [Pas]. Therefore, for the 'lower bound' estimation, we aimed to have most of Greenland's viscosity points at depth of 150 and 200 [km] to be below the 1e20 [Pas] viscosity threshold. Concerning the 'upper bound', the same method was replicated but in this case, in order to get most points above 1e21 [Pas].

The thought with these two profiles, is that the 'upper bound' will be better suited for taking into account the effect of ice melting during the de-glaciation era, and the 'lower bound' profile will be more sensitive to the changes in ice heights closer to today.

Finally, additionally to these two 3D viscosity profiles, we also test another one dimensional viscosity profile, which overestimates the viscosity in the first 400 [km], by implementing a viscosity of 1e22 [Pas] there. It is an

over estimation as we know that the viscosity in Greenland is according to Khan et al. (2016), which managed to fit the modern uplift rates to modern measurements, and according to Lecavalier et al. (2014) most likely lower. However, because we wish to have multiple scenarios to compare in the final results, in order to asses the impact of using a 3D viscosity, and to consider a wide range of plausible solutions, we include it as a profile to be tested.

It is also interesting to note that that this last 1D viscosity profile set up, is close to the over estimation at 200 [km] depth using the 3D viscosity profile.

6.2. Results

As done in the previous parametric studies, we can present the results through the prism of the uplift rates in the last three decades, from 1992 to 2019 at the four already used GPS stations.

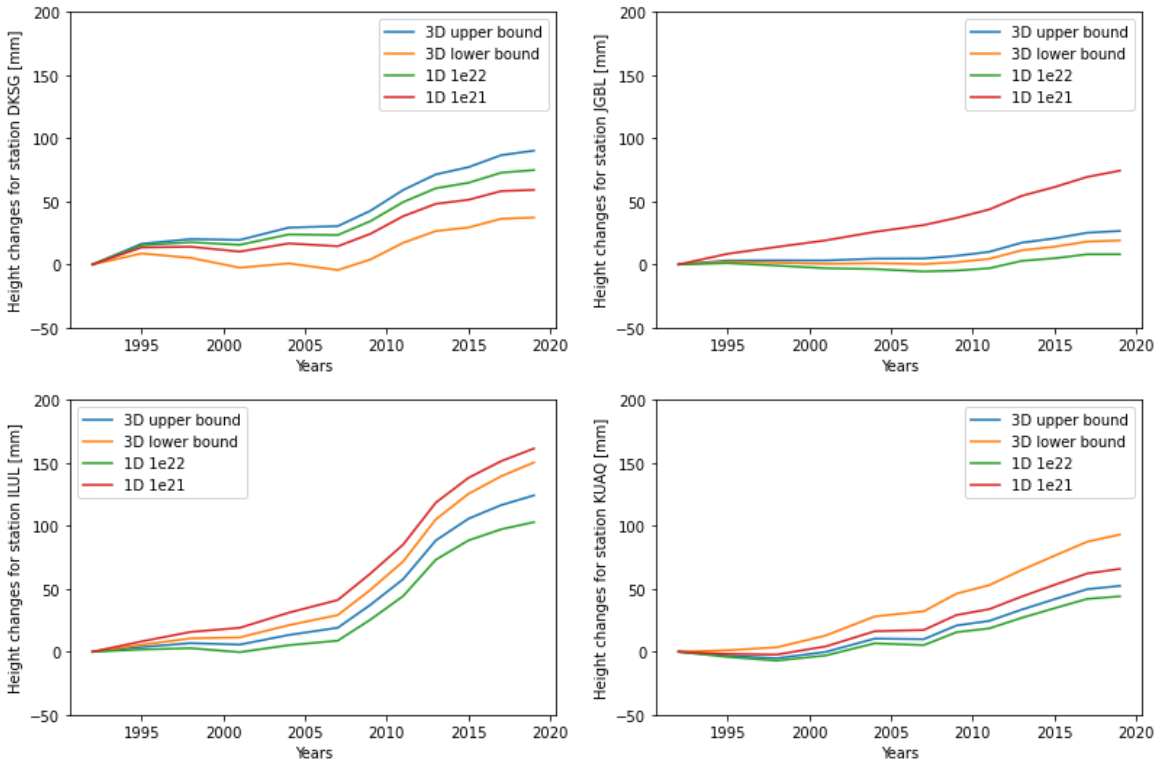

Figure 6.3: Variation of the uplift trends since 1992 at four GPS stations: DKSG (top left), JGBL (top right), ILUL (bottom left) and KUAQ (bottom right). The '1D 1e21' setting is the same as the draft model, but with the ice height difference w.r.t. the ice height 122000 years ago loaded in the simulation.

When analysing Figure 6.3, three major aspects can be noticed, and from which we can make conclusions. Firstly, the 3D viscosity profiles do make a large difference, whether it is the lower bound or upper bound profile. The 3D viscosity profile, for all four GPS stations, although it may have a higher overall mean and maximum viscosity compared to the 1D viscosity draft setting in the case of the over estimation, the 3D profile generally still yields overall a smaller uplift since 1992. This maybe because in the developed viscosity maps, below depths of 150 [km], all four GPS stations have viscosity lower than 1e20 [Pas], which is smaller than both 1D model viscosity at those depths.

A second aspect which can be noted from the deflection analysis is that varying a one dimensional varying viscosity by whole magnitude, does not provoke significant changes in the mean uplifts for the past 10000 years of deflections. Although locally the changes might be noticeable, as proved in Figure 6.3, the mean of the uplifts in the finer region does not change nearly at all. Instead, it is the how the data is distributed which changes. The variation of the standard deviation of the deflections changes more when the 1D viscosity profile is varied then when the 3D viscosity profile is varied, varying by about 14 [m] and 6 [m] respectively. Same is true for the variation of the minimum and maximum of the data, which varies by about 19 [m] and 23 [m] for the minimum and maximum between the 1D models, and for the 3D models by 3 [m] and 4 [m] respectively.

A third aspect we can note is how the station's uplift compared with each when the viscosity is varied. For instance we notice that the lower bound model uplift at the locations of the ILUL and KUAQ stations is higher since 1992 than he upper bound model uplift, which is due to their a lower viscosity, and therefore a supposed strong recent ice melt, possibly in the past few thousand years. For the DKSG station, the uplift maybe stronger for the upper bound model, perhaps because there has not been large recent ice melts. Lastly, the response of the upper and lower bound 3D models is similar at the JGBL station, as there has not been large ice mass changes there in the past centuries and millennia. The difference between the 1D models at JGBL may be due to external factors which need more investigation.

7
Final results & Discussion

Before concluding this report, we should present the final results, for the four viscosity profile settings, that is: Final0, Final1, Final2 and Final3. Final0 and Final2 are the 1D viscosity profiles, 1e21 [Pas] and 1e22 [Pas] between 70 and 420 [km] depth respectively, and Final1 and Final3 are the higher and lower bound viscosity profiles for the upper mantle and lithosphere, developed in Chapter 6 using the viscosity model presented in Section 2.2.

The results will be presented through the deflections in the last 10000 years before present till 2019, as this is often a benchmark in GIA studies due to the fact that accuracy beyond 10000 years ago is smaller. The results will also be presented through the modern day deflection rates, that is the uplift rates since 1992. This is useful because there are GPS measurements for these uplifts since about that time. Also 1992 is the year where we start to use significantly more detailed ice mass data, hence we expect higher elastic accuracy from that point on. Adding on, we can also present the results, through the four GPS station's uplifts used this far, a reminder that these are the DKSG, JGBL, ILUL, KUAQ stations from Appendix A (Khan et al., 2016), in order to properly compare the data outputs with the active measurements. The reasoning behind their specific choice is explained at the start of Chapter 4.

Finally, a detailed discussion will accompany these results, in order to better explain them, and provide clues for the conclusions and recommendations chapters. Namely, an in depth discussion is present for the deflection in the South-West of Greenland.

7.1. Computation times

First we should compare the computation times between Final0, Final1, Final2 and Final3, and the respective evolution from 25 by 25 [km] to 10 by 10 [km] resolution. This section aims to inform any reader who would wish to replicate or improve these results. The run times for the four final models are shown below. The reader should note that TU Delft's servers was used here, with 21 Abaqus licenses.

- Final0: about 40 hours
- Final1: about 2 weeks
- Final2: about 30 to 40 hours
- Final3: about 3 weeks

Although the 1D draft model runs in Chapter 6 have less time steps than Final0 and Final2, 35 against 57, the draft model only took 15 hours while Final0 and Final2 took 30 to 40 hours. The draft models with 3D viscosity took 4 days and 1 week while Final1 and Final3 took 2 and 3 weeks. It should also be noted that in the draft model, the 14 last steps take fewer computation time as they are shorter, and in the final runs it is the 20 last time steps which do so.

We can therefore stipulate that passing from 25 [km] resolution to 10 [km], while changing the amount of time steps from 35 to 57, changed the time taken by a factor of 1.8 to 2.3, depending on the type of viscosity profile. Introducing a 3D varying viscosity profile increases the time taken by a factor of 11.2 to 12.6, depending on the resolution used. Higher resolutions tend to increase in time, proportionally, if a 3D varying viscosity profile is used.

7.2. Deflections from 10000 years ago till 2019

We can now present the uplift results for the total uplifts between 10000 years ago till 2019. The maps for the uplifts are presented in Figure 7.1, and the range of simulated values is presented in Figure 7.2.

In order to get a high level overview of the results, Figure 7.1 presents the maps of Greenland for each final run, with the net deflection since 10000 years ago till present day 2019.

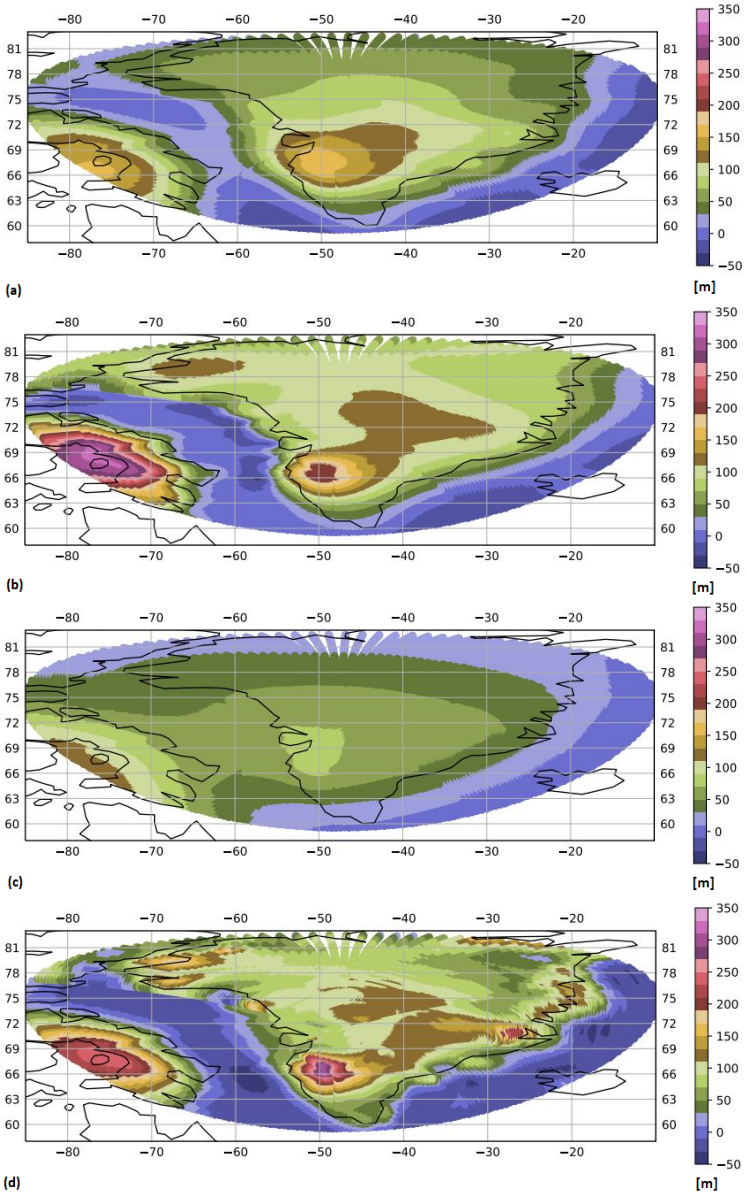

Figure 7.1: Uplift maps [m] since 10000 years ago (before present) till 2019, for final0 (a), Final1 (b), final 2 (c), final3 (d), for the 'tight' region. This plotted on a longitude, latitude grid.

In Figure 7.1, the main difference between the two 1D viscosity profile models is the intensity of the uplift since 10000 years ago. The model which has a constant viscosity of $1e22$ [Pas] between 70 and 420 [km] depth, Final2, has a smaller uplift in the last 10000 years. This is due to the fact that Earth layers with a higher viscosity, have a higher response time to load changes on the surface. Thus, the model with the larger 1D viscosity, has not yet had the time to fully react to ice load changes previous to 2019. This can be the de-glaciation period, from 17000 to 1000 years ago, but also to ice changes in the last 10000 years.

The two 3D varying viscosity profiles differ by the magnitude and resolution of the total deflections over the past 10000 years. In Final3 results, we see a more detailed map, which shows overall higher uplifts, namely in the South-West and coastal regions, and a more varying uplift response. This may be due to Final3's lower viscosity profile than Final1, and hence its ability to react to ice changes quicker. These load changes are presented in Figure 7.8, between 4500 and 100 years ago, and may explain the strips in the Final3 results: part (d) of Figure 7.1. Figure 7.2 presents the range of deflection values estimated between the models.

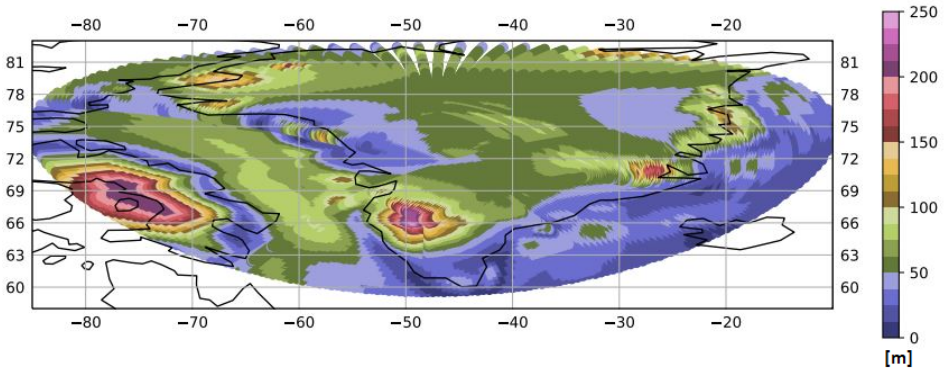

Figure 7.2: Range of uncertainty in uplift [m] since 10000 years ago (before present) between all four final models, for the 'tight' region. This plotted on a longitude, latitude grid.

7.3. South-West of Greenland: highest uplift region during de-glaciation

Through studying Figure 7.1 and Figure 7.2, it becomes apparent that the South-West region, just as later for the present day uplift rate, displays unique characteristics when compared with the rest of Greenland. During the last 10000 years it has the highest deflections, whether that is in Final0, Final1, Final2 or Final3. However, Final1 and Final3 present by far the largest positive uplifts in this region.

A first point which should be made, when analysing deflections in the South-West region, in the last 10000 years before present, is that the ice melt in this region is the quickest and most abrupt ice melt, when compared with other regions of Greenland, see Figure 7.9 in Section 7.6. This brutal ice melt, between about 13000 and 5000 years prior to the present times, can be attributed to the Holocene Thermal Maximum, when the temperatures were roughly 2.5 [$^{\circ}C$] warmer than today, as shown in Figure 7.3. This sudden increase of temperatures mostly affected the South-West region, where the ice present after the retreat was at some instances lower than today's ice masses (Simpson et al., 2011), reaching 80 [km] retreats along the surface over the Holocene Thermal Maximum. Moreover, the ice loss during the de-glaciation is there, in the South-West, quite extensive, where the mean ice height drops nearly 1 [km] in just 15000 years, which can be seen in Figure 7.9. Furthermore, contrary to the region North of it in Greenland, called region 3 in Figure 7.9, the South-West ends its de-glaciation closer to our time frame, which is at 45000 years before present. Hence, a higher viscous response is present from this region, than in any other in Greenland during the time frame upon which the maps in Figure 7.1 are plotted.

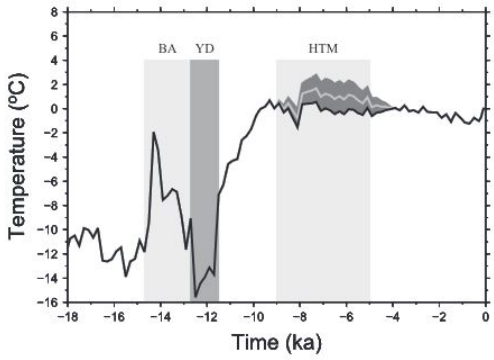

Figure 7.3: Temperature function used in the development of the Huy3 ice model and directly taken from Lecavalier et al. (2014). Bølling-Allerød (BA), Younger Dryas (YD), and Holocene Thermal Maximum (HTM) are climatic events labelled here. The Huy3 model was developed within the grey region during HTM (Lecavalier et al., 2014).

We can already state here, something which is discussed in more detail later in order to explain the modern day uplift rates, that the 3D varying viscosity profiles are more sensitive to ice changes; in the sense that they have higher overall displacements within the same time frame and with the same loads than the 1D viscosity models. This is because they display higher uplifts, in reaction to the same ice load changes, in the same amount of time, as the 1D varying viscosity profiles. This is thought to be due to their laterally varying viscosity, as the 3D

upper bound viscosity profile, Final1, has clearly higher uplifts then Final0, although it has overall a higher or equal viscosity in Greenland until 200 [km] depth as seen in Figure 6.2. See Chapter 6 for the associated 3D varying viscosity maps.

However, the 3D lower bound viscosity profile, has a more varying uplift map than the upper bound 3D. This is also true for the South-West region. This particularity is thought to exist because the under estimated viscosity profile, Final3, has a lower viscosity for its mesh elements, and thus reacts with a quicker and stronger deflection reaction to ice load changes than the upper bound profile. This is also seen in Figure 7.6, where Final3 always reacts the fastest and the strongest to ice changes. The recent ice melt in Greenland, which creates the peak in the South-West region happens, between 10000 years ago and 5000 years ago, over a low viscosity region. Thus, the deformations are high, and happen within a smaller time frame than other models, especially over the South-West region.

7.4. Disparities in other regions: during de-glaciation

We can also investigate the central region of Greenland, the West and East extremities of region 4, as defined in Table 7.1, and the sea regions around Greenland.

The central region's deflections varies most between the 3D and 1D profile category than within the settings for each dimensional type of profile. This is due to the fact that the highest viscosity region in the 3D varying models is located in the centre of Greenland, as depicted back in Figure 6.1 and also viewed in the temperature profile used in the model and shown in Appendix D, while the 1D viscosity profiles do not have, by definition, this large region of higher viscosity in the centre of Greenland. This region of disagreement between types of viscosity profiles in deflection is mostly represented by the dark green region in Figure 7.2.

Concerning the North lighter green and East-West coastlines of the Norther most region of Greenland, above 75 [°] latitude, in Figure 7.2, the differences there can be explained by the fact that, this area, called region 4, undergoes a small increase in mean ice height during the 4 to 5 thousands of years prior to present day, as seen in Figure 7.9. This increase in ice height between 4500 and 100 years ago is also seen in Figure 7.8. This fact, in combination with lower viscosity from depths of 150 [km] for the 3D models, as seen in Figure 6.1, results in disparities of prediction in Figure 7.2, mostly coming from the Final3 simulation which has the lowest viscosity below 150 [km] depth in this region.

A final point which can be made is that the during the Holocene Thermal Maximum, the ice retreat in the North is smaller (Simpson et al., 2011), and thus creates a smaller uplift rate than in the Southern region, therefore having a total uplift during that period which is smaller than in the South or Centre of Greenland. This change in ice load is better represented in the 3D models, as they have higher viscosity, about 1e22/1e23 [Pas], in those regions, above 150/100 [km] depth than the 1D models. Hence they have a longer reaction time to these ice load changes. The underlying point is then that the uplift velocity is smaller then the down-lift velocity at the extremities of the North most region, for the 3D models, when they are more similar in the central part of the North most region. Rather, the 1D models do not see as much this clear disparity in deflections between the central and coastal regions, especially for Final2.

Lastly, the sea regions west of Greenland, as mentioned previously, see a difference due to the fact that they have a lower viscosity in the 3D varying viscosity profiles than in the 1D varying viscosity, and also because they are not loaded with the same ice masses as the lands. However, it should be noted that the disparity between the models takes mostly place in the sea region between North-America and Greenland, where the 3D profiles can vary up to 10000 [Pas] difference between land and sea, when the 1D models are constant through out the land sea separation .

7.5. Deflections from 1992 to 2019

The same process as in the previous two sections can now be repeated for the uplift rate maps for modern day deflections, resulting from the four final models which the ice history from 122000 years ago to 2019. These are presented for the years 1992 to 2019 in Figure 7.4, including total range of predictions map, Figure 7.5, while also discussing the uplift rates at certain stations and the reasons why a negative rate is observed in the South-West region of Greenland in models Final1 and Final3, as done in Section 7.6 .

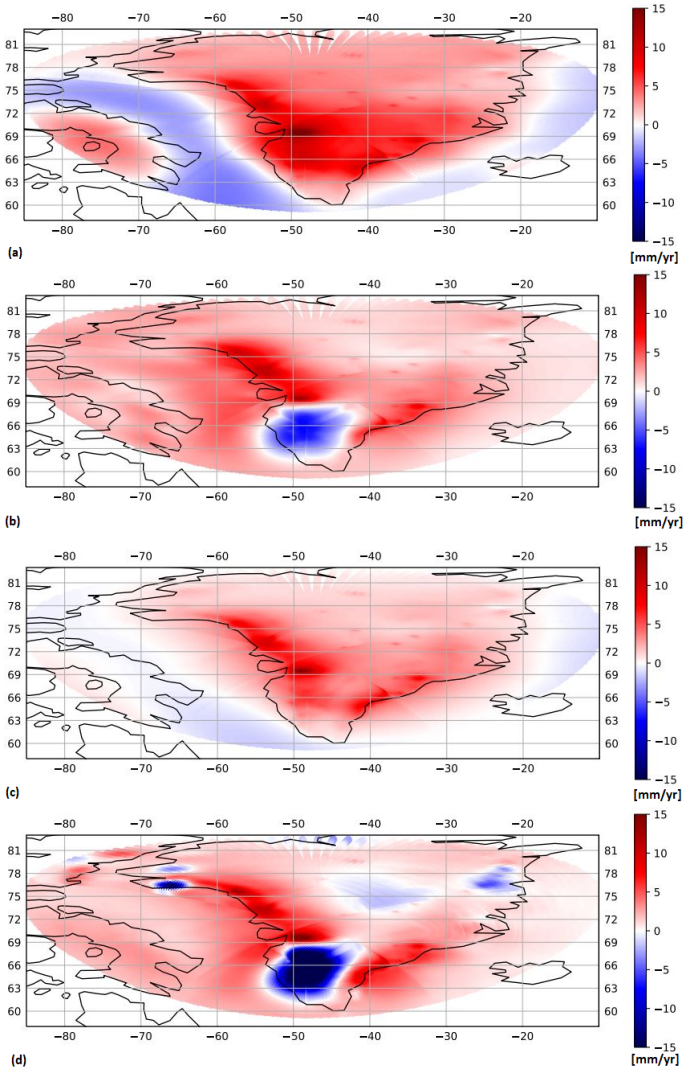

Figure 7.4: Rate of uplift maps [mm/yr] since 1992 till 2019, for Final0 (a), Final1 (b), Final2 (c) and Final3 (d).

Similar to the comparison of the Final0 and Final2 models in the previous sections, alike conclusions can be drawn here for the uplift rates between 1992 and 2019. The difference between the two models, is purely on the intensity of the values for the uplift rates. The higher viscosity model, has a lower uplift rate. This is due to its higher reaction time. We can here stipulate that its uplift is slower because it might not yet be fully reacting to ice load changes between 5000 years before present till now, whereas the lower 1D viscosity model is already reacting to those load changes. We should also note that the downward deflection which took place before de-glaciation was also smaller for the higher viscosity model. Hence, it also 'needs' to cover a smaller amplitude of deflection.

The behaviour change between the two models which use 3D varying viscosity profiles, Final1 and Final3, is the same as for the ones which use 1D varying viscosity profiles. From Figure 7.4 we can clearly see that the major difference between Final1 and Final3 is the intensity of the uplifts and down-lifts. The positive uplifts tend to be greater, and the negative uplifts tend to be further negative. However, this is not as clear of a difference, between the two models, then with Final0 and Final2, as seen in Figure 7.12. At some GPS stations, on the coastlines, although the uplift was positive, Final1 still has higher uplift rates. This difference in observation, between the two 3D varying viscosity models and the two 1D varying viscosity models, is certainly due to the lateral variations in viscosity present in the 3D viscosity models. The lateral variations in viscosity in the 3D viscosity models clearly react more to the ice height changes in the time frame 4500 years ago till 100 years ago, as the pattern is similar between Figure 7.4's Final1 and Final3 graphs, and Figure 7.8. I.e., the 3D viscosity models react more strongly to recent ice changes.

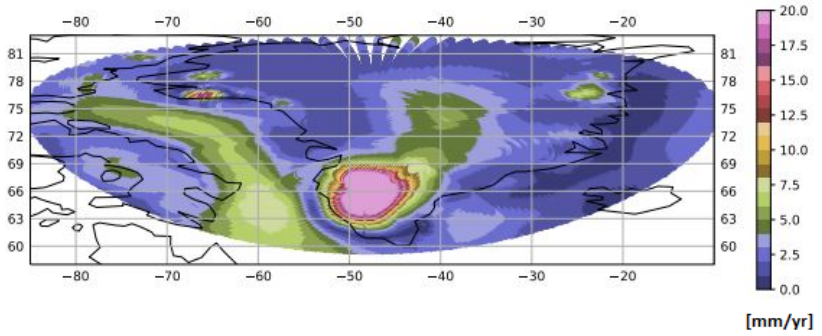

Figure 7.5: Range of mean uplift rates simulated [mm/yr] across all four final models, from 1992 to 2019.

There are then multiple differences, interesting to note, between the models which have the 3D viscosity profile and the 1D viscosity profile in the upper mantle. The effect of these differences is dominating in Figure 7.5. Firstly, the run Final0 and the run Final1 have similar magnitudes of uplift rates between 1992 and 2019, except for the uplift rate in the sea regions and in the South-West of Greenland. This entails that in Final0, just as in Final2, it is where the loads are placed which determines the areas of uplift, whereas in the 3D varying viscosity, where the uplift is more spread across regions which do not have land, the uplift rate is more influenced by the lateral variation in viscosity which in turn react with a larger deflection in accordance with the ice height changes, as made evident in the South-West. As the viscosity varies vastly across Greenland, so does the uplift rate, but because it does not vary as much on the regions covered by sea, the uplift rate is there more homogeneous and similar to the uplift rate of areas with similar viscosity in Greenland. See Figure 6.1 for a reminder on the 3D viscosity profiles over Greenland. Also, see Section 7.6, the next sub section, for a detailed explanation on the South-West negative uplift region in Final1. The higher 'convergence' time for the 3D varying viscosity models is discussed below.

7.6. The negative uplift rate region in modern times in Final1 and Final3

In this section, we can take the time to explain what appears as an anomaly in the results, which is present in Figure 7.5 and Figure 7.4 in the figure for Final1 and Final3. The anomaly there is a negative uplift rate region in the South-West of Greenland between 1992 and 2019. Reasoning this apparent specific anomaly can help us better understand our model, and other results too. Furthermore, after reasoning and explaining it, we should compare our conclusion to both literature and measured uplift rates about/in the region, in order to better understand how the model could be improved further on.

In order to properly analyse this phenomenon, we need to plot the deflections of this region, on a long and shorter time scale, and compare it to the trend in the whole of Greenland, as done in Figure 7.6. Notice that the change in trend in the last 4500 years in the Final1 and Final3 models corresponds to the negative uplift region.

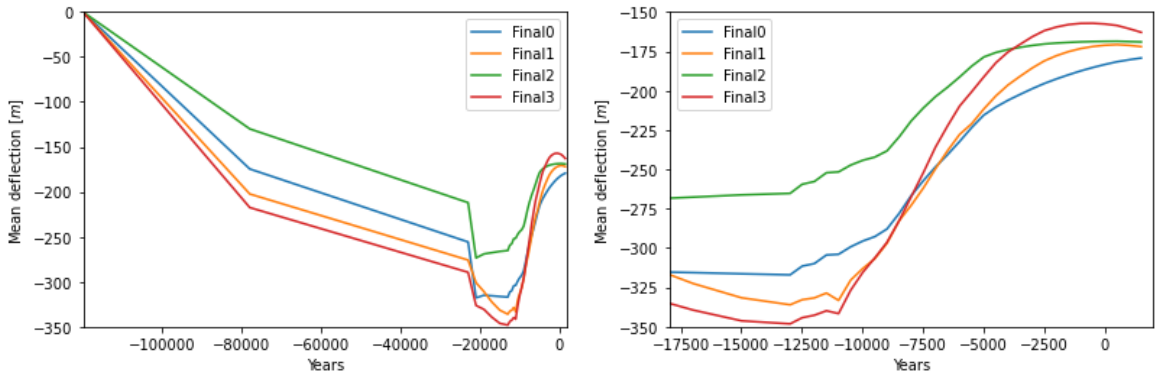

Figure 7.6: Mean deflections in the South-West region through the whole simulation (left) and in the last 20000 years (right). The definitions of these regions is shown in Table 7.1.

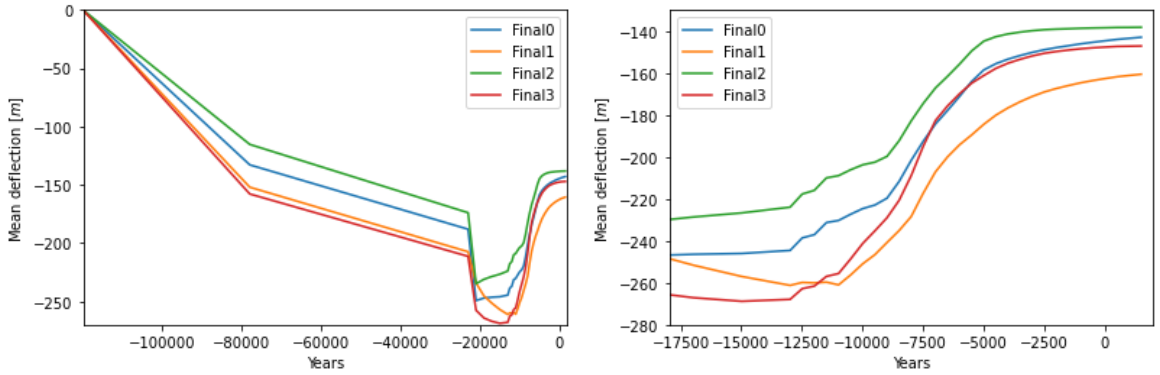

Figure 7.7: Continuation of Figure 7.6. Mean deflections through the whole simulation for the whole of Greenland, respectively left and bottom right graphs. The definitions of these regions is shown in Table 7.1.

There are thought to be two main reasons, which work together, to explain this anomaly. The first is the fact that the 3D viscosity profiles are more sensitive to ice changes, although they have a higher viscosity in Greenland than the 1D profiles at depths between 100 and 150 [km]: ranging from 1e24 to 1e25 [Pas] against 1e21 to 1e22 [Pas]. What is meant by sensitivity is that they have a larger deflection response in the same time frame as the 1D models. This can clearly be seen in all the graphs in Figure 7.6. The Final1 and Final3 curves have higher amplitudes, and achieve these higher amplitudes much faster than Final0 and Final2. This reason is important to consider in order to explain the trend of the two 3D profiles. However, this aspect should in principle alarm us, as we know the viscosity to be higher at shallow depths in the 3D upper bound model than in the 1D models. The first explanation we can present is that lateral variations in viscosity seem to make the entire profile more sensitive although its viscosity is larger in shallow depths. For the Final3 model results we can also bring forward that the viscosity profile below 150 [km] depth in the upper mantle, which we know to be about 1e18/1e19 [Pas] in the South-West region, may also cause this more rapid reaction to load changes. For Final1, the viscosity in the South-West below those depths in the upper mantle is more similar to the 1D profiles: about 1e21/1e22 [Pas]. This is extremely interesting to note.

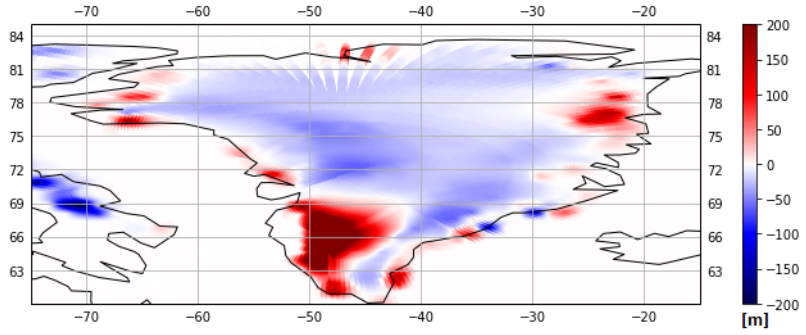

Figure 7.8: Ice height change between 45000 years ago till 100 years ago, from Huy3 (Lecavalier et al., 2014). This is used in the models.

The second main reason is that the South-West region entered about 4.5 thousand years ago a period of increase in ice history by the end of its de-glaciation era, with a large increase in mass, as seen in Figure 7.8. In Figure 7.6's top right figure, we see that all curves enter a stabilising phase about 7000 years ago, around year -5000 B.C. As discussed previously, this is due to the de-glaciation phase induced uplift rate gradually decreasing. The increase in mass in the South-West region lasts between 4500 and 100 years ago, and is thought to be due to the slight decrease in temperature between 6500 and 4000 years ago, as seen in Figure 7.3. The increase in ice spans most of the area and has a magnitude on average of 10 to 200 [m]. Furthermore, because of the general lower viscosity of the South-West region compared to the rest of Greenland in the 3D models, as seen in Figure 6.1 and Figure 6.2, and its viscosity of 1e18/1e19 [Pas] below depths of 150 [km], we believe that this increase in ice created this negative uplift region.

This increase in ice mass is also visible in Figure 7.9, where the South-West is substantially the only region

which sees its mean ice height increase after de-glaciation. It is interesting to note how the increase in mean ice height in Figure 7.9 directly finds a correlation in Figure 7.6, i.e. it is the inverse graph: when ice forms in Figure 7.9, the deflection towards the centre of the Earth increases in Figure 7.6.

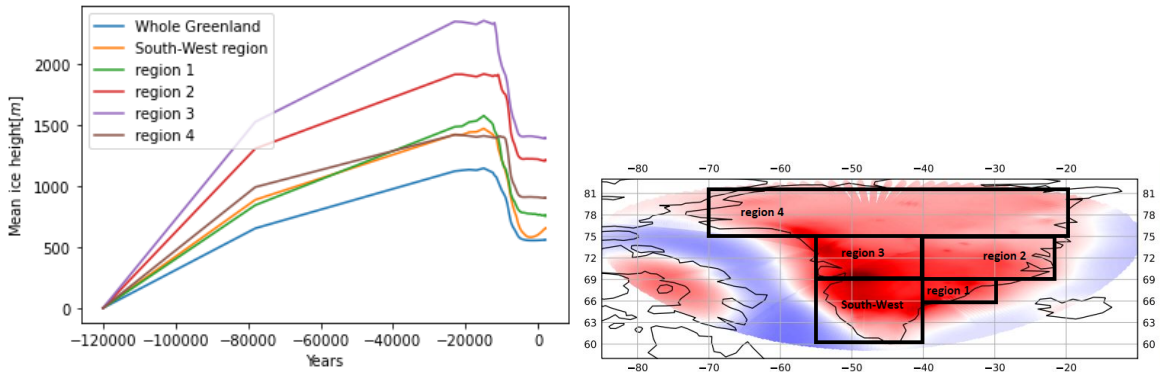

Figure 7.9: Time series of mean ice height loaded in the simulation in different regions in Greenland, as defined in Table 7.1 (right), and map of regions (left).

Moreover, as described and explained, the 3D viscosity profiles have higher sensitivity to the same load changes than the 1D viscosity profiles. However, they also have a higher convergence time, which is thought to be due to the higher variations in viscosity. Hence, because of the 3D nature, more points can move differently to each other, as they have different physical Earth characteristics, and it is thought then that the overall system may take longer to come to equilibrium because of this.

Below, in Table 7.1, the regions used to analyse the ice height variations are defined. Important to note is that these cover nearly all of Greenland, and that region 3, a region of large variations is situated just up north of the South-West region. Note: the regions were designed to cover all of Greenland, and 'nearly' is used just for precaution.

Table 7.1: Definition of the regions of Greenland used in Section 7.6 for the explanation of the negative uplift rate region, between 1992 and 2019, in Final1.

	Latitude [°]		**Longitude [°]**	
	Maximum	**Minimum**	**Maximum**	**Minimum**
Whole Greenland	82	61	-15	-73
South-West region	69	61	-40	-55
region 1	69	66	-30	-40
region 2	75	69	-25	-40
region 3	75	69	-40	-55
region 4	82	75	-20	-70

All of these reasons, lead us to hypothesis that the ground in the South-West region is now deflecting downward because: the uplift rate due to de-glaciation was starting to come to equilibrium, after a strong and long de-glaciation phase; which combined the high reactivity of the 3D viscosity profiles and the quick formation of ice between 45000 and 100 years ago, about 10 to 200 $[m]$ on average, 'kick started' a negative uplift rate era in this region. All of the reasons specific to the South-West region are made possible because of its relatively low viscosity compared to the rest of Greenland in the 3D models, as well as its lower viscosity than the 1D models beneath depths of 150 $[km]$ for Final3.

The negative uplift region, can also be explained through both measurements and literature, as done below. While measurements are more comparable to the simulated uplift rate values, they are more scarse and do not give an insight into the behaviour of this negative uplift region in time. For the 'literature' part of this subsection the papers by Simpson et al. (2011) and Lecavalier et al. (2014) are used.

The negative uplift region in the South-West is right over two GPS stations which have a modelled negative uplift for ”GIA” (viscous) response (Khan et al., 2016), in the order of magnitude of -1 $[mm/yr]$. The reason here, for such a large down-lift rate both in Final1 and Final3, which is respectively about -3 and -7 $[mm/yr]$, could, as explained above, stem from the 3D varying viscosity. There are two possible reasons for this, that can both coexist together.

The first reason for such a low and negative uplift rate in the South-West region since 1992, is the fact that the elastic uplift is not modelled in an accurate enough manner. This could be due to a too large mesh, as elastic changes are instantaneous and ice loss is extremely discrete. As the elastic deformations are now smoothed out over a mesh with several kilometres resolution, the proper local effects of elastic changes can not be properly accounted for. Thus, there is a need for a more refined ice history since at least 1992 if not 1972, both in time and space, and a corresponding refined mesh. The final models were loaded with a resolution above Greenland of minimum 10 by 10 $[km]$, which we here deem too coarse. This was pointed in Chapter 4's Figure 4.5, where the 10 by 10 $[km]$ resolution was identified as close to the convergence point, but still not fine enough. *Note: We still assume that the number of mesh points are the number of loaded points for future work.*

The second is that the 'long term' ice history for this South-West region is not accurate enough. This lack of accuracy could be due to the fact that it was developed with a 1D varying viscosity profile, or that there was another mistake in the development of the model.

In literature, it becomes apparent, that an area of negative uplift is not a coincidence in this region. For instance, given Figure 7.10 (Simpson et al., 2011), it seems that when modelled, there is a negative viscous response in the South-West region.

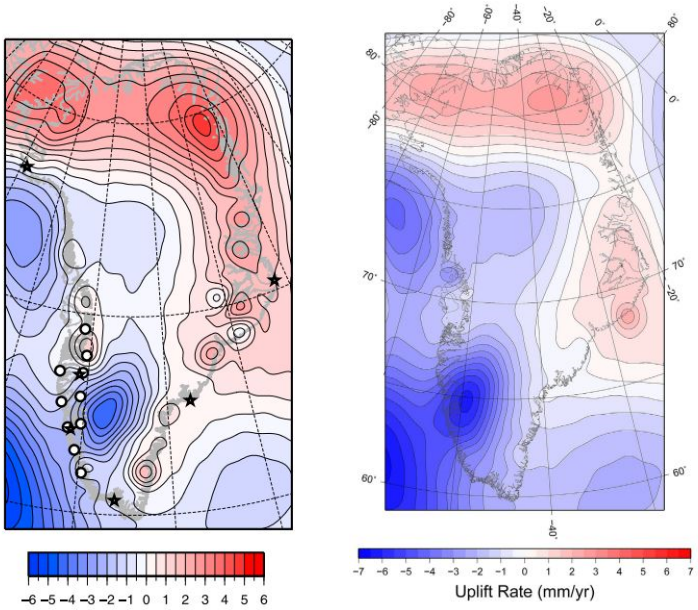

Figure 7.10: Right taken from Simpson et al. (2011). It is the uplift rates generated using the Huy2 ice history (left) and from Lecavalier et al. (2014) using the Huy3 ice history (right), also taken directly from the paper.

Both maps in Figure 7.10 display a negative uplift area in the South-West. We can here proceed to point out the similarities between these two papers, with respect to viscosity profiles, and our 3D models, in order to obtain possible clues for the existence of the down-lift region in the South-West of Greenland. From the start we knew that the main driving reason for this negative uplift rate region was the viscosity profile, as the 1D models in the final runs do not have this negative uplift region.

Both maps, from Lecavalier et al. (2014) and Simpson et al. (2011), have a viscosity of 5e20 $[Pas]$ from about 120 to 670 $[km]$ depth. We know that in our lower bound 3D viscosity model, Final3, the viscosity at the depth of 150 $[km]$ is closer to 1e21 $[Pas]$, and that at lower depths than 200 $[km]$ it is closer to 1e19 $[Pas]$. This is the first similarity, and the fact that our viscosity in the upper mantle may be slightly lower than the ones from the two papers, may explain the stronger reaction from the lower bound 3D viscosity model. The upper bound 3D viscosity model, Final1, has a viscosity about 1e21 $[Pas]$, which may explain why its uplift rate magnitude is closer to those presented in Figure 7.10.

Furthermore, the second main similarity, is that the lithosphere, in both papers, is about 120 [km] thick. This means that we can assume there to be viscosity values which are higher than 1e30 [Pas]. The upper bound 3D viscosity model, Final1, has viscosity values at 50 and 100 [km] depth higher than 1e25 [Pas] as seen in Figure 6.1. The lower bound 3D model, Final3, has a viscosity higher than 1e25 [Pas] at 50 [km] depth and one of about 1e24 [Pas] at 100 [km] depth. Again, this slightly lower, although still very viscous compared to the 1D models, viscosity value than the one in both papers, may explain why Final3 has a stronger negative uplift rate than the maps in Figure 7.10, and why Final1, with a thicker lithosphere, may have an uplift rate in the South-West closer to that of the two mentioned papers. It is hypothesised that the 1D models do not display this negative uplift rate region because their thinner effective lithosphere, which only span 70 [km] depth, while it is made evident in this paragraph that the 3D viscosity profiles have a larger effective lithosphere.

Finally, the reader should also note that in Simpson et al. (2011), a study was conducted to find what and where were the highest discrepancies in modern day viscous uplifts, if the Earth structure beneath Greenland was changed. From this, it was found that the area in Greenland with the highest variation in uplift rates, was the South-West region, when the upper mantle viscosity was changed. In other words, we can, with this study, directly link the fact that we have varying viscosity profiles to the existence of the negative uplift region in our results in the South-West of Greenland, as it seems to be the region, from Simpson et al. (2011), which sees the highest effect in its modern day viscous uplift rate due to upper mantle viscosity change.

7.7. Deflections from 1992 to 2019 results, continuation

The deflections and deflection rates since 1992, can as done previously in other chapters, be presented through the prism of known GPS stations. This apparents itself to a validation of the results. However, the reader should have in mind that the uplift rate in all GPS stations on Greenland's coast is significantly, if not majorly, affected by the elastic uplift due to present day ice melts (Khan et al., 2016); this was also seen in Chapter 5 where the changes in ice loads since 1914 are on average 1.8 [mm/yr] against a mean of 2.56 [mm/yr] for Final0 in that period. To properly model an elastic uplift, a sub 10 kilometre resolution should be used, as changes in ice primarily happens at glaciers in very local regions. This sub 10 kilometre resolution is indicated because the smallest resolution setting in this research is 10 [km] for a surface mesh. However, we stipulate in reality the mesh to have to be at least sub 5 kilometre in order to accurately simulate elastic uplifts. Nevertheless, it is useful to compare the results as done in Figure 7.11.

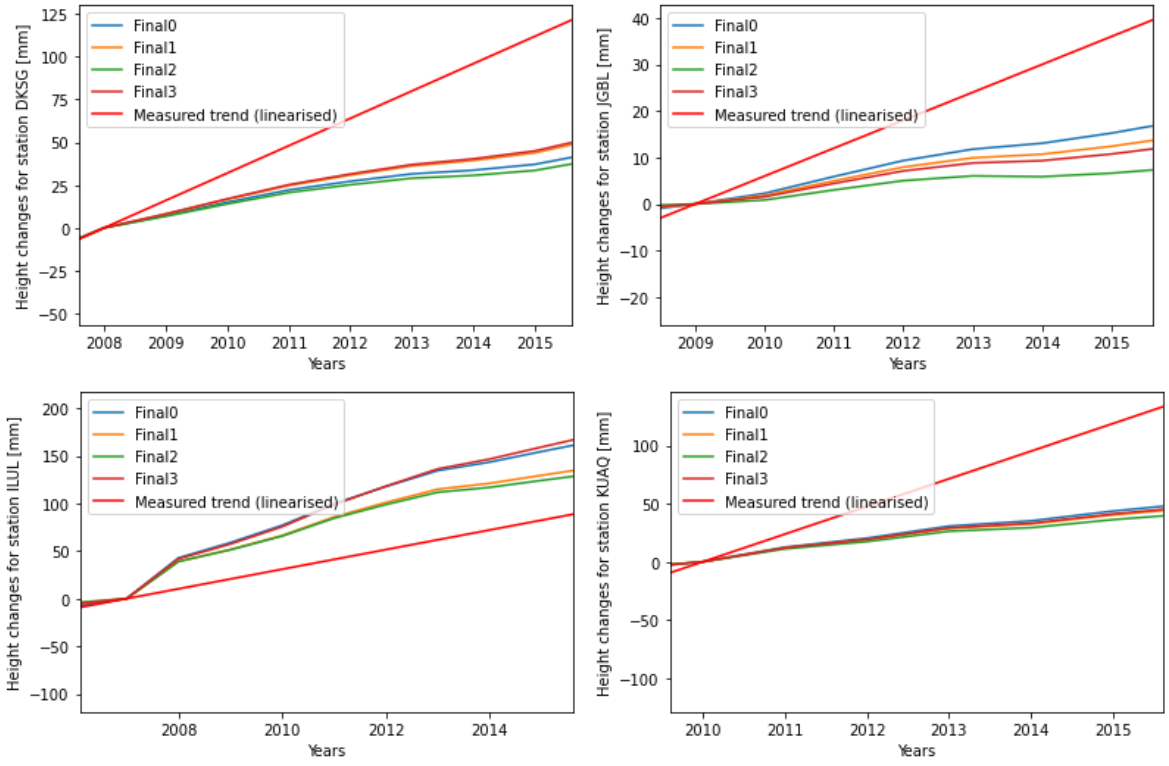

Figure 7.11: Uplifts since 1992 for GPS stations: DKSG (top left), JGBL (top right), ILUL (bottom left) and KUAQ (bottom right), againts the measured linearised trend at each station from Khan et al. (2016).

From Figure 7.11 there are multiple teachings, both considering the ability for the models here to approximate modern day uplifts and the possible future improvements.

The first is that for the station DKSG, where low viscous velocities are expected and high elastic velocities (Khan et al., 2016), the point mentioned in the introduction of this section stands. That is, that a finer grid is most certainly needed, in order obtain more accurate modern uplift rates. The gradient for all models is now about 4.25 +/- 0.5 [mm/yr], which is equivalent to the expected viscous signal. This means that the elastic signal, is vastly under estimated at this GPS station, and the 10 [km] resolution is not sufficient.

In station JGBL, the viscous effect is supposed to be dominant (Khan et al., 2016) over the elastic effect. However, the trend presented here, which is supposed to incorporate both the elastic and viscous effects, does not match measurements. Final0 provides the best approximation, which is sensible as it has the closest viscosity, which Lecavalier et al. (2014) used for the development of the ice model Huy3 for Greenland: 1e21 [Pas] in our model against 5e20 [Pas] for Lecavalier et al. (2014). Here again, we could point to a finer mesh in order to more accurately approximate the elastic uplift, but there is definitely also an issue in modelling the viscous response. The issues could be multiple, and this needs to be more investigated.

At ILUL, the gradient for models with a higher viscosity, namely Final1 and Final2, is more accurate with respect to the measured trend. This could indicate towards the fact that the simulated viscous response is higher than the real life viscous response, due to an over estimation of the ice masses, as we know that the elastic component of the uplift rate is supposed to be dominant (Khan et al., 2016). Moreover, this could also mean that in this region the resolution used is enough to properly model the elastic uplift, as it is the second highest region of ice mass loss (Milne et al., 2018).

Lastly, at the KUAQ station, both the elastic and viscous response are underestimated. We know this because the gradient simulated is lower than both individuals gradients estimated in Khan et al. (2016) for the elastic and viscous response. In reality, this station shows a high uplift rate, along with the MIK2 station, although the regions around have lower rates. Khan et al. (2016) made their simulation fit to reality by approximating a lower viscosity: 0.1e20 [Pas] in the aenosphere and 5e20 [Pas] in the upper mantle (Khan et al., 2016), compared to the surrounding areas.

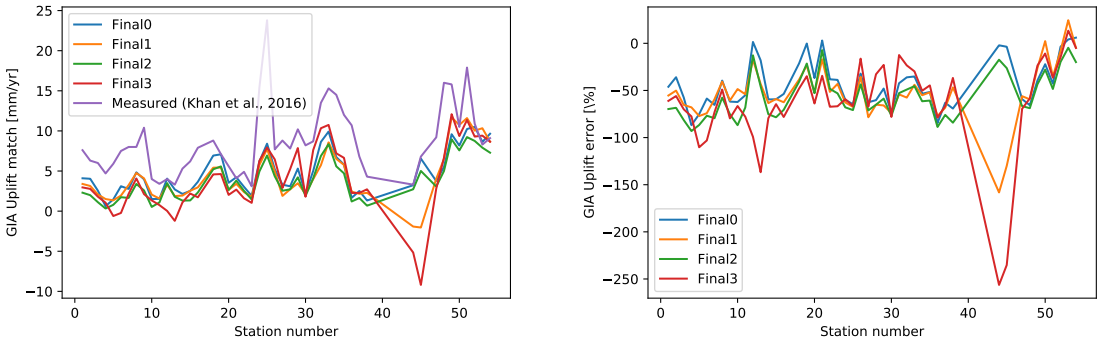

Figure 7.12: Rate of uplift [mm/yr] for each GPS station, in the same time range, compared against the measured linearised trend (left), and the percentage error between each final model trend and the measured linearised GPS trend (right). The respective GPS station numbers for JGBL, DKSG, ILUL and KUAQ are: 3, 48, 42 and 25. *Note: stations 16, 38, 39, 40, 41, 42, 43 and 46 are not included because the time range of the measured trend did not fit fully in our time steps taken in the models.*

From Figure 7.12 multiple conclusions can be drawn. Firstly, that the model with the 3D viscosity upper bound profile follows, in terms of shape of the trend, much better the trend of the measured uplift rates at the GPS stations, than the 1D viscosity profiles. We hypothesis that the 3D viscosity profile is closer to reality, in terms of pattern of viscosity, then the one dimensional viscosity profile. For instance, the upper bound model run correctly identifies a decrease of the uplift rates between stations 44 and 45, when the 1D viscosity runs do not find this trend.

Secondly, the 3D upper bound trend sometimes matches results from one 1D model or the other. This is stipulated to be because the viscosity in the 3D overestimated viscosity profile either matches about 1e21 [Pas] or 1e22 [Pas], especially on the coastal regions where the GPS stations are located. One can see in Figure 6.2 that the viscosity at for instance 200 [km] depth is about 1e21 [Pas] on the coast, while it varies between 1e21

and 1e25 [Pas] at 150 [km] depth on the coasts. Final3, the lower bound model, is quite unique in the sense that it provides more often than Final1, larger divergence from 1D viscosity models. This may be due to its viscosity, on the coastal regions, being lower than both 1D models overall.

Thirdly, it can be seen that the fit with reality for the Final1 model is generally worse than Final0 and Final2. We think this could be due to the fact that the 'long term' ice histories, from Huy3, where developed with a one dimensional varying viscosity profile, and not a three dimensional one similar to our 3D models in terms of pattern (Lecavalier et al., 2014). This effect can also be seen in Figure 7.11. However, from Khan et al. (2016), we know that the elastic uplift is a large contributor to modern day uplift rates on the coasts. Hence, the difference in fit to the real uplift rates, is less visible in Figure 7.12 than in Section 7.2.

Lastly, we can here point out again the inability of the model to simulate the elastic uplift, especially in the South-West region, which we think is mainly due to the mesh for both the input loads and the model being too coarse, and the model not therefore being able to register sub-10 [km] resolution changes in ice heights. For this we can use results from Figure 7.13 (Milne et al., 2018), which presents their modelled viscous present day responses.

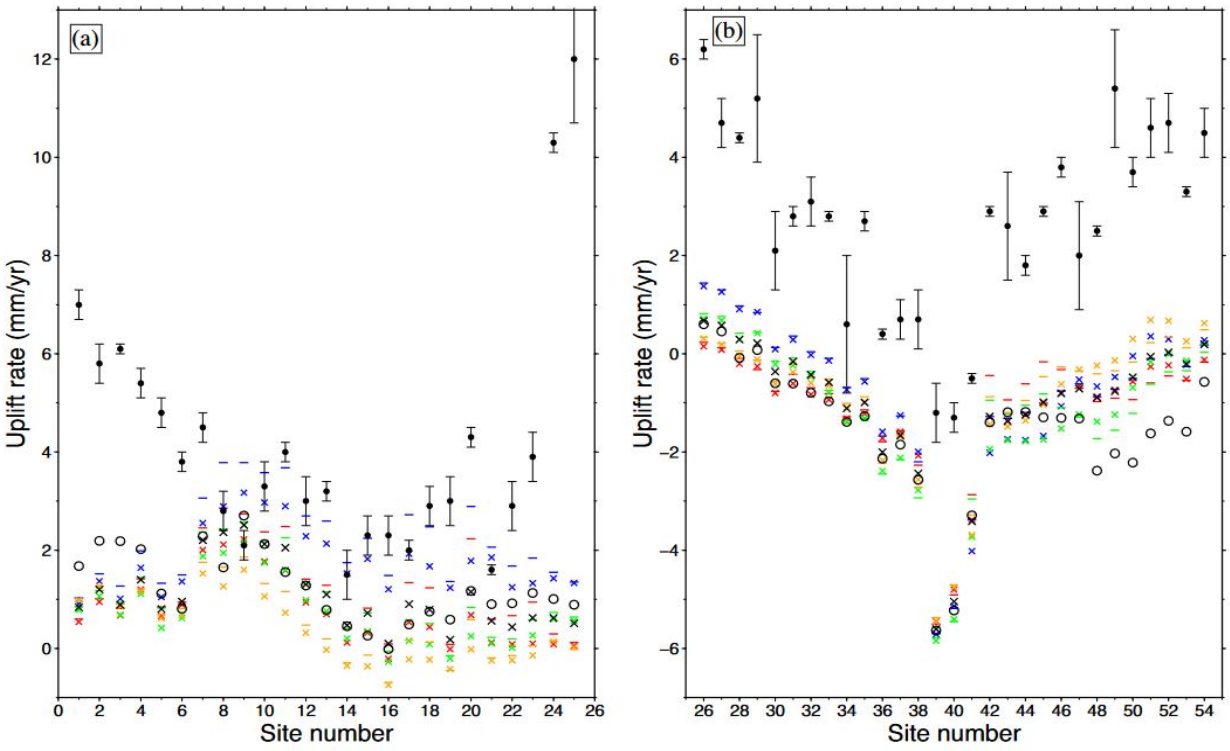

Figure 7.13: Comparison of GPS stations uplift rates and modelled uplifts rates for the viscous uplift, directly taken from Milne et al. (2018). The rates from the GPS uplifts are corrected for elastic motion. Black circles indicate the use of a 1D reference model, and the colours refer to 3D models: Results for the 1-D reference model are indicated by black circles and the 3-D model output is given by coloured symbols: S40RTS (red), Savani (blue), SEMUCB-WM1 (green) and SL2013sv (orange). The black crosses indicate the mean of the 3D model, and coloured dashes refer to the lithosphere model (Milne et al., 2018).

We see in Figure 7.13 that the uplift in the South-West region, which is roughly stations 44 and 45, present the same or similar modelled uplift rates than for stations in our 3D models, Final1 and Final3: about -2 to -7 [mm/yr]. However, our model is supposed to also include elastic uplifts. This then points to the fact that elastic uplift velocities in the South-West region are underestimated, and that an even finer region is there needed.

A last argument can be put forth, concerning the model's inability to accurately simulate elastic uplift. In a paper which partially investigated the error variation as function of surface resolution in elastic uplift at the marine ground line in West Antarctica, it was found that errors brought from the grid resolution drastically decreases below a surface resolution of 3.75 [km] (Wan et al., 2021). This is additional proof that the 10 by 10 [km] resolution setting is clearly not fine enough to properly simulate elastic uplift rates.

On a final note, we plot the deflection at one last GPS station, KULU, as we can compare the data to the actual

measured one, and not just the linearised trend.

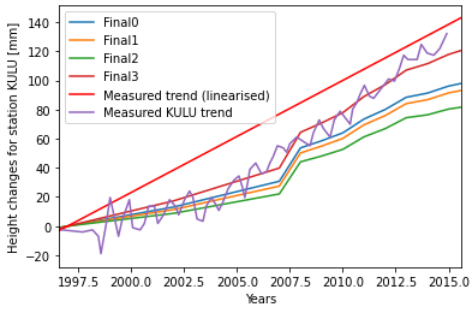

Figure 7.14: Simulated uplift rate [mm/yr] at the KULU station versus the measured and linearised measured uplift (Khan et al., 2016).

Figure 7.14 presents how the model results compare to the actual measured uplift. Unlike other graphs, we were able to get the actual data points, which were extracted from Khan et al. (2016). In Figure 7.14, we can see that the Final3 line is actually the best fit line. Final3 is also, contrary to other graphs, the one which yields the highest uplift rate. KULU is located on the central East coast of Greenland, a bit South of the KUAQ station, which we know from Figure 7.8 sees a slightly higher loss than the rest of Greenland between 45000 and 100 years ago. We can conclude from Figure 7.14, that for the region surrounding the KULU station's position, the Final3 model is adapted, but that as seen previously, the accuracy varies vastly across geographical locations in Greenland.

8

Conclusions & Recommendations

We can now present the main conclusions of this Master Thesis. Later on, these conclusions will be used to formulate structured recommendations in order to solve inquiries which are left after this research.

The aim of this Master Thesis is to simulate Glacial Isostatic Adjustment in Greenland, both the viscous and elastic deformations, while synthesising an ice history spanning 122000 years before present until 2019, and testing this model with 3D varying viscosity profiles. The GIA responses were simulated on a spherical Earth.

The chosen Earth spherical model, simulated in Abaqus 6.14, has a finer region which was originally set with a resolution of 25 by 25 [km], as seen in Subsection 3.2.1 and then changed to a setting of 10 by 10 [km] after Chapter 4, and which en-globed Greenland. It also has a coarser region, the rest of the globe's surface, with a setting of 100 by 100 [km].

We structured this conclusion according to the main three research questions posed in the introduction of this Master Thesis.

8.1. How can we design a spatial resolution which accurately models modern day uplifts rates, given the use of a unified ice history since 122000 years ago till now?

The parameter study on the surface resolution, performed in Chapter 4 is perhaps the study which had the greatest effect both on uplift rates at the present day, while also heavily impacting the uplifts in the finer region in the past 10000 years before present. An important point to remember here is that the resolution of the ice loads used is the same as the mesh of the model, i.e. each element is loaded, and there is in theory no element which has two loads on it.

For the maximum deflection behaviour, we noticed that the 10 by 10 [km] setting approached convergence, and we stipulate that the convergence point may be laying between 1 and 10 [km], given the 'area correction' scheme used when converting the ice masses to ice heights. We tested this by analysing what was the corresponding ice height change in the first time step of the model to the maximum deflection, and found that the distance was getting considerably smaller between the 25 [km] and 10 [km] settings then the previous increases in resolution. *Quick reminder: Abaqus does not use the resolution indication as a hard constraint. Instead it aims towards it. The result from this is that not all mesh areas are 10 by 10 [km], and many, if not most, are larger. This means that when converting from ice masses to ice heights, a scheme was needed to be developed in order to aim for mass conservation. This scheme was verified against a benchmark model which used interpolated ice heights instead of interpolated ice masses.*

For instance, concerning the mean deflection in the finer region, it was found that with a 100 by 100 [km] setting, the maximum deflection was only about 180 [m] upward, with an ice height change of about 0.5 [kg/m^2], when for the 50 by 50 [km] it was closer to 600 [m] for about 1.8 [kg/m^2] change and for the 25 by 25 [km] it was nearly the same as the 10 by 10 [km] area corrected: about 650 to 700 [m] maximum deflection for about 2.25 [kg/m^2] ice height/surface density change. With this study on the 'long term' ice history's effect on deflections, we found that a resolution of 10 by 10 [km] is close to the convergence point.

For the short term and local uplifts, the 10 by 10 [km] setting also approached a convergence point, but it was clearly not a high enough resolution to approach absolute accuracy with respect to present day GPS uplift measurements. This is thought to be due to the fact that this GIA model underestimates elastic uplifts. As elastic uplifts are instantaneous, and happen on a very small wavelength, simulating them with a minimum 10 by 10 [km] mesh is unfeasible. Hence, in the final results of Chapter 7, it was found that the elastic uplift was poorly approximated, due to the deflections being closer to the viscous estimations in other papers.

The modern viscous deformations are, notably according to Khan et al. (2016), Lecavalier et al. (2014) and Simpson et al. (2011), supposed to be mostly situated between -7 and +7 [mm/yr] rates on the coasts of Greenland, with some exceptions at certain GPS stations. Total uplift rates, on coastal regions are then supposed to be situated in the range of 0 to 22 [mm/yr] (Khan et al., 2016). However, we notice that deformation

rates, for coastal regions, are mostly between -10 and +10 [mm/yr], and thus more similar to the viscous range of uplift rates than the total one, encompassing the elastic uplift rate. This is further indication that our model may not properly simulate elastic uplift rates, which then points to a lack of high enough resolution in the models.

This was especially true in the South-West region which saw a significant down-lift rate in our 3D viscosity simulation in the 1992 to 2019 period, although it is supposed to have a significant uplift rate according to Khan et al. (2016). We can here recommend to establish a finer mesh size, at least in this region, but also in stations where the elastic uplift is also known to be dominating, as shown in Khan et al. (2016). This research into the surface resolution needed for deflection convergence resonates with recent research conducted in GIA modelling in West Antarctica by Wan et al. (2021). In this paper, they found that errors in modelling due to grid resolution decreased significantly when resolutions below 3.75 [km] were used. The contribution in research from this Master thesis may then indicate that the convergence point, where the deflection only varies little when the resolution is increased, is most likely around a 5 [km] resolution. This is a first approximation for this finer mesh size.

We then present the conclusions regarding the radial resolution and lithosphere structure. *Note: when we discuss here the radial resolution of the layers, it is important to remark that for the lithosphere forcible division, we talk about the layers we define, whereas for the radial resolution, we discuss the layers Abaqus creates. As mentioned and discussed numerous times in this overall research project, these two are not the same, as Abaqus takes a lot of freedom on layer definition.*

We have developed a radial resolution in the upper mantle which proved to show convergence for the entire simulation deflections. It consisted of mesh layers at distance from the centre of the Earth of: 6355, 6319, 6281, 6241, 6181, 6108, 6040 and 5980 [km]. This is an important aspect as it then allows for the research to concentrate on surface resolution and finding a convergence in the deformations by varying it. The new mesh configuration in the radial direction was found by indicating to the Abaqus software to add a separation at 150 [km] and 300 [km] depth on top of the others already present, taken directly from Spada et al. (2011). This is a clear addition to the Abaqus model which was originally given by Caroline van Calcar and Bas Blank, which inputed in the software the layer definition from Spada et al. (2011), and not with the added layers at 150 and 300 [km]. Using less layers or a different configuration in the first 420 [km] depth proved to yield deflection results out of this 'convergence' state.

In the layers beneath the upper mantle, it was investigated if making the seed size coarser affected the results, and how long it increased computation time. This investigation was performed over a 42000 year long propagation, with initial full ice heights. The study either made the layers 1, 2, 3 or 4 times coarser than the upper mantle ones. It was concluded that 3 times coarser was the most appropriate choice as it made the simulation gain 83% computation time, while changing the maximum deflection by less than 0.5%, while 4 times coarser only gained 1% more time than 3 times coarser while changing the results, relative to the finest setting, by 0.41%.

Convergence in deformations was also reached when structuring the lithosphere. We set in the first 70 [km] depths in the Abaqus FEM model 1 imposed layer, as 2 or 3 imposed layers increased the computation time by 30% to 80% respectively, and only changed the deflection results from 1972 by about 0.006%.

8.2. How can an ice history be designed and built, which represents the ice thickness differences from 122000 years ago till now and which is also pertinent for a GIA model?

The ice models/data schemes used were the 'long term' ice loads from the Huy3 model (Lecavalier et al., 2014), spanning 122000 years ago till 1914, and the 'short term' ice history made from glaciers measurements from 1972 till 1992 (Mouginot et al., 2019), and satellite data from 1992 till 2019 (Simonsen et al., 2021).

The ice loads were interpolated in order to fit the mesh developed for the simulation. These loads were then also corrected for, in order to obtain mass conservation, and converted to ice heights, as they were given in ice masses. The previously mentioned 'area correction' method was here used for the final simulations. The model worked by inputting ice heights and not ice masses per element. Expanding on this, we conclude that the interpolation methods which use complex mathematical functions, such 'gaussian', work generally less well than simpler functions like 'linear', because more complex functions create a range of values which is unrealistic: increasing the range of values by several magnitudes, whereas the simpler functions keep the original range

of values much better. Adding on, it was also found that if one wishes to skip a percentage of the original data when doing the interpolation, in order to decrease computation times, simpler mathematical functions such as 'linear' preserved the statistics from the original data better than when more complex functions were used. This is true when a large number of points are used. The choice of simpler functions also impacted the model modern uplifts, which proved to be unrealistic - that is suddenly increasing by several magnitudes over 1 year for instance - when complex functions were used. This is logical as elastic uplifts are directly correlated to the loads input: if more complex functions increase the magnitudes of loads by a unrealistic amount, then the deflections will vary by unrealistic amounts.

However, during the interpolation procedure, we were faced with a major limitation, which was that the ice history from 1972 to 1992 is only for certain glaciers. Hence, we had to first project these glaciers ice mass balances on a grid before interpolating these ice mass losses for the whole of Greenland. This led our model to be less precise in that time frame for the elastic uplifts, and also less accurate. The projection of the ice masses on a longitude latitude grid, before the interpolation, was clearly identified as the step which degraded the quality of the interpolated data. However, this degradation of quality was thought to have a minimal impact on modern day uplifts, as it was estimated in Simpson et al. (2011) that the viscous component of the deflections due to the ice mass changes in the past 100 years, was below 0.5 $[mm/yr]$ magnitude; this point was also confirmed in our research where we found that the ice changes since 100 years ago provoke a similar pattern in time and place as the deflections, pointing then towards an elastic deflection. Since we do not use or investigate elastic deflections between 1972 and 1992, we did not think that this worsening of interpolated ice masses significantly impacted our uplift rates since 1992. A recommendation here would be to use a 3D interpolation function which has the 'nearest' interpolation setting. This way the mass change at glaciers would not change geographically during grid conversions.

Concerning the timeline used when inputting the ice loads, we should now present our conclusion. It was found that the timeline resolution prior to 25000 years ago, does not seem to significantly impact the present day deflections as the propagation time prior is long enough to allow the model's deflections to stabilise. Moreover, as the viscosity below 150 $[km]$ depth is smaller for the 3D profiles along the coasts, the ice history prior to 25000 years ago may be even less relevant for them, as these would have quicker reaction time.

From 25000 years ago till 100 years before present, two major findings were concluded. The first is that the gain in accuracy was higher when the resolution was made finer from 11000 years ago onward. Moreover, custom timelines made according to the variation of ice masses in the lower half of Greenland - this area had on average a lower viscosity than the rest of Greenland - found that a key factor to include in the timelines, was the inclusion of steps of 500 years between 15000 years ago till 5000 years ago, due to the proximity in time and ice load between 17000 years ago, the ice maximum in Greenland, and 15000 years ago in Greenland.

Finally, we came to the conclusion that the timeline should have four steps between 1972 and 1992 instead of two, as the ice changes there do change the end deflections by about 1.1% while not increasing the computation time significantly. Furthermore, the ice history from 1992 to 2007 was set to three steps, which demonstrated less than 1 $[mm]$ difference with the 5 steps configuration. Lastly, the ice history was set to 12 steps from 2007 to 2019, as the end deflections changed by up to 0.7% with the 6 steps configuration, and because this timeline is of high interest, we decided to double the time steps in that time period.

The ice heights were, in the final results, loaded as the difference with the ice heights 122000 years ago. This was done in order to properly consider and apply the assumption that the Earth was in isostatic equilibrium 122000 years ago. Applying this assumption also decreases computation times, as the deflections are smaller in the first time step. However, applying this assumption, and testing it against a model which did not apply this assumption, does not significantly change the outputs for present times. This difference may arise from the model loading, and the internal stresses in the model differing when full ice heights are loaded against when partial ice heights are input. We can now formulate the major limitations of this ice history.

The major limitation noted through out this Master Thesis with regards to ice loads is the fact that, although the 'long term' ice history was developed to fit Greenland relative sea level data, it was developed assuming a 1D viscosity profile (Lecavalier et al., 2014). This becomes an issue in the sense that the deflections using 3D viscosity profiles therefore fit less uplift rate measurements than the 1D profiles. This limitation is intricately linked to Section 8.3, as it could also be viewed that the limitation of the model here is the use of a 3D viscosity and not the use of a 1D developed ice history. Nevertheless, it stands that more research should be conducted

in ice histories development for GIA, when 3D viscosity profiles are used in the GIA deflection simulations.

Another limitation was the absence of the ice masses from 1914 to 1972. Only the changes since 1972 were obtained. Thus, we had to interpolate the ice history from 1914 to 1972, using all the previous files, to find the ice masses in 1972. This led to a general trend over Greenland being applied for all the data points in the 'tight' region around Greenland, and only represents in a very coarse manner the ice history in that time frame. However, this was only a minor limitation as the ice history, from 1900 to 1983 of Greenland, varies about roughly 4 times less in ice change per year for all regions, then the ice history from 1983 to 2003 (Kjeldsen et al., 2015).

8.3. What are the effects of including a 3D varying viscosity in a GIA model in Greenland which uses a unified ice history from 122000 years ago till present day, on deflections throughout the simulations and on present day uplift rates?

The 3D varying viscosity profiles were found to have higher sensitivity, that is a higher deflection in the same time frame, to ice load changes in the 'long term' and the 'short term' periods than the 1D varying viscosity models, especially in the South-West region. We think this is due to their lateral variations, which are not present in the 1D viscosity models and make the coastal regions a factor of 100 to 1000 less viscous than the central region of Greenland, but also because the viscosity below depths of 150 or 200 [km], was lower for the 3D viscosity profiles than the 1D profiles: about $1e19$ to $5e20$ [Pas] against $1e21$ [Pas] and $1e22$ [Pas]. This is important as it may suggest that in reality, the ice loads or ice load changes might have been smaller than expected, as these were developed with 1D viscosity models.

This effect of a higher response to loads for 3D varying viscosity profiles, is even more accentuated when these viscosity profiles have a lower viscosity. The higher sensitivity of 3D viscosity profiles is best illustrated through the case of the South-West region, where it starts down-lifting around 4500 years ago for the 3D profiles when the 1D profiles stabilise. We believe this large down-lift rate area, which is of higher magnitude for the lower bound 3D profile, is caused by its lower viscosity in the upper mantle, in combination with a thick lithosphere, a finishing de-glaciation phase (Lecavalier et al., 2014) and an increase in ice mass between 4500 and 100 years ago. As mentioned previously, this could mean that the elastic deformation is underestimated at present times, as the viscous one is clearly dominant, but it could also mean that in this region the ice mass changes are overestimated between 4500 and 100 years ago, in light of the effect produced when a 3D viscosity is used: the creation of a large down-lift rate area in present times although measurements point towards an uplift.

Aside from the obvious, which is that the knowledge about the 3D viscosity of the Earth is limited, and that the 'long term' ice model is not developed with a 3D viscosity profile, we can formulate some limitations to the use in this Master Thesis of the 3D viscosity profiles, upper and lower bounds, as well as the use of 1D viscosity profiles.

Firstly, the reactions of the 3D models to load changes seem unreasonably large; although we discussed in the previous chapter that the negative uplift region deflection rates, in the South-West, were closer for the upper bound 3D profile than to the lower bound 3D profile, to uplift rates in previous research, namely in Lecavalier et al. (2014) and Simpson et al. (2011). This was a clear characteristic of the 3D viscosity profile results. However, it is a disadvantage as it induces large negative uplift rates from 4000 years ago onward, while 1D models do find an equilibrium state within the simulation.

Furthermore, the viscosity profiles, whether they are 3D or 1D, do not change over time. However, we know that surface pressures, affect the pressures in the layers beneath the surface, and therefore change the viscosity, as suggested by experimental data by Faul and Jackson (2005). As a large portion of Greenland's ice melts about 10000 years ago (Lecavalier et al., 2014), at the start of the Holocene Thermal Maximum, a non-linear rheology could prove to yield different results as the viscosity beneath Greenland may have had time to vary. This is for now a recommendation and needs further research. This non-linear effect is not taken into account, and therefore could be inducing errors in the viscosity profile behaviour and thus in the simulation uplifts.

Another limitation, is that the viscosity profiles do not seem to be accurate enough. This is shown through the example of the GPS station KUAQ, where we know that a low viscosity should be present in the aenosphere and

the upper mantle (Khan et al., 2016) but is clearly not the case. The limitations mentioned just before this one could be linked to the low viscosity expected at KUAQ and MIK2 stations. There are multiple reasons why the 3D viscosity profiles here may lack accuracy. The first, but only minor reason, is that the contribution in gravitational acceleration due to the lithosphere, upper mantle and lower mantle is difficult to dissociate (Fullea et al., 2021), which then affects the pressure of each layer, and finally the viscosity. Additionally, a more important limitation is that the translation from seismic velocity anomalies into temperature profiles is also uncertain at this stage. As pointed out in the paper of WINTERC-G, Fullea et al. (2021), multiple different seismic models exist, which give temperature profiles varying between 200 and 600 [K] at specific depths between models. Lastly, more concretely, as made evident in the base research used to generate the 3D viscosity models, Hirth and Kohlstedt (2003), there are also uncertainties in the wet diffusion and wet dislocation constants used in the modelling of the viscosity. For example, the melting ratio can vary between 30 and 45, when the specific energy can vary anywhere between 260 [kJ/mol] and 410 [kJ/mol] for wet diffusion and between 440 and 520 [kJ/mol] for wet dislocation (Hirth and Kohlstedt, 2003).

The last limitation with the 3D varying viscosity profiles used in this research is the fact that the constants used in the Olivine flow model, assuming a wet diffusion and dislocation creep, may be outdated. The paper used here for reference is Hirth and Kohlstedt (2003). However, this method of developing the 3D viscosity model was also used in van der Wal and Xu (2016), so finding a more up to date version may not be yet available.

8.4. Recommendations

Finally, we can now formulate recommendations based on the conclusions made in the previous sections and through out the report. Conclusions which often try to explain found phenomena but also try to identify the key limitations of model characteristics, parameter estimations and modelling. Recommendations lead to further improvements of the current model.

There are three main recommendation orientations which we can list and explain for this investigation of GIA in Greenland: Earth modelling, ice history synthesis and 3D viscosity profiles used in the 3D Earth.

8.4.1. Recommendations for the Earth modelling

The first area of recommendations are made with respect to Earth modelling, this includes meshing, computation time or even geological characteristics, excluding viscosity. The order of the following recommendation was chosen so because the first two address directly one of the main issues found in the conclusions of this Master Thesis, that is the surface resolution. The third recommendation addresses practicality in simulations but is to our knowledge difficult to implement, while the last three recommendations are considered easy to implement, given that such codes and models exist for self-gravity and ocean loading.

1. **Making two models with different surface resolution.** One model for long term, who's outputs are inputted into the short term model. The models would be divided in a chronological manner across the timeline. This way a coarse resolution could be implemented until 1914, and then a much finer resolution than 10 [km] could be implemented after 1914, in order to more accurately simulate the elastic uplifts. Although a two model system is what this Master Thesis avoids, this two model system would not be the same as the one found in literature, as done for instance in Khan et al. (2016). What is usually done is to simulate the elastic uplift with a completely different model. However, what this recommendation recons is to have exactly the same model, but change its resolution from a certain point in time onward. This is doable if the displacements, as well as the ice heights, of all the nodes are taken and converted into a finer grid. This recommendation therefore recommends two clear parts in the model instead of one unified section which constantly has the same properties throughout the entire simulation. The limitation of this recommendation is that converting internal stresses from the first to the second model, would be a key issue to overcome.
2. **Including a finer resolution in the upper layers.** This recommendation would be to better approximate recent elastic deformation. It would be achieved by finding methods to lower computation time. This is of course a general recommendation. However, more research should be done into developing conventions destined to reduce computation time in the Abaqus software for GIA simulations. As in Chapter 7 and Section 4.1, it was found that the computation time increases by resolution of the mesh and greatly by 3D viscosity inclusion. Thus, finding ways of passing from a run time of 2 to 3 weeks to for instance half

or three quarters of that time, would be beneficial to all researchers. Multiple leads can be explored to reduce computation times, for example: having an even more adaptive meshing by dividing the globe in multiple regions of different mesh types in order to more effectively mesh the Earth or scaling down the loads and the spherical Earth model. As the use of a 3D viscosity was clearly the factor which increased the simulation time the most, and we assume it to be an essential contribution to future modelling, we do not think that we should go back to a 1D viscosity profile in the upper mantle.

3. **Loading in our own mesh**. This would be done in order to gain more control over the element creation and overall simulation, and to also provide higher traceability of results. We can imagine to share common 'mesh files' between different researchers. This is addressed with a proposed method in Appendix C. Also, this way, more complex shapes could be created for the finer region: ones which would better enclose areas of known low viscosity or high ice mass changes. This would greatly reduce the dependence on the Abaqus software; the modellers would be much more knowledgeable about their own models and would be more able to guide their experiments and research instead of Abaqus.
4. **Investigating the density and Young's Modulus at depths 150 [km] and 300 [km].** In our model, we use the layer definition and material characteristics as specified in Spada et al. (2011). However, in this paper, layers at 150 [km] and 300 [km] depths are not present, and hence we simply assumed that they had similar characteristics as the layers in the upper mantle. Applying new characteristics at these layers could lead to higher accuracy, and if the investigations prove that these should be left un-changed, higher confidence in the model would be obtained. At this stage, we have not found any specific studies on the effect of layer density or Young's modulus at those depths on GIA deflections. However, we can speculate that varying the Young's modulus will affect the elastic response at the surface, and that varying the density, by for instance including a 3D density profile, may also change the deflections by creating less or more gravitational pull by the Earth's layers and ice on the model's structure, and will change the buoyancy of the crust on the mantle underneath it.
5. **Including the effects of self-gravity.** Both the effects of the changing gravitational acceleration due to deflections, and the gravity rate due to ice being present on the surface of the Earth should be taken into account in order to improve the accuracy of the model. They are complex and complicated but necessary effects to implement.
6. **Including ocean loads.** As ocean and sea loads were not included in the model, some error in the deflections were created due to this absence. Ocean loads often counter act uplift deflections in the sea regions. They are necessary in order to accurately model GIA.

Self-gravity and ocean loading inclusion

We believe that now is an appropriate moment in this chapter to expand on why self-gravity and ocean loads were not taken into account in this Master Thesis, and why they are a useful recommendation, as pointed out in the list above.

Self-gravity is not included in any model run. The first reason is that the computation time is already so high for the models including 3D varying viscosity profiles, that including self-gravity, which doubles the run time, would be very costly. This is for self-gravity, with respect to the gravity change that the ice creates by just being present on the Earth's surface.

Furthermore, the gravity value per layer is kept constant through the simulation, assuming a spherical Earth. Hence, the gravitational acceleration is not changed in the model, when calculating the weight of the ice loads, when in fact it should be, as deformations in the Earth's sphere do locally change the gravity at those points. This effect of self-gravity is neither taken into account for programming and practical reasons.

Lastly, we did not take into account ocean loads for the same reasons: in the time had, and for practical reasons, it was unfeasible. Also, just as with self-gravity, it would have increased computational times. Including ocean loads is, however, more realistic. As ice melts over the globe, it distributes the liquid water through the oceans. This in turn creates new sets of loads on the Solid Earth, which then interact with the load changes due to the ice.

However, we can stipulate that including the self-gravity might change deflections by a maximum of 10% (Spada et al., 2011). It was discussed in the referenced paper that differences between two models which were compared, were attributed to grid effects, sphericity and self-gravity, and the error was about 10%. As there was no separation between between the three sources of error in order to display their individual contribution, we assume the worst case scenario, and place the error due to self-gravity at 10%. Another study, pointed out

that after a load is unloaded from a surface, the self-gravity could create differences in deflection up to 20 [m] in the 2000 years which follow the unloading (Amelung and Wolf, 1994). It also found that the errors due to sphericity and self-gravity partially cancelled each other out. This would mean that imposing self-gravity on a spherical Earth model may be an important recommendation for future research in this models(Amelung and Wolf, 1994).

Moreover, including ocean loads, may increase present day uplifts. As oceans exert a force oriented towards the centre of the Earth of sea floors, they create a slight negative deflection. Hence, because grounds in Greenland are overall uplifting in modern times, this may create a feedback effect, where the uplift rates may be slightly higher than in the models in this Master Thesis. This effect may be increased by the melting of ice, around and in Greenland in the past 10000 years. This difference in uplift was evaluated in a benchmark study. It was found in that paper that the root-mean square and maximum differences for the individual solutions of the vertical displacements varied between 0.1 [m] and 1.5 [m] (Martinec et al., 2018), between models which included the ocean loads, also called sea level equation, and ones which did not. This represented about 1.5% of the displacements for the used ice loads (Martinec et al., 2018). These results are only mentioned, in order to give to the reader an idea of the effect created when including ocean loads.

8.4.2. Ice history synthesis recommendations

The second main area of recommendation concerns the ice history, and this area covers topics such as, but not limited to: interpolation of ice loads, ice history development, ice height conversion or missing ice history values. The first two recommendations are a more direct continuity of this Master Thesis; hence their order w.r.t. the third recommendation. Moreover, the first recommendation is more important as it concerns the entire ice history Huy3 prior to 1914, when the second only concerns the ice history between 1914 and 1972.

1. **A Greenland specific 'long term' ice history, developed with a 3D varying viscosity structure should be used.** The ice history used here until 1914, is made using a 1D varying viscosity structure. It is not made with a viscosity structure which varies as much as the 3D upper or lower bound profiles (Lecavalier et al., 2014). The impact on the results is partially unknown. However, we do know that 1D viscosity profiles perform better than 3D profiles if the ice history was developed with a 1D viscosity. Hence, as 3D varying viscosity profiles are assumed more accurate than 1D varying viscosity profiles, using an appropriate ice history should then be done. Note that this recommendation could become obsolete if the third recommendation is applied, as the GIA deflections with a 3D viscosity would already bias the ice sheet reconstruction process, if a 3D varying viscosity is used in the ice model. However, an ice history like Huy3, which is obtained from inversion, may still be useful to validate the ice (de)glaciation process in a GIA-ice model feedback loop. Lastly, such a history may be as, if not more, difficult to constrain as the number of available measurements is the same as when a 1D viscosity is used.
2. **Research into the ice history between 1914 and 1972.** Due to time constraints a crude method was developed to find the ice mass change between 1914 and 1972, in order to obtain the ice height in 1972. This was not thought crucial as the viscous response in modern times, due to these ice mass changes is thought negligible (Simpson et al., 2011). However, the lower bound 3D viscosity profile, could potentially be affected by a more accurate ice reconstruction there. As a final point for this recommendation, we do not believe this is a crucial one, as the ice history in Greenland does not change significantly between 1900 and 1983 (Kjeldsen et al., 2015), compared to the changes after 1983. The mass balances are about 25%, between 1900 and 1983, of the magnitude of the changes between 1983 and 2003 for instance (Kjeldsen et al., 2015).
3. **Coupling of the ice history and the GIA response for the 'long term' GIA effects.** As proven and shown in van Calcar et al. (2021) for Antarctica, coupling an ice model and GIA deflections, could help to uncover more accurate uplift velocities during the last glacial maximum, as the Earth's physics are better represented in such a model than in ours, and it allows to investigate effects such as the ice (de)glaciation - GIA feedback. Although this was only done for Antarctica so far, implementing it for Greenland is promising. It should be noted that with such a technique, only viscous effects in the present time would be present, i.e. we would still need to use satellite data and measurements for the ice history since 1972. However, the ice history and deflections prior to the last centuries could be more accurate, as well as the modern day viscous response due to the last glacial cycle.

8.4.3. 3D viscosity profiles recommendations

The last main area of recommendations concerns the inclusion of the 3D varying viscosity profile in the model, and the possible solutions which could be brought to improve this inclusion. The first recommendation is first as it is more in line with what research was conducted in this Master Thesis. The third recommendation is last, as the first two apparent themselves more to fundamental and high level recommendations, whereas the third is more considered a parameter tuning/research. Recommendations on the viscosity profiles:

1. **Further investigation into the uses of 3D varying viscosity profiles, and comparison with 1D varying viscosity profiles, when using different ice histories/models.** This research would be to investigate how the models we have developed here, and perhaps new ones too, react to different ice histories or ice models. For this Master Thesis, we only used one ice history per time frame. On a research perspective, it would be more interesting to observe how the Earth models developed here react to different ice histories, as this may give us more insight on these Earth models' limitations. This could also help to either comfort us in the idea that 3D viscosity profiles are a real improvement, or if they are a necessary step forward, while worsening the results.
2. **Including a non-linear steady state rheology.** The underlying assumption in this Master Thesis is that the viscosity of an element, or a region in the Earth's mantle does not change throughout time. However, we know very well that this is a wrong assumption. Equations which calculate creep typically take pressure into account. This pressure changes as the loads on the Earth change, namely the ice loads in polar and medium latitude regions. Hence, including a rheology which changes over time, depending on the ice heights loaded at different locations, would be more interesting on a research perspective, in order to converge towards a unified Earth model.
3. **Reviewing the constants used in the 3D varying viscosity profile.** Potentially more up to date constants, from the ones used, could be chosen for the diffusion and dislocation creep equations. The ones used in the wet diffusion and dislocation model date back to 2003 (Hirth and Kohlstedt, 2003).

Bibliography

F. Amelung and D. Wolf. Viscoelastic perturbations of the earth: significance of the incremental gravitational force in models of glacial isostasy. *Geophysical Journal International*, 117(3):864–879, 06 1994. ISSN 0956-540X. doi: 10.1111/j.1365-246X.1994.tb02476.x. URL https://doi.org/10.1111/j.1365-246X.1994.tb02476.x.

B. Blank, V. Barletta, H. Hu, F. Pappa, and W. van der Wal. Effect of lateral and stress-dependent viscosity variations on gia induced uplift rates in the amundsen sea embayment. *Geochemistry, Geophysics, Geosystems*, 22(9):e2021GC009807, 2021. doi: https://doi.org/10.1029/2021GC009807. URL https://agupubs.onlinelibrary.wiley.com/doi/abs/10.1029/2021GC009807. e2021GC009807 2021GC009807.

U. H. Faul and I. Jackson. The seismological signature of temperature and grain size variations in the upper mantle. *Earth and Planetary Science Letters*, 234(1):119–134, 2005. ISSN 0012-821X. doi: https://doi.org/10.1016/j.epsl.2005.02.008. URL https://www.sciencedirect.com/science/article/pii/S0012821X05001044.

J. Fullea, S. Lebedev, Z. Martinec, and N. L. Celli. WINTERC-G: mapping the upper mantle thermochemical heterogeneity from coupled geophysical–petrological inversion of seismic waveforms, heat flow, surface elevation and gravity satellite data. *Geophysical Journal International*, 226(1):146–191, 03 2021. ISSN 0956-540X. doi: 10.1093/gji/ggab094. URL https://doi.org/10.1093/gji/ggab094.

C. Hirt, S. Claessens, T. Fecher, M. Kuhn, R. Pail, and M. Rexer. New ultra-high resolution picture of earth's gravity field. *Geophysical Research Letters*, 40, 08 2013. doi: 10.1002/grl.50838.

G. Hirth and D. Kohlstedt. Rheology of the upper mantle and the mantle wedge: A view from the experimentalists. *Washington DC American Geophysical Union Geophysical Monograph Series*, 138:83–105, 01 2003. doi: 10.1029/138GM06.

E. R. Ivins, W. van der Wal, D. A. Wiens, A. J. Lloyd, and L. Caron. Antarctic upper mantle rheology. *Geological Society, London, Memoirs*, 56, 2021. ISSN 0435-4052. doi: 10.1144/M56-2020-19. URL https://mem.lyellcollection.org/content/early/2021/11/16/M56-2020-19.

S. A. Khan, I. Sasgen, M. Bevis, T. van Dam, J. L. Bamber, J. Wahr, M. Willis, K. H. Kjær, B. Wouters, V. Helm, B. Csatho, K. Fleming, A. A. Bjørk, A. Aschwanden, P. Knudsen, and P. K. Munneke. Geodetic measurements reveal similarities between post–last glacial maximum and present-day massloss from the greenland ice sheet. *Khan et al. Sci. Adv*, 2, 2016.

K. Kjeldsen, N. Korsgaard, A. Bjørk, S. Khan, J. Box, S. Funder, N. Larsen, J. Bamber, W. Colgan, M. Van den Broeke, M.-L. Siggaard-Andersen, C. Nuth, A. Schomacker, C. Andresen, E. Willerslev, and K. Kjaer. Spatial and temporal distribution of mass loss from the greenland ice sheet since ad 1900. *Nature*, 528:396–400, 12 2015. doi: 10.1038/nature16183.

B. S. Lecavalier, G. A. Milne, M. J. Simpson, L. Wake, P. Huybrechts, L. Tarasov, K. K. Kjeldsen, S. Funder, A. J. Long, S. Woodroffe, A. S. Dyke, and N. K. Larsen. A model of greenland ice sheet deglaciation constrained by observations of relative sea level and ice extent. *Quaternary Science Reviews*, 102:54–84, 2014. ISSN 0277-3791. doi: https://doi.org/10.1016/j.quascirev.2014.07.018. URL https://www.sciencedirect.com/science/article/pii/S0277379114003011.

D. Leroux and T. Pellarin. 11 - remote sensing data assimilation: Applications to catchment hydrology. In N. Baghdadi and M. Zribi, editors, *Land Surface Remote Sensing in Continental Hydrology*, pages 363–399. Elsevier, 2016. ISBN 978-1-78548-104-8. doi: https://doi.org/10.1016/B978-1-78548-104-8.50011-5. URL https://www.sciencedirect.com/science/article/pii/B9781785481048500115.

S. B. Luthcke, H. J. Zwally, W. Abdalati, D. D. Rowlands, R. D. Ray, R. S. Nerem, F. G. Lemoine, J. J. McCarthy, and D. S. Chinn. Recent greenland ice mass loss bydrainage system from satellitegravity observations. *SCIENCE*, 314:1286–1289, 2006.

Z. Martinec, V. Klemann, W. van der Wal, R. E. M. Riva, G. Spada, Y. Sun, D. Melini, S. B. Kachuck, V. Barletta, K. Simon, G. A, and T. S. James. A benchmark study of numerical implementations of the sea level equation in GIA modelling. *Geophysical Journal International*, 215(1):389–414, 07 2018. ISSN 0956-540X. doi: 10.1093/gji/ggy280. URL https://doi.org/10.1093/gji/ggy280.

G. Milne, K. Latychev, A. Schaeffer, J. W. Crowley, B. Lecavalier, and A. Audette. The influence of lateral earth structure on glacial isostatic adjustment in greenland. *Geophys. J. Int*, 214:1252–1266, 2018.

J. Mouginot, E. Rignot, A. A. Bjørk, M. van den Broeke, R. Millan, M. Morlighem, B. Noël, B. Scheuchl, and M. Wood. Forty-six years of greenland ice sheet mass balance from 1972 to 2018. *Proceedings of the National Academy of Sciences*, 116(19):9239–9244, 2019. ISSN 0027-8424. doi: 10.1073/pnas.1904242116. URL https://www.pnas.org/content/116/19/9239.

G. Ramillien, F. Frappart, and L. Seoane. 6 - space gravimetry using grace satellite mission: Basic concepts. In N. Baghdadi and M. Zribi, editors, *Microwave Remote Sensing of Land Surface*, pages 285–302. Elsevier, 2016. ISBN 978-1-78548-159-8. doi: https://doi.org/10.1016/B978-1-78548-159-8.50006-2. URL https://www.sciencedirect.com/science/article/pii/B9781785481598500062.

S. B. Simonsen, V. R. Barletta, W. T. Colgan, and L. S. Sørensen. Greenland ice sheet mass balance (1992–2020) from calibrated radar altimetry. *Geophysical Research Letters*, 48(3):e2020GL091216, 2021. doi: https://doi.org/10.1029/2020GL091216. URL https://agupubs.onlinelibrary.wiley.com/doi/abs/10.1029/2020GL091216. e2020GL091216 2020GL091216.

M. Simpson, L. Wake, G. Milne, and P. Huybrechts. The influence of decadal to millennial-scale ice mass changes on present-day vertical land motion in greenland: Implications for the interpretation of gps observations. *Journal of Geophysical Research*, 116, 02 2011. doi: 10.1029/2010JB007776.

G. Spada, V. R. Barletta, V. Klemann, R. E. M. Riva, Z. Martinec, P. Gasperini, B. Lund, D. Wolf, L. L. A. Vermeersen, and M. A. King. A benchmark study for glacial isostatic adjustment codes. *Geophysical Journal International*, 185(1):106–132, 04 2011. ISSN 0956-540X. doi: 10.1111/j.1365-246X.2011.04952.x. URL https://doi.org/10.1111/j.1365-246X.2011.04952.x.

C. van Calcar. Interactions between ice sheet dynamics and glacial isostatic adjustment. Master's thesis, TU Delft, Delft, Netherlands, 2020.

C. van Calcar, B. de Boer, B. Blank, R. van de Wal, and W. van der Wal. The effect of the GIA feedback loop on the evolution of the Antarctic Ice sheet over the last glacial cycle using a coupled 3D GIA - Ice Dynamic model. In *EGU General Assembly Conference Abstracts*, EGU General Assembly Conference Abstracts, pages EGU21–15773, April 2021.

W. van der Wal and Z. Xu. 3D viscosity maps for Greenland and effect on GRACE mass balance estimates. In *EGU General Assembly Conference Abstracts*, EGU General Assembly Conference Abstracts, pages EPSC2016–10010, April 2016.

L. M. Wake, B. S. Lecavalier, and M. Bevis. Glacial isostatic adjustment (gia) in greenland: a review. *Curr Clim Change Rep*, 2:101–111, 2016. doi: 10.1007/s40641-016-0040-z.

J. Wan, N. Gomez, K. Latychev, and H. Han. Resolving gia in response to modern and future ice loss at marine grounding lines in west antarctica. 08 2021. doi: 10.5194/tc-2021-232.

P. Whitehouse. Glacial isostatic adjustment modelling: Historical perspectives, recent advances, and future directions. *Earth Surface Dynamics*, 6:401–429, 05 2018. doi: 10.5194/esurf-6-401-2018.

P. Wu. Using commercial finite element packages for the study of earth deformations, sea levels and the state of stress. *Geophysical Journal International*, 158(2):401–408, 08 2004. ISSN 0956-540X. doi: 10.1111/j.1365-246X.2004.02338.x. URL https://doi.org/10.1111/j.1365-246X.2004.02338.x.

H. S. B. L. A. D. D. R. S. G. E. R. I. A. W. M. Xiaoping Wu1, Michael B. Heflin and S. E. Owen. Simultaneous estimation of global present-day water transport and glacial isostatic adjustment. *Pure and Applied Geophysics - PURE APPL GEOPHYS*, 3:642–647, 08 2010. doi: 10.1038/NGEO938.

A

Uplift results from Khan et al. (2016)

Table A.1 displays the the measured uplift rates at various GPS stations in Greenland, as well as the viscous and elastic components estimation (Khan et al., 2016).

Table A.1: Table taken directly from Khan et al. (2016). It shows the total uplift measured at each GPS station, the calculated elastic uplfit and the calculate 'long term' GIA uplfit.

Site	Latitude	Longitude	t_start	t_end	Up rate	Elastic Up rate	GIA Up rate	Basin #
	Deg	deg	Year	Year	mm/yr	mm/yr	mm/yr	
BLAS	79.53861 N	22.97472 W	2008.5	2015.6	7.6 ± 0.2	4.3 ± 0.5	3.3 ± 0.5	1
LEFN	80.45668 N	26.29346 W	2008.5	2015.6	6.3 ± 0.2	4.3 ± 0.2	2.1 ± 0.3	1
JGBL	82.20876 N	31.00420 W	2008.5	2015.6	6.0 ± 0.2	1.5 ± 0.2	4.5 ± 0.3	1
KMJP	83.64324 N	33.37708 W	2008.5	2015.6	4.7 ± 0.2	0.9 ± 0.1	3.8 ± 0.2	1
JWLF	83.11165 N	45.11983 W	2008.5	2015.6	5.9 ± 0.2	1.1 ± 0.2	4.8 ± 0.3	1
HRDG	81.87983 N	44.51737 W	2008.5	2015.6	7.5 ± 0.2	2.1 ± 0.2	5.4 ± 0.3	1
KMOR	81.25271 N	63.52739 W	2007.7	2015.6	8.0 ± 0.1	1.9 ± 0.1	6.1 ± 0.1	1
SCBY	80.26013 N	59.59362 W	2007.7	2015.6	8.0 ± 0.2	2.2 ± 0.3	5.8 ± 0.4	1
KAGZ	79.13196 N	65.85295 W	2007.7	2015.6	10.4 ± 0.1	3.4 ± 0.3	7.0 ± 0.3	1
NORD	81.60014 N	16.65545 W	2006.7	2015.2	4.0 ± 0.3	1.3 ± 0.2	2.8 ± 0.4	1
DMHN	76.77107 N	18.65568 W	2010.6	2015.6	3.4 ± 0.3	1.2 ± 0.2	2.3 ± 0.4	2
LBIB	75.89380 N	23.85294 W	2009.6	2015.6	4.0 ± 0.2	1.7 ± 0.4	2.3 ± 0.4	2
YMER	77.43289 N	24.32633 W	2009.6	2015.6	3.3 ± 0.2	1.8 ± 0.5	1.5 ± 0.5	2
GMMA	77.80943 N	19.65212 W	2009.6	2015.6	5.3 ± 0.2	2.1 ± 0.1	3.2 ± 0.2	2
NRSK	79.15503 N	17.72542 W	2008.5	2015.6	6.2 ± 0.2	2.2 ± 0.1	4.0 ± 0.2	2
GROK	78.44270 N	22.90376 W	2008.5	2015.6	7.9 ± 0.2	4.9 ± 0.5	3.0 ± 0.5	2
SCOR	70.48534 N	21.95032 W	2004.7	2015.6	3.8 ± 0.1	2.2 ± 0.1	1.6 ± 0.1	3A
VFDG	70.29992 N	29.81764 W	2009.6	2015.6	8.8 ± 0.2	4.9 ± 0.5	3.9 ± 0.5	3A
DGJG	71.78653 N	29.85020 W	2009.6	2015.6	7.1 ± 0.2	4.2 ± 0.5	2.9 ± 0.5	3A
MSVG	72.24082 N	23.91286 W	2009.6	2015.6	5.6 ± 0.2	1.3 ± 0.1	4.3 ± 0.2	3A
HMBG	73.67598 N	28.12907 W	2009.6	2015.6	4.1 ± 0.2	1.1 ± 0.5	3.0 ± 0.5	3A
WTHG	73.95520 N	24.30892 W	2009.6	2015.6	4.9 ± 0.2	2.0 ± 0.4	2.9 ± 0.4	3A
DANE	74.31195 N	20.19983 W	2009.6	2015.6	3.1 ± 0.2	1.1 ± 0.1	2.0 ± 0.2	3A
MIK2	68.14030 N	31.45180 W	2009.6	2015.6	15.4 ± 0.2	5.1 ± 0.1	10.3 ± 0.2	3B
KUAQ	68.58700 N	33.05270 W	2009.6	2015.6	23.8 ± 0.3	11.8 ± 1.3	12.0 ± 1.3	3B
KULU	65.57933 N	37.14935 W	1996.6	2015.6	7.7 ± 0.1	3.3 ± 0.1	4.4 ± 0.1	4
UTMG	62.92721 N	43.30641 W	2007.6	2015.6	8.8 ± 0.7	8.2 ± 1.2	0.6 ± 1.4	4
HJOR	63.41821 N	41.14787 W	2007.6	2015.6	7.8 ± 0.1	5.0 ± 0.1	2.8 ± 0.1	4
TREO	64.27707 N	41.37508 W	2007.7	2015.6	10.2 ± 0.2	7.1 ± 0.5	3.1 ± 0.5	4

Table A.2: Continuation of Table A.1.

Site	Latitude	Longitude	t_start	t_end	Up rate	Elastic Up rate	GIA Up rate	Basin #
	Deg	deg	Year	Year	mm/yr	mm/yr	mm/yr	
TIMM	62.53554 N	42.28616 W	2007.6	2015.6	8.2 ± 0.2	5.5 ± 0.1	2.7 ± 0.2	4
LYNS	64.43048 N	40.19806 W	2007.7	2015.6	8.7 ± 0.2	5.9 ± 0.1	2.8 ± 0.2	4
KBUG	65.14368 N	41.15755 W	2007.7	2015.6	13.5 ± 0.2	11.4 ± 0.8	2.1 ± 0.8	4
HEL2	66.40116 N	38.21570 W	2007.6	2015.6	15.3 ± 0.1	10.1 ± 1.3	5.2 ± 1.3	4
KSNB	66.86328 N	35.57632 W	2007.6	2015.6	14.5 ± 0.1	9.8 ± 0.5	4.7 ± 0.5	4
PLPK	66.89773 N	34.03347 W	2007.6	2015.6	12.0 ± 0.1	5.8 ± 0.2	6.2 ± 0.2	4
SENU	61.06958 N	47.14131 W	2008.4	2015.6	10.7 ± 0.1	10.7 ± 0.6	0.7 ± 0.6	5
NNVN	61.63188 N	44.90105 W	2007.6	2015.6	6.8 ± 0.4	6.1 ± 0.1	0.7 ± 0.4	5
QAQ1	60.71526 N	46.04776 W	2001.8	2015.6	4.3 ± 0.1	3.9 ± 0.1	0.4 ± 0.1	5
KELY	66.98742 N	50.94483 W	1995.7	2015.6	3.2 ± 0.1	3.7 ± 0.1	-0.5 ± 0.1	6
AASI	68.71932 N	52.79334 W	2005.7	2015.6	7.9 ± 0.1	5.0 ± 0.1	2.9 ± 0.1	6
QEQE	69.25263 N	53.52232 W	2005.9	2015.6	7.9 ± 0.1	5.0 ± 0.1	2.9 ± 0.1	6
ILUL	69.24041 N	51.06075 W	2006.1	2015.6	10.3 ± 0.1	8.5 ± 0.2	1.8 ± 0.2	6
KAGA	69.22230 N	49.81463 W	2006.4	2015.6	22.1 ± 0.1	19.5 ± 1.1	2.6 ± 1.1	6
NUUK	64.18355 N	51.73116 W	2009	2015.6	3.3 ± 0.3	4.6 ± 0.1	-1.3 ± 0.3	6
KAPI	64.43235 N	50.27121 W	2009.5	2015.6	6.8 ± 0.3	8.0 ± 0.5	-1.2 ± 0.6	6
THU2	76.53705 N	68.82503 W	1999.2	2015.6	6.4 ± 0.1	3.1 ± 0.1	3.3 ± 0.1	7A
MARG	77.18704 N	65.69462 W	2007.7	2015.6	9.2 ± 0.1	4.7 ± 0.5	4.5 ± 0.5	7A
DKSG	76.35162 N	61.67767 W	2007.6	2015.6	16.0 ± 0.1	11.3 ± 0.6	4.7 ± 0.6	7B
ASKY	75.72613 N	58.25735 W	2007.6	2015.6	15.8 ± 0.1	11.2 ± 0.6	4.6 ± 0.6	7B
KULL	74.58062 N	57.22706 W	2007.6	2015.6	10.5 ± 0.2	6.8 ± 0.2	3.7 ± 0.3	7B
SRMP	72.91068 N	54.39370 W	2007.6	2015.6	17.9 ± 0.1	12.5 ± 1.2	5.4 ± 1.2	7B
RINK	71.84850 N	50.99396 W	2007.7	2015.6	10.9 ± 0.2	8.9 ± 1.1	2.0 ± 1.1	7B
UPVK	72.78829 N	56.12800 W	2007.4	2015.6	8.3 ± 0.1	5.8 ± 0.1	2.5 ± 0.1	7B
QAAR	70.74041 N	52.68837 W	2007.7	2015.6	9.1 ± 0.2	5.3 ± 0.1	3.8 ± 0.2	7B

B

Synthesizing the ’short term’ ice history

As discussed in Figure 2.3.4, we synthesise the ice history from 1972 to 2019, using two sources of data. One which spans 1972 to 1992[1], and which repertories the ice mass loss per glacier, and one which spans 1992 up to but not including 2020, and gives a detailed ice mass change calculated from GRACE and altimetry data[2].

We only consider as far back as 1972, due to the fact that no viable plausible measurements have been found plausible before then, and that ice history measurements in Greenland are a recent endeavour.

In fine, the ’short term’ ice history, before interpolation, is the glacier history until 1992, and then the detailed history from 1992 to 2020.

[1] This one actually spans until 2018, but it is less precise than the second data set so it is thus left out.
[2] This data has a precision of 0.01 [°].

C

Building the mesh lay-out: a recommended approach for future work

In Section 2.1 we defined the mesh used in the simulations for this Master Thesis. However, as a recommendation we can show how a mesh with an extra fine region would be implemented, in order to have more control over the meshing process, usually performed by Abaqus. We thus repeat the process in Appendix C but with the intent of designing a mesh which the user would have more control over.

C.1. General structure & approach

When building the mesh model, we can first assign a global mesh, as although our area of interest is Greenland, what happens over the rest of the Earth cans till have an influence on Greenland. Furthermore, a finer region is then designed which englobes the whole of Greenland. Lastly, we create an even finer region which we place in a particular of interest, i.e. where we expect the highest land uplifts or the strongest reactions to load changes.

C.2. Global mesh setting

For the global mesh setting, it is only needed to determine the mesh size, as the area is by definition the whole Earth except for finer mesh regions. For this we use the mesh size found in literature (Xiaoping Wu1 and Owen, 2010). It is of 100 by 100 [km], which is roughly 1 degree in any direction for the Earth at the equator[1] A demonstration of this global mesh is done in Figure C.1.

[1] Important to note for the reader, that when building the mesh model, the Earth is assumed a perfect sphere.

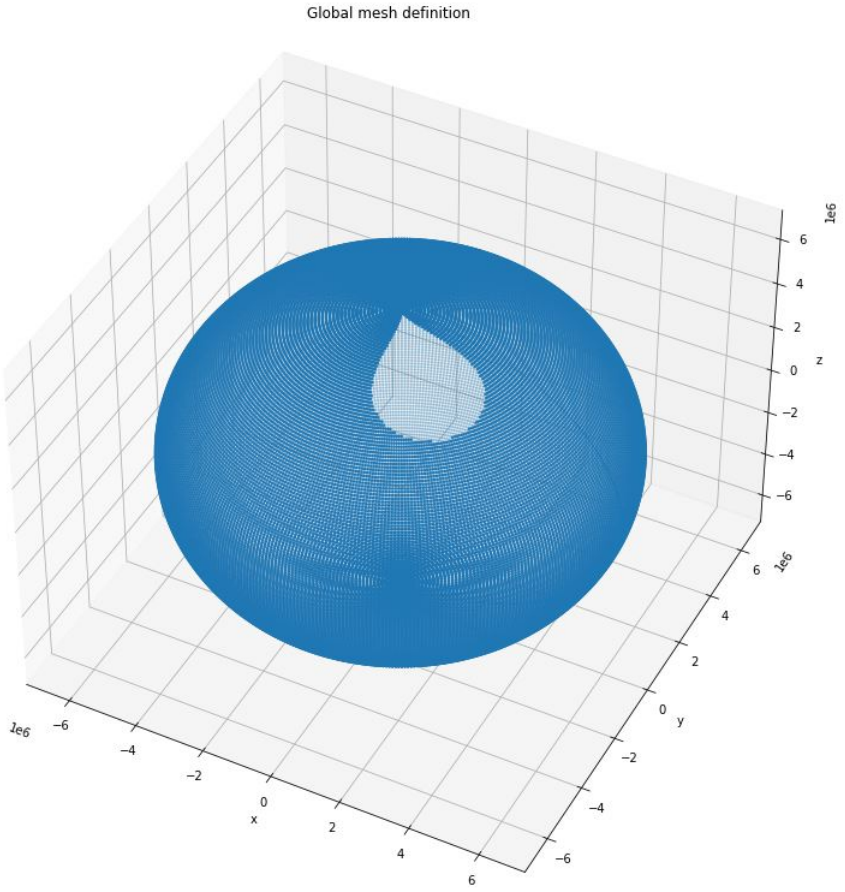

Figure C.1: 3D global mesh. The reader can already observe that the finer mesh regions are cut out.

C.3. Finer mesh region 1

When modelling this finer region, we are left with two design choices: the area of this finer mesh region and the mesh size. These two are both discussed in this finer region and in the even finer one. In general, and this is valid also for the other region, we make the choice of an ellipse for the region, as it is a flexible shape in both longitudinal and latitude directions, when a rectangle has too rigid edges and a circle is inefficient in space for an area such as Greenland.

C.3.1. Area definition - finer mesh region 1

The first finer mesh region should at least include Greenland. If not, then we will not be able to guarantee a certain level of quality and accuracy in our results. By first then establishing this criterion, we can delimit the contours of Greenland, and come up in Table C.1 with a list of points, inspired from Figure C.2 (Luthcke et al., 2006), which the limit of the first finer region should at least pass through.

Table C.1: List of points on the Greenland coast, inspired from (Luthcke et al., 2006).

Longitude [°]	Latitude [°]
316	60
288	78
336	70
335	80
308	66
296	80
316	82
328	68
300	76
337	74
291	76
298	81.5
308	66
304	74
328	68
320	64
328	82

This is the figure the points are estimated from, see Figure C.2.

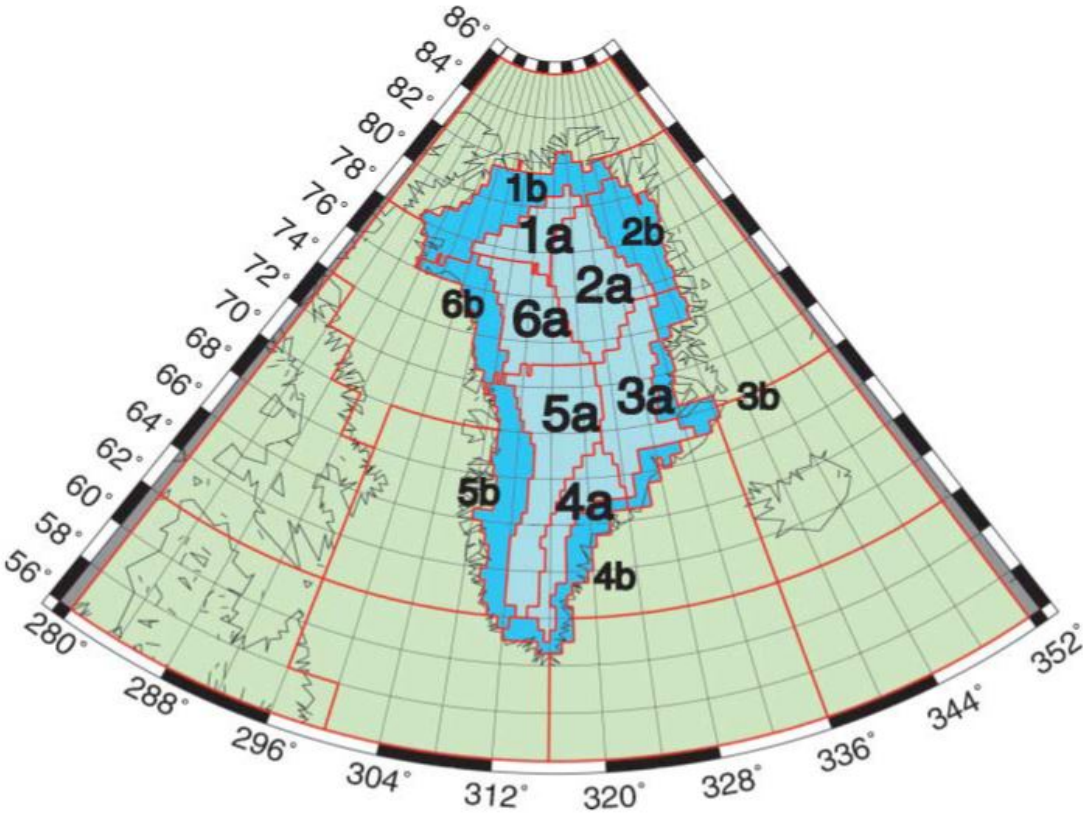

Fig. 1. Greenland DS mascon regions: regions above 2000 m elevation are labeled "a," and those below are labeled "b." Exterior region mascons outside of Greenland are also shown outlined in red.

Figure C.2: Divisions of Greenland in regions to analyse the mass loss of the whole region (Luthcke et al., 2006).

However, only taking into account these points as the limiting zone is assuming that areas just around Greenland are not affecting Greenland itself. This is a wrong assumption, and we thus add 8 degrees extra in both longitude and latitude directions, to increase the 'Greenland effective modelling area'[2].

C.3.2. Mesh dimensions - finer region 1

The shape of each mesh determined a square[3] within the finer region, and is more complex at its outside boundaries with the 'global' mesh and at the boundary with the second finer region.

When determining the size of the mesh, we should keep in mind the end goal of this thesis: that we wish to link modelled uplift to the change in gravity field change, as measured by GRACE, over Greenland. Thus, our mesh should be a finer than GRACE's resolution, but not significantly. GRACE's resolution is situated around 300 [km] (Leroux and Pellarin, 2016), and getting gravity field measurements below 10 [km] (Hirt et al., 2013) is deemed for now not possible. So when modelling the uplift, we can assign a ratio of 144 mesh points to 1 gravity field measurement, yield a mesh of 25 by 25 [km]; roughly 0.25 [°] in both latitude and longitude. This ratio is high, in order to take into account Greenland's complex shape, and the fact that the defined area is non-squared when the mesh is.

In sum, combining both the limits of the first finer region determined in Subsection C.3.1, and the mesh size here, we can plot this finer region over a 2 dimensional and polar grid; in Figure C.3 and Figure C.4 respectively.

[2]From now, abbreviated to Gema.
[3]Although it is deformed as it is projected on a sphere.

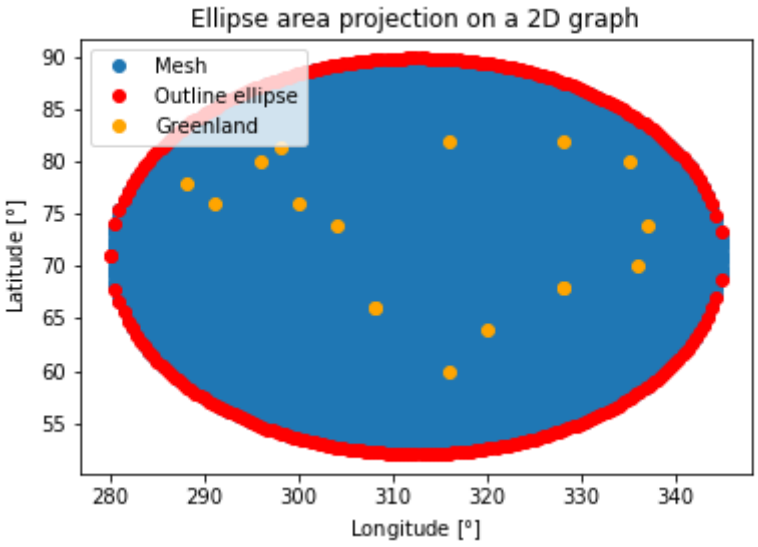

Figure C.3: 2D plot of finer region 1, over points of Greenland.

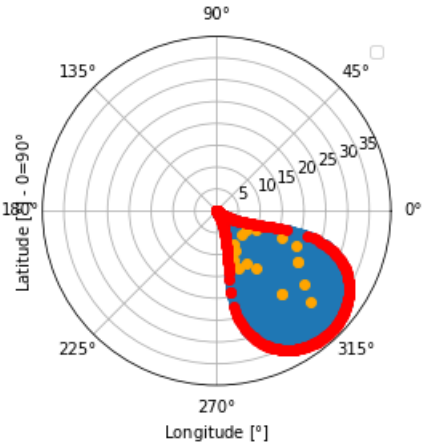

Figure C.4: Polar plot of finer region 1, over points of Greenland.

C.4. Finer mesh region 2

C.4.1. Area definition - finer mesh region 2

The first finer mesh region aimed to englobe the whole of Greenland, as it is our area of study. However, this second finer mesh region should contain (an) area(s) where higher uplifts or higher sensitivity to load changes are expected.

In order to find such a region, we should first acknowledge that we should use GPS stations and find their uplift rates. Higher uplift rates in the last decades would be more advantageous for an even finer mesh region. For this, we can refer ourselves to Khan's paper (Khan et al., 2016), which performed a similar study but in 1 dimensions[4].We can clearly rely on this paper as it is relatively recent, and it analyses uplift rates on average between 2007 and 2016.

In this paper, the mean total uplift[5] is 8.69 $[mm/yr]$. Therefore, we first select the GPS stations which show uplift rates above this one. Furthermore, we subdivide this category into ones which have an uplift rate up to

[4]The reader can refer him/her self to the literature study (REFERENCE) done previously to this thesis, where this study is more explained in detail.

[5]For the selection of relevant GPS stations we do not make a difference between elastic and GIA uplift, especially because there is usually a positive correlation between high elastic and GIA uplifts.

11 $[mm/yr]$[6], then an uplift rate between 11 and 16 $[mm/yr]$[7], and finally ones with an uplift rate higher than 16 $[mm/yr]$[8]. These can be plotted over Greenland's contour, as done in Figure C.5, with the help of their coordinates (Khan et al., 2016).

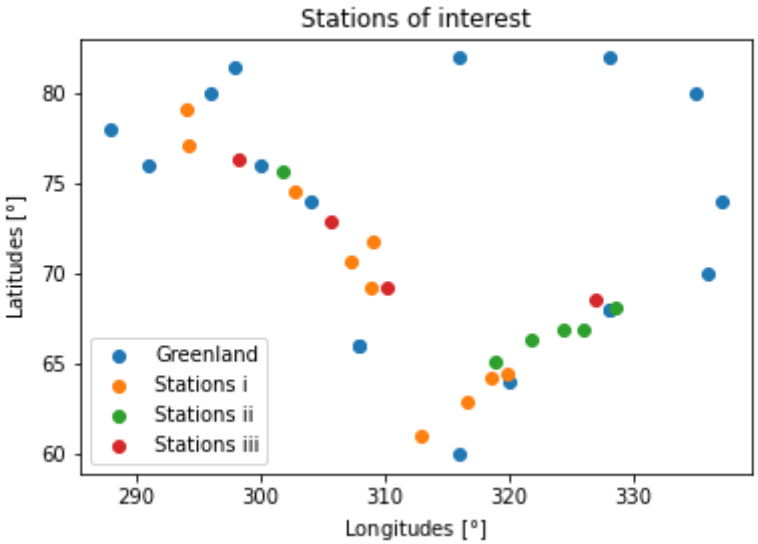

Figure C.5: Stations of interest in Greenland.

We can define here a region which englobes all category ii and iii stations, i.e. the most important ones, and nearly all category i, except for the two on the highest latitudes. This is deemed acceptable nearly all category ii and iii are below those latitudes.

C.4.2. Mesh dimensions - finer region 2

The mesh size should definitely be smaller than in the finer region 1, which is 25 by 25 $[km]$. For this region we could thus rely on the analysis made in (Hirt et al., 2013), which was realistically having measurements of the gravity field below 10 $[km]$ is close to impossible. In other words, 10 $[km]$ is a suitable size for the surface mesh, i.e. 0.12 [°] in both latitude and longitude directions. It yields a ratio of 900 mesh points for 1 gravity field measurement.

In conclusion we can then plot the mesh, the stations of interest and this second finer region on a graph to better illustrate it, in Figure C.6.

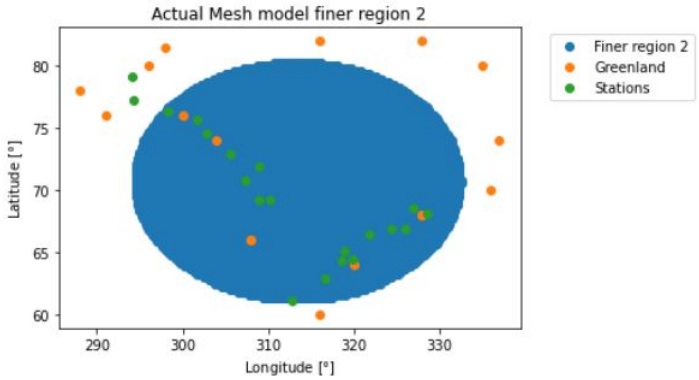

Figure C.6: Finer region 2.

[6]These stations are designated of category i.
[7]These stations are designated of category ii.
[8]These stations are designated of category iii.

C.5. Overall mesh model summary

We can now summarise our mesh model, shown in Table C.2, which we will use when modelling the uplift at different epochs.

Table C.2: Mesh model summary, when modelling the uplift.

	Mesh sizes [km,km]	
global	100, 100	
finer region 1	25, 25	
finer region 2	10, 10	
	Elliptical limits	
	Longitude [°]	**Latitude [°]**
finer region 1	280, 345	52.0, 90.0
finer region 2	294.32233, 332.5482	61.14368, 80.35162

We can present part of this summary in Figure C.7.

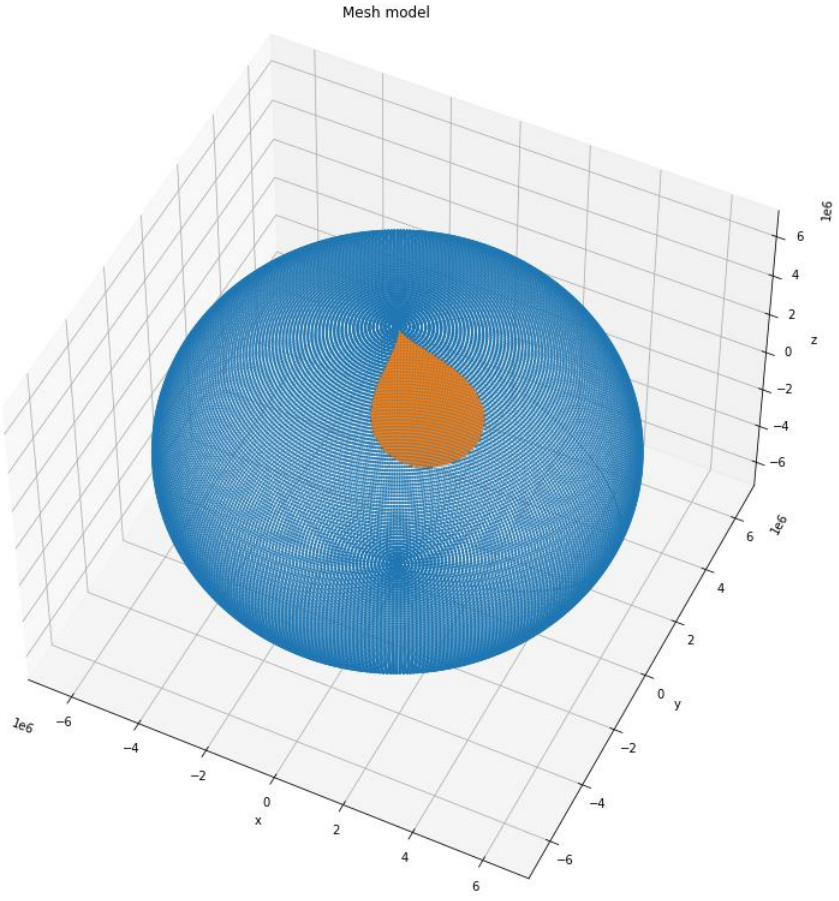

Figure C.7: Global and finer region 1 meshes.

C.6. Uploading the mesh into Abaqus

What has been discussed so far is the design of the mesh. However, one of the main limitations faced into this procedure is how to input this mesh into Abaqus. This has only been partially explored, but some leads can be

given in order to perform this. A possibility which could be used is to input the nodes files into a software such as CATIA, also by DASSAULT systemes, create the elements between the nodes, and then save it into a CAD file which would then be input in Abaqus. An example of this loading of the nodes is shown in Figure C.8.

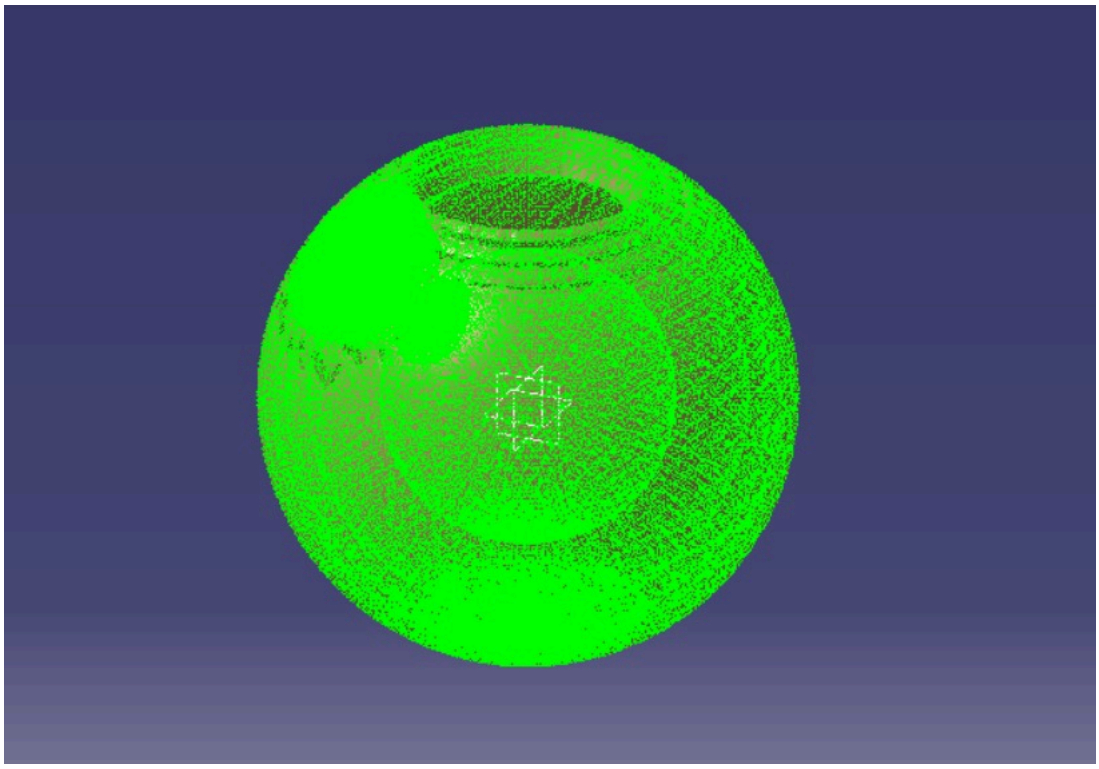

Figure C.8: Screen shot of an example of the nodes loaded in the CATIA software. One can notice a fine mesh region over Greenland.

It was note found possible to just input nodal coordinates into Abaqus. Hence, first developing the elements, and inputing nodes and elements in CAD file is found to be a more plausible option, which was partially experimented with.

D

Temperature profile used

Below, in Figure D.1, we see the temperature profile at 150 [km], used in the development of the viscosity profiles developed in Figure D.1.

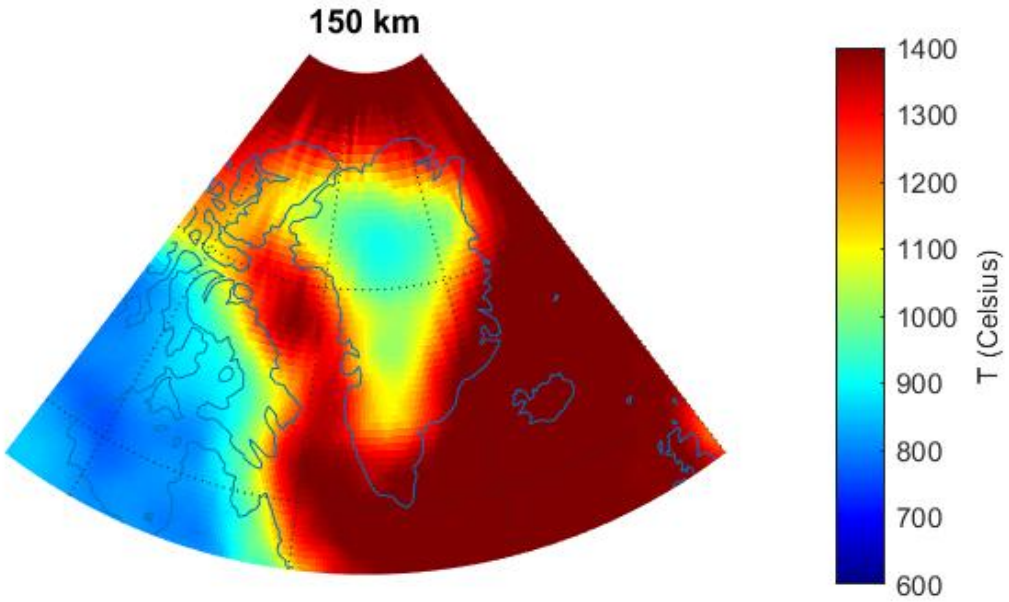

Figure D.1: Temperature profile at 150 [km] depth used in the wet and dry 3D varying viscosity models in Chapter 4. Figure is self made.

E

Short-term interpolation method choices

Table E.1 presents the choice of interpolation methods if method 1 and 3 of corrections of mass were applied after interpolation, when Table E.3 presents the choice of interpolator per year after having applied method 1 and 2 of mass corrections. These methods are elaborated in Subsection 2.3.5.

Table E.1: Alternative interpolation method per year for the 'short term' ice history data. The grades provided are just the sum of the difference in mean and difference in range between the pre-interpolation and post-interpolation data. This data had, in the project grid in Greenland between 1972 and 1992 method 1 and 3 corrections, contrary to the below table which had method 1 and 2 of correction.

Year	Method	Function	Grade	Year	Method	Function	Grade
1972	gaussian	RBF	11.95144	1996	quintic	RBF	0.03154
1973	gaussian	RBF	12.06177	1997	quintic	RBF	0.028799
1974	gaussian	RBF	4.277968	1998	gaussian	RBF	0.042544
1975	gaussian	RBF	4.809083	1999	gaussian	RBF	0.052161
1976	gaussian	RBF	12.05632	2000	quintic	RBF	0.039763
1977	gaussian	RBF	17.97735	2001	quintic	RBF	0.038656
1978	gaussian	RBF	13.28075	2002	quintic	RBF	0.044643
1979	gaussian	RBF	30.06304	2003	quintic	RBF	0.034039
1980	gaussian	RBF	18.90103	2004	quintic	RBF	0.042702
1981	gaussian	RBF	13.54734	2005	quintic	RBF	0.07678
1982	gaussian	RBF	10.66479	2006	quintic	RBF	0.070677
1983	gaussian	RBF	22.89866	2007	quintic	RBF	0.059682
1984	gaussian	RBF	26.3549	2008	quintic	RBF	0.055628
1985	gaussian	RBF	12.20547	2009	quintic	RBF	0.044148

Table E.2: Continuation to Table E.1.

Year	Method	Function	Grade	Year	Method	Function	Grade
1986	gaussian	RBF	8.146801	2010	quintic	RBF	0.047091
1987	gaussian	RBF	11.77387	2011	inverse_multiquadric	RBF	0.020431
1988	gaussian	RBF	2.956189	2012	quintic	RBF	0.033617
1989	gaussian	RBF	3.993861	2013	gaussian	RBF	0.022274
1990	gaussian	RBF	4.136251	2014	quintic	RBF	0.042191
1991	gaussian	RBF	6.263722	2015	quintic	RBF	0.029298
1992	quintic	RBF	0.023854	2016	quintic	RBF	0.016698
1993	quintic	RBF	0.025649	2017	quintic	RBF	0.029583
1994	quintic	RBF	0.024153	2018	quintic	RBF	0.047305
1995	quintic	RBF	0.02255	2019	quintic	RBF	0.067695

Table E.1 and its continuation Table E.2, clearly show that if methods 1 and 3 are applied, where the error in total is constantly shared between the points of interpolation, the quintic and gaussian methods are the only ones chosen.

Table E.3: Chosen interpolation method per year for the 'short term' ice history data. The grades provided are just the difference in mean between the pre-interpolation and post-interpolation data. This data had, in the project grid in Greenland between 1972 and 1992 method 1 and 2 corrections, contrary to the above table which had method 1 and 3 corrections.

Year	Method	Function	Grade	Year	Method	Function	Grade
1972	linear	RBF	0.131299	1996	quintic	RBF	1.51E-05
1973	linear	RBF	0.011256	1997	cubic	RBF	1.69E-06
1974	inverse_multiquadric	RBF	0.008842	1998	linear	RBF	0.000101
1975	cubic	RBF	0.084133	1999	inverse_multiquadric	RBF	4.47E-05
1976	linear	RBF	0.01901	2000	quintic	RBF	0.000151
1977	inverse_multiquadric	RBF	0.065484	2001	cubic	RBF	0.000203
1978	multiquadric	RBF	0.088283	2002	cubic	RBF	0.000218
1979	multiquadric	RBF	0.100658	2003	gaussian	RBF	0.000155
1980	linear	RBF	0.087439	2004	gaussian	RBF	0.000254
1981	cubic	RBF	0.034508	2005	quintic	RBF	0.000603
1982	inverse_multiquadric	RBF	0.02036	2006	quintic	RBF	0.000471
1983	quintic	RBF	0.03512	2007	quintic	RBF	0.000287
1984	linear	RBF	0.129549	2008	quintic	RBF	0.000124
1985	linear	RBF	0.119245	2009	cubic	RBF	7.76E-05
1986	inverse_multiquadric	RBF	0.028914	2010	cubic	RBF	0.000147
1987	inverse_multiquadric	RBF	0.011823	2011	thin_plate	RBF	1.75E-05
1988	inverse_multiquadric	RBF	0.145847	2012	cubic	RBF	0.000347
1989	linear	RBF	0.149228	2013	cubic	RBF	5.06E-06
1990	inverse_multiquadric	RBF	0.017371	2014	cubic	RBF	7.56E-06
1991	thin_plate	RBF	0.004834	2015	cubic	RBF	0.000335
1992	inverse_multiquadric	RBF	0.000111	2016	multiquadric	RBF	4.59E-06
1993	inverse_multiquadric	RBF	5.57E-05	2017	cubic	RBF	1.39E-05
1994	inverse_multiquadric	RBF	7.23E-05	2018	gaussian	RBF	5.02E-06
1995	quintic	RBF	6.77E-05	2019	cubic	RBF	9.35E-06

Table E.3 and Table E.1 are tables which differ by the kind of correction which is made on the projection of the data from 1972 to 1992[1] on the 16 by 16 point grid, before rotation. We can clearly see that Table E.3 has better 'grades' from 1972 to 1992, and a higher variety of interpolation methods chosen. This comforts us in the idea, explained in Subsection 2.3.5, that the proportional method of correction[2] is more accurate than the constant approach in correction[3].

The table above, Table E.3, provides two main useful teachings. The first is that having more points in the original data set, that is prior to the interpolation, increases the quality of the interpolated data. This is supported by the fact that the grades for the years 1992 onwards, which have 16 times more points that the data sets prior to 1992[4].

The second major teaching is that the correction methods 1 and 2 together are more adapted for correcting ice mass, with regards to the conservation of the mean, than methods 1 and 3 together.

[1] Reminder: this data is extremely coarse, only 260 points over the entirety of Greenland.
[2] This is method 2 of correction.
[3] This is method 3 of correction.
[4] This takes into account that fact that only every 50 values is taken. In reality the data from 1992 to 2019 has 800 times more data points.

Errors due to skips in the given data - theoretical case

In order to increase the computation time we skip values in the given data. We skip 9/10 of the values in the 'short-term' ice histories - this applies to the data sets from 1992 to 2019, as we do not skip any values for the data between from 1972 to 1992 - and every 5/6 of the values in the 'long term' ice histories outside of the so called finer region, and 5/6 too inside this finer region.

Skipping these values means that the interpolation functions have less points from which to interpolate. This thus creates an uncertainty in the interpolated values. However, it can be quantified, in the following way.
We create a random data set of pre-interpolation data, and a random set of coordinates on which to interpolate. The size of the new data set is randomly picked smaller or larger than the initial data set. Furthermore, this pre-interpolation data set is then interpolated, using basic Rbf linear interpolation, and the difference in mean between the new and pre-interpolation values is taken. Then the same is done, but every 5/6 values is skipped in the initial data. This process is repeated 3 times per initial population size. The initial population size is varied between in steps of 1 between 100 and 500 individuals. In Figure F.1 we can see the behaviour difference of the interpolation between the partial and full data set, along with a close-up version for when the error is below 5%.

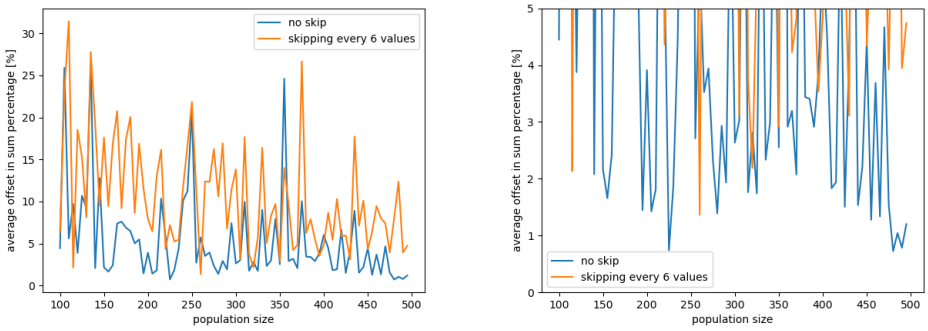

Figure F.1: View of the error behaviour (left). The equation which describes the error in percentage when using the skipped initial data set is Equation F.1. View of the error behaviour beneath 5% error (right).

$$E_{percentage,mean} = \exp(2.65871485) \cdot \exp(n \cdot -1.62298145e - 3) \tag{F.1}$$

Where $E_{percentage,mean}$ is the error of the mean in terms of percentage of the pre-interpolation mean, and n is the size of the initial population. If we use the equation given in Figure F.1, and apply the population data set of 1000 and 5000 in size, which corresponds roughly to the size of the data sets interpolated in terms of magnitude, we get a percentage error between 2.695% and 0.003%. Seeing that skipping about 5/6 of values, within the long term ice history, does not affect significantly the data outcome, we deem possible the use of this method to increase the speed, i.e. decrease the computation time, of the interpolations.

Lastly, as the previously shown study investigates an error over the entire globe's surface, and in the 'short term' ice history we only have the Greenland 'tight' region over which we interpolate, we deem that skipping 90% of the values there, should probably not be a significant issue, as that is still more points used than for the global 'long term' interpolation. I.e, the 'long term' ice history is 13000 points long, which divided by 6 roughly makes 21000 points, when the Greenland 'short term' ice history is 210000 points long, about 160000 thousand in the actual 'tight' , which divided by 10 roughly makes 16000 points, while the Greenland 'short term' ice history is over a much smaller region.

This point is only valid if the variations in the detailed 'short term' ice history do not significantly impact the GIA model, as the ice mass variations in the 'tight' region are resolution-wise more refined than in the 'long term' ice mass variations. Because the technique used to skip values is nondiscriminatory, and most ice mass points do not significantly change in the 'short term' period, we only deem probable, but not certain, that this skipping effect does not significantly impact the final results' accuracy. *Note: Aspects such as spherical Earth model resolution and the resolution of the load maps applied are believed to have a much larger impact on the final results than this skipping effect.*.

This topic is further explored in Chapter 4, where it is referred to as the 'quality of the interpolated ice loads'. The principle is the same as here, but the effect on the uplift is accounted and measured, to find the most convenient way to interpolated these loads. In Chapter 4, we skip different ratios of the data, to try to more accurately account the effect of skipping ice masses in the original data on the simulated uplift.

F.1. Mapping the interpolated loads

The need for mapping comes from the fact that instead of writing a complex code which would assign each element a load, Abaqus presents a mapping function which allows to just enter the coordinates of a load, and it will assign it to an element. However, coordinates can be entered in different manners, and choosing this manner is what this chapter focuses on.

'.MappedField' is the command used[1]. It notably allows to specify the coordinate system in which the data is inputed, and which mapping format is used. These mapping formats are discussed below.

There are two possible formats for the input data into the mapping function when mapping the load field. We can map the loads in a grid format, which was done in the original model given by Caroline van Calcar, or in a 'XYZ' format. These two options are discussed and weighted here.

F.1.1. Grid format

The grid format inputs the loads in a matrix format, as the name suggests. The values of ice heights are entered in the latitude, in the vertical direction, and longitude, in the horizontal direction[2]. The clear advantage in this method is that the radius of each node is not taken into account, as the loads are directly applied to the surface. *Reminder from the previous chapter: the radius of each node will change after each time step deformation.*

The disadvantage of this method is that it is clearly and highly time consuming when loading in the loads in the mapping function. This is because of the shear size of the grid matrix: longitudes and latitudes rarely repeat. For instance, if we have 3 data points, and they all have different latitudes and longitudes, the grid format will require 9 data points with 6 of them being 0, instead of the original 3 data points. Thus, most ice height values in the matrix are 0, and the software has to register these values although they are useless to the simulation.

F.1.2. 'XYZ' format

The 'XYZ' format contains the pressure loads in a list, where each load has its own three dimensional spherical coordinate: radius, longitude and latitude in that order[3]. The advantage with this method is that it is considerably quicker than when the loads are in the grid format method, as it has less loads to enter in Abaqus. If the example provided above is continued, the 'XYZ' format only requires the 3 data points, and will only load 3 data points, contrary to the grid format which will load 9 data points.

However, it looses in accuracy, as the radius matters in this method, and as it was already discussed in Subsection 2.3.7, the mesh points will displace themselves as well in the vertical direction. As also discussed in Subsection 2.3.7, we assume for all load files that the radius is the volumetric radius of the Earth, when in fact the nodes coordinates may have significant deviations from this radius. We expect this loss in accuracy to be small.

[1] More on this command can be read in the Abaqus scipting user guide: http://130.149.89.49:2080/v6.11/books/ker/default.htm?startat=pt01ch21pyo06.html.

[2] Abaqus manual on the grid format for more information: https://abaqus-docs.mit.edu/2017/English/SIMACAECAERefMap/simacae-c-fldusingmappointgrid.htm.

[3] Abaqus manual on the 'XYZ' format for more information: https://abaqus-docs.mit.edu/2017/English/SIMACAECAERefMap/simacae-c-fldusingmappoint'XYZ'.htm.

F.1.3. Trade-off

We thus need to make a trade-off, on whether the errors in the 'XYZ' format, provoked by the non-alignment of radii between the nodes and the ice loads, are at acceptable levels or not, given that the grid format has an excessive amount of run time.

Elastic sensitivity analysis

From the initial runs, where only the static step, i.e. elastic load, is taken into account from 122000 years ago, we can set up an experiment where we compare the results from the volumetric radius setting equivalent, when there is no deformation, as having a grid formatted input, as the radius of the nodes are all 6371 [km] initially, to the settings of: 100 [m] smaller radius, 1 [km] smaller radius. This is in the goal to simulate the radii disparities in the actual simulation. *Note: The deviation of the node's radius from the volumetric radius are expected to be between the range of magnitudes of a 1000 [m] to 0 [m]. 1000 [m], as results later suggests, is in reality the upper realistic magnitude bound for GIA deflections.*

Lastly, we can do this error analysis on 'XYZ' versus 'Grid' format by performing it on two different load data sets, to test how the number of loading points, i.e. the number of elements which are loaded, affects the deflection statistics and errors. Table F.1 and Table F.2 show these results respectively, for 2231 points loaded and 18556 points loaded. We expect and find that with a higher number of points loaded, the error decreases. This is to support the fact that in the final model, where more than 50000 points will be loaded, that the error will me minimal, and the 'XYZ' format will be deemed acceptable.

Table F.1: Statistics of the absolute percentage error and distance error of the elastic displacement, for three different radii. 2231 load points were used. The original deflection data, that is with the volumetric radius of the Earth, is also presented.

Amount of values: 2231			
Absolute error percentage in elastic loading			
	R - R100	**R - R1000**	
Mean	9.40E-02	0.26976	
Max	229.4537	1511.401	
Min	0	0	
Median	0.044183	0.041358	
Amount of values: 2231			
Absolute error in elastic loading [m]			Original data [m]
	R - R100	**R - R1000**	**R**
Mean	0.228	0.498507	-14.08181999
Max	104.8911	439.7734	418.5990601
Min	0.	0	-7840.087891
Median	0.170471	0.156799	318.8971252

Table F.2: Statistics of the absolute percentage error and distance error of the elastic displacement, for loads of different radiis. 18556 load points were used. The original deflection data, that is with the volumetric radius of the Earth, is also presented.

Amount of values: 18556			
Absolute error percentage in elastic loading			
	R - R100	**R - R1000**	
Mean	2.37E-07	0.000754	
Max	0.001218354	4.530996	
Min	0	0	
Median	0	0.000334	
Amount of values: 18556			
Absolute error in elastic loading [m]			Original data [m]
	R - R100	**R - R1000**	**R**
Mean	7.00E-08	0.00024	-1.926709834
Max	0.00012207	0.232147	52.25845718
Min	0	0	-989.3812866
Median	0	0.000156	40.07298279

From Table F.2 and Table F.1, there are multiple conclusions, which are enumerated below:

1. The increase of loading points, decreases in a near linear fashion, the deflection statistics. This is due to the fact that these are purely elastic deformations, and that the pressure on the loaded elements is higher when there are less points, as the total ice mass is the same in both sets of loads. Elastic deformations at discrete points is proportional to the load applied.
2. The error, when there is a radial offset between the load and the nodes at the start at the simulation, decreases when more load points are used. The trend here is unclear.
3. Lastly, the error increases as the radial offset increases. This is the third 'clear' trend of these elastic results. It seems that the general trend is that, in the distance error - not percentage error - the error increase by one or two magnitudes when the radius offset goes from 100 [m] to 1000 [m].

Visco-elastic sensitivity analysis

A similar analysis can also be performed, with exactly the same data and settings, on the visco-elastic response. The only change now is that the response will also be viscous, so not only instanteneous. For this, we assign a simulation time of 50 years with the loading of 122000 years ago. *Note: In reality, the first time step, from 122000 years to 25000 years, is much longer. However, for the purpose of this sensitivity analysis we wish to make the run times quicker, and thus perform this sensitivity on a much smaller period, one which is comparable for instance to the size of the time steps between the years: 1000 and 500 years ago.*.

Furthermore, the way the visco-elastic deformation is investigated is by running the visco-elastic step but with a varying radius, as done in the elastic step: first no radius change, then 100 [m] change and then 1 [km] change for all values. We will do this for both data sets again, with the particularity of the 2231 point large data set being run as well with 100 years of propagation, in order to check the behaviour of the results and the errors. This will only be done with the 100 [m] radial offset. Table F.3 and Table F.5 present the results, both for the data set of size 2231 and for the one of size of 18556.

Table F.3: Statistics of the absolute percentage error and distance error of the visco-elastic displacement, for loads of different radiis. 2231 load points were used. The original deflection data, that is with the volumetric radius of the Earth, is also presented.Additionally, the simulation is also ran for a 100 years.

Values: about 2000, exact: 2231, 50 years			
Absolute error percentage in visco-elastic loading			
	R - R100	**R - R1000**	
Mean	0.124684	3.06E-01	
Max	2.24E+03	4.63E+03	
Min	0.00E+00	7.47E-06	
Median	0.044173	0.041095	
Values: about 2000, exact: 2231, 50 years			
Absolute error in visco-elastic loading [m]			Original data [m]
	R - R100	**R - R1000**	**R**
Mean	2.27E-01	0.502005	-17.11616543
Max	106.6035	446.8594	412.1262817
Min	0.00E+00	3.05E-05	-8042.76709
Median	0.167938	0.153839	316.7922211

Table F.4: This figure is the continuation (sideways) of Table F.3. Statistics of the absolute percentage error and distance error of the visco-elastic displacement, for loads of different radiis by a 100 [m]. 2231 load points were used. The original deflection data, that is with the volumetric radius of the Earth, is also presented. Contrary to the previous table, the propagation is a 100 years.

Values: about 2000, exact: 2231, 100 years	
Absolute error percentage in visco-elastic loading	
R - R100	
0.200495751	
4995.984157	
0	
0.044163879	
Values: about 2000, exact: 2231, 100 years	
Absolute error in visco-elastic loading [m]	Original data [m]
R - R100	**R**
0.225707374	-19.96657088
108.3032227	406.1164551
0	-8241.344727
0.16557312	314.8033295

Table F.5: Statistics of the absolute percentage error and distance error of the visco-elastic displacement, for loads of different radiis. 18556 load points were used.

Values: about 18000, exact: 18556, 50 years			
Absolute error percentage in visco-elastic loading			
	R - R100	**R - R1000**	
Mean	3.13E-07	1.20E-03	
Max	2.47E-03	1.44E+01	
Min	0.00E+00	0	
Median	0	0.000334	
Values: about 18000, exact: 18556, 50 years			
Absolute error in visco-elastic loading [m]			Original data [m]
	R - R100	**R - R1000**	**R**
Mean	7.95E-08	0.000239	-2.310729531
Max	0.00012207	0.235779	51.44263077
Min	0.00E+00	0.00E+00	-1014.911438
Median	0	0.000153	39.80755043

The main conclusions of this short study can be summarised, as done below:

1. The conversion ratio between the 18556 load point deflections and the 2231 one is the same as the elastic conversion: just the ratio of load data sets.
2. Also, the variation per radius offset has the same pattern, although the magnitude change of the error is larger between offset options.
3. Propagating the visco-elastic deflection for 50 years more did not change the errors in any clear direction, but reduced the gap ratio between the mean, max, min and median.
4. The visco-elastic deflection is similar to the elastic deflection, and the rate of the viscous response in the first 50 years is larger than in the second 50 years, although this may depend on the viscosity profile values.

These conclusions point towards the fact that, assuming our GIA deflections in the final model stay beneath the 1 [km] magnitude, the 'XYZ' format does not change the results by a distance which is significant enough.

Computation time

Till now, we have often mentioned the increase in speed procured by the use of the 'XYZ' format over the grid format. In this section we detail this finding by proposing three aspects of the modelling which vary when using the 'XYZ' format instead of the grid format.

The first is the mapping field function, which is at the heart of this whole trade-off. The second is the simulation time, and the third is the total modelling time. Table F.6 displays the time differences between the two formats for an elastic response, and Table F.7 displays it for a visco-elastic response. The reason why we only present the magnitudes, and this is also valid for the visco-elastic deformation run time, is that CPU run times can significantly vary in value. However, the magnitudes are usually respected, and as we do not wish to repeat these runs multiple times as it would take up too much time, only the magnitudes of the run times are recorded. What is meant is that we would need to repeat these runs multiple times and statistically analyse the run times, i.e. write down the mean and standard deviation. However, this procedure, for these simulations would take too much time for the contribution they would add. Thus, as we know magnitudes do not vary by definition much in magnitude, only the CPU run time magnitudes are presented. *Note: what matters here is the ratio between the grid format and the 'XYZ' format. This is because if other fellow engineers/ scientists would want to replicate this experiment, the computer characteristics they would be using would most likely be different, thus yielding different CPU run times.*

Table F.6: Time taken magnitude for the 'XYZ' and grid format within the modelling for an Elastic response.

Elastic	**'XYZ' format**	**Grid format**
Mapping time [s]	0.03	5.5
Simulation time [s]	510	>1200
Total run time [s]	530	>1200

Table F.7: Time taken magnitude for the 'XYZ' format and grid format within the modelling for a visco-elastic response of 50 and 100 years.

Propagation time	*Visco-elastic*	**'XYZ' format**	**Grid format**
50 years	**Mapping time [s]**	0.03	0
	Simulation time [s]	1380	4046.24205
	Total run time [s]	1390	4066.79429
100 years	**Mapping time [s]**	0.03	0
	Simulation time [s]	1380	
	Total run time [s]	1390	

All of these computation times were obtained from the elastic and visco-elastic sensitivity analysis, when the radius of the loads coordinates both in the elastic or visco-elastic deformation is the volumetric radius of the Earth: 6371 [km].

The computation times for the 'XYZ' format in the visco-elastic response are found to be about a third than that for the grid format. Furthermore, when performing a similar analysis on the visco-elastic response, the computation times for a 100 years of propagation compared to 50 year propagation were not noticed to be any different. This may be because the difference in propagation time is too small. The grid format clearly takes more time, and we thus are reinforced in the opinion that the 'XYZ' format is better for use.

We can then conclude, that in light of the results in the computation time and in the results' disparity between the grid format and 'XYZ' format mapping techniques, that the 'XYZ' format provides results faster and with an error which is negligible, when compared with the grid format results.

G

Time ramps in time steps

When simulating behaviour of models and materials over very large time steps, several thousands of years as seen in the Section 2.4, it is useful to ramp the loads exerted on the objects and elements, as it allows us to more precisely in time load the model. What is meant by a ramp is the variation of the load in between the time steps. This ramp is explained and designed in this chapter in detail.

G.1. Usefulness of the ramp

What is now set in the model is to load the ice sheet data at each time step, as defined in Abaqus. This is called a step function, as the load is constant inside each time step. However, it is not realistic as no ice mass can suddenly appear. Thus, we can include a ramp to gradually change the load during the time step in order for it to reach the value of ice mass at the end of the time step, for the next time step. This way, there is no brutal change between both time steps.

Figure G.1 shows both the step function and the ramp function applied in an ideal way. Further on, we will see that having a perfect ramp function, i.e. one which ideally estimates all of the loads at all times inside the time step it is used, is close to impossible.

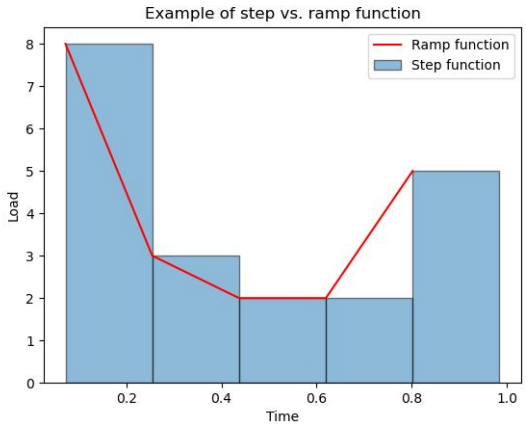

Figure G.1: Time step function versus an ideal ramp function.

G.2. Designing the ramp

This sections details how the time ramp is included and found.

G.2.1. General set up

Firstly, we need to define how the ratio of the input load varies over time. In the case of Figure G.2, the ramp is linear as there is only a starting time and ratio, and a finishing time ratio[1]. However, this can vary at will, and many steps can be added.

[1] The link to the MIT Abaqus documentation on time ramps is: https://abaqus-docs.mit.edu/2017/English/SIMACAEPRCRefMap/simaprc-c-amplitude.html.

$$\begin{bmatrix} Time & RelativeLoad \\ t_1 & r_1 \\ t_2 & r_2 \end{bmatrix}$$

Figure G.2: Tabular amplitude of the ramp, directly taken from the MIT Abaqus documentation, see link above. t_1 and t_2 are the starting and finishing time respectively. These should correspond to the ones in the model. r_1 and r_2 are the ratios of the input loads.

Then once this matrix is defined with the help of the '.TabularAmplitude' Abaqus scripting function, we need to include this amplitude variation in the actual loads. This is done by inputing the name of the ramp, given in the 'TabularAmplitude' function, in the 'amplitude' variable in the '.Pressure' command, where the load map is specified.

Note: An important point to mention is that, as it stands with the Abaqus scripting interface, only one ratio can be given for the whole data set. Linking back now to what was discussed at the start of this chapter, the ramp function here would not look like Figure G.1, but more like Figure G.3, where the error is randomly situated above or below the actual point.

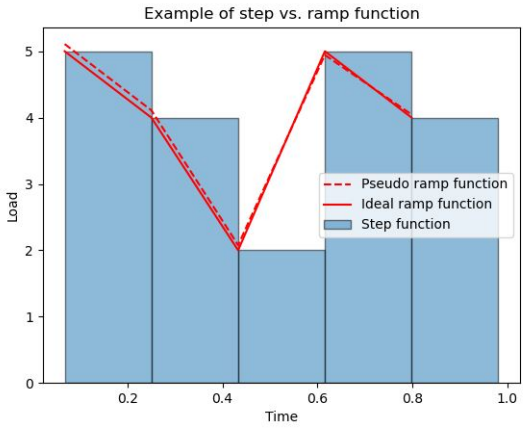

Figure G.3: Depiction for illustrative purposes of how the ramp will be implemented.

G.2.2. Determining ratios

Ideally, the end values of a time step are the starting values of the next time step for every point. This means that we find ideal ratios which represents every point in the pressure field. However, this actual scenario is not possible, as only one ratio of load change can be given for the whole data set, not for every point in it.

Every point has an own variation throughout the time step. Thus, even if we get closer to reality by including a ramp load, there will still be a slight total mass offset at the transition between the two time steps. So rather then to create an ideal ramp, we create a hybrid between a true ramp and a step function.

The most fair assumption we can formulate for these ratios, is through Equation G.1, where r_1 is the input load[2], and $R_{optimum}$ refers to the optimum found ratio. The optimum ratio is found by brute force: we define an arbitrary ratio between 0.85 and 1.15, with a resolution of 0.00001, and check for each ratio if it has a lower mean error than the previous.

$$r_2 = r_1 \cdot R_{optimum} \tag{G.1}$$

The error is the difference between the actual ice masses and the ice masses of the previous time step when multiplied with the ratio, as demonstrated in Equation G.2.

$$c = ||r_2 - v| \tag{G.2}$$

[2]The starting load ration, r_1, being the load we know at a certain time step, so 1.

Where c is the error between the approximation of the ice loads, r_2, and and the true ice loads from the ice model, v. Furthermore, it order to get a better approximation of the loads along the surface, we can apply this scaling to represent inside the time steps, the variation, as we have data in between time steps. For instance, between 122000 years ago and 80000 years ago, which is our first time step, we are aware of the ice data at 7 time steps. As discussed in Section 2.4, we do not include them in the actual simulation but we can acknowledge their presence by filling in a table the ratios.

So, for the first time step, if we apply in each part of the time step this ratio, we come to Figure G.4 as the graph for the mean error per part of the time step. Each part of the time step is defined by the ice mass data sets available, discussed in Section 2.2.

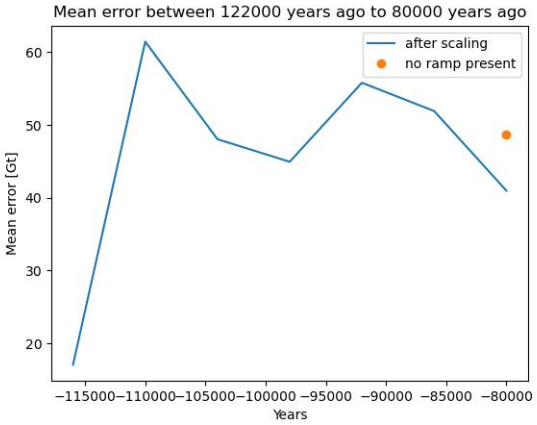

Figure G.4: Mean error through out the ramp, in comparison with the mean error at the final step, if no ramp was included. The correction referring to the scaling method. The 'no ramp present' refers to the mean error, when the ramp is not applied and we just have a step function. This is for the years 122000 to 80000 years ago.

Table G.1 shows the statistics of the ice model data at 122000 and 80000 years ago, which if subtracted from one another is the change in ice data in the model 80000 years ago, as well as the ice masses 80000 years if a time ramp is applied. We notice then a much smaller difference between loads at 80000 years ago and the scaled loads, than between the loads at 122000 years ago and 80000 years ago from the model data.

Table G.1: Table comparing the statistics at 80000 years ago, the statistics of the approximated data at 80000 years ago (Scaled), and the data at 122000 years ago. This is meant to show that the difference in data when including the ramp is smaller and thus smoother (transition from the scaled 80000 years ago data to the 80000 years ago data) than when having effectively a step function (transition from 122000 years ago to 80000 years ago).

	Data sets [Gt]		**Scaled [Gt]**
	122000 years ago	**80000 years ago**	**80000 years ago**
Max	3423	3607	3698.925674
Min	0	0	0
Range	3423	3607	3698.925674
Std	671.589	736.7239	725.7253282
Mean	203.4938	252.1029	219.8972897

It can clearly be seen from Figure G.4 that the ratio coefficient does improve the fluidity of the data, especially from the fact that at 80000 years ago, where we would like the minimum shift in values, the mean error is smaller than if the ramp was not included. The mean error is 13.42 $[Gt]$, when the mean loading is 252.102 $[Gt]$ and the maximum loading 3607.0 $[Gt]$. Note that we are now working in Gt when in the model this is converted to a pressure. However, this is does not change the ratios of loads. Lastly, we also provide the data in comparison,

to show the jump in values between the unscaled and scaled data sets at 80000 years ago.

We can perform another example to show how this complex ramp improves ours approximation of the results, for the time step between 80000 years ago and 25000 years ago.

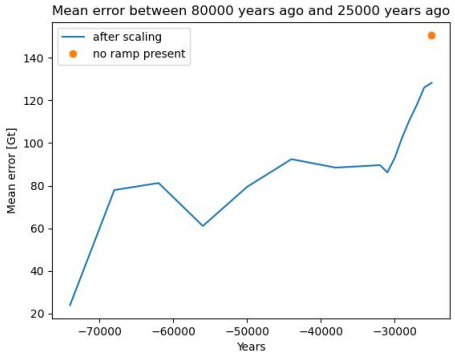

Figure G.5: Mean error throughout the ramp, in comparison with the mean error at the final step, if no ramp was included. The correction refers to the scaling method. The 'no ramp present' refers to the mean error, when the ramp is not applied and we just have a step function. This is for the years 80000 to 25000 years ago

Table G.2: Table comparing the statistics at 25000 years ago, the statistics of the approximated data at 25000 years ago, and the data at 80000 years ago. This is meant to show that the difference in data when including the ramp is smaller and thus smoother (transition from the scaled 25000 years ago data to the 25000 years ago data) than when having effectively a step function (transition from 80000 years ago to 25000 years ago).

	Data sets [Gt]		Scaled [Gt]
	80000	**25000**	**80000**
Max	3607	4494	4238.340354
Min	0	0	0
Range	3607	4494	4238.340354
Std	736.7239	959.0747	865.6740927
Mean	252.1029	402.2561	296.2289542

The main conclusion from Table G.2 and Table G.1 is that applying a ramp seems at first glance to bring steps closer to a smoother transition between each other than if the ramp was not applied.

G.3. Simple & complex ramps

Lastly, we can conclude this chapter by presenting why a complex ramp, that is one which is not simply linear but has multiple 'kinks', is more accurate. To answer that we first investigate how much the final deflections vary when using a simple linear ramp and a complex one.

Thereafter, it is possible to set up one simulation where there is no ramp, one where there is a simple linear ramp, and one where there is a complex one[3]. We will be using the first time step of the simulation as an example, but instead of making it stop at 80000 years ago[4], we will make a time step ranging from 122000 years ago to 98000 years ago. Shortening the first time step, is purely done for computational time reasons, as for a simple experiment it is not deemed worthy to have a long computational time[5]. Lastly, as seen in Figure G.6, the period between 122000 years ago and 98000 years ago, has some fluctuations, therefore giving

[3] A complex one referring to adding variations in the magnitudes of the loads between the start and end point of the simulation.
[4] In the actual simulation the first time step spans 122000 years ago to 80000 years ago.
[5] The underlining assumption is that if we simulate 98000 years of deformation, the run time will be longer than if we simulate 24000 years of deformation.

this analysis more worth.

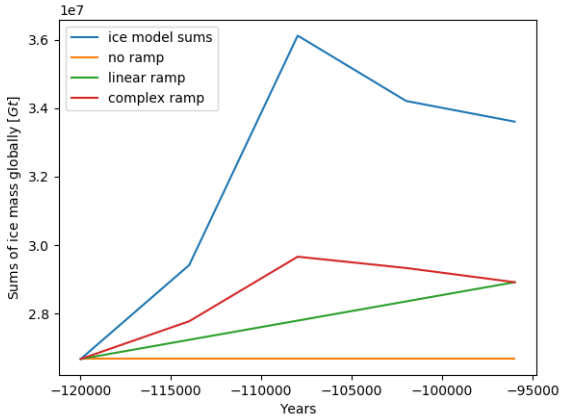

Figure G.6: Variation of the total ice mass on the globe between 122000 years ago and 98000 years ago. This trend can be found again in Figure 2.13. Are also plotted the linear, complex and 'no time ramp' settings from this test.

After simulating with the three different ramp configurations, we can present the results as in Table G.3. The CPU time was only recorded once, so the stipulated time should only be interpreted as a magnitude, as it was rounded to the nearest ten seconds. This is because the CPU run time can vary in function of computer settings, or in function of the use at that moment of the servers.

Table G.3: Table showing how the final deflection varies after a 24000 years long propagation, when using various ramp settings: step function, linear ramp, complex ramp.

	Deflections [m]		
	no ramp	linear ramp	complex ramp
Min	-1153.73	-1234.0906	-1255.567383
Max	79.97501	80.3846588	87.60253143
Range	1233.709	1314.47523	1343.169914
Median	11.56108	12.489378	12.55819035
Std	107.6808	115.519883	117.2091348
Mean	-2.66641	-2.8856073	-2.893692887
	CPU run time [s]		
Simulation	1830	1850	1780
Total	1840	1860	1790

The main conclusion from Table G.3, is that the largest difference in results between the setting's results presented comes from the use of the ramp or the use of the step function. As the ramp takes into account that the ice loads increases over the time step, it is only natural that building a ramp increases the deflections in this specific scenario. However, the complex ramp changes the statistics of the deflections by a maximum of 10% for the maximum deflections and a minimum of 1% for the mean results, from the linear ramp results. This change is not negligible by any means. Therefore, because the linear and complex ramp configurations have about the same run time, and the complex ramp, which is by definition more accurate, has significantly different deflections, we can conclude that the complex ramp in the actual uplift modelisation should be used.

G.4. The time ramp in relation to the reality

Finally, we find it useful to discuss the time ramp's contribution to accuracy. From the subsections above, it has becomes clear that include the time ramp increases accuracy and fidelity to the original ice mass data sets. In developing the time ramp is key underlying assumption is that the ice models are accurate. Hence, the data sets themselves have uncertainties. This means that including time ramps could only be a small improvements on the large errors of the ice models.

However, because we are at this stage unaware of the values of the errors in the ice model, including the time ramp as done here in the final simulations is an assumed design choice to try and mitigate errors.

Lithosphere division parametric study: insight in the behaviour of the deflection

We created this appendix in order to explain and justify the fact that we directly start loading from 1972 onward, and we neglect the effects prior. We prove here that there is a variation in uplift rate due to the recent ice melts.

The first setting is the one where the lithosphere is as in Subsection 3.2.1: there is one imposed layer, with a target mesh size of 70 [km]. Figure H.1 shows the variation of the statistics of the rates of deflection across the years. The one at 1982 is not shown, as it is very high, due to the fact the model is unloaded before the year 1972[1].

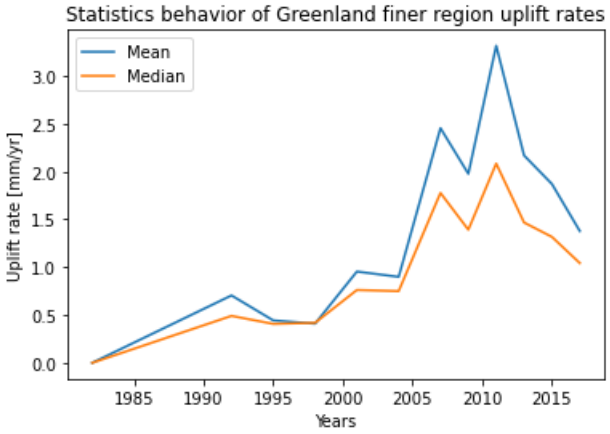

Figure H.1: Graph displaying the mean and median of the deflection rates across Greenland, when loading only from 1982 onward, while forcing 1 lithosphere layer. We do not load from 1972 onward, as this was is not worth showing because of its really high value due to the fact that the model is not loaded before this step. This is all relative to the uplift in 1982.

We see in Figure H.1, that rates at each year remain largely constant, although there is a small slope of increase. The variations across years can be attributed to elastic deformations, as the negative viscous response is assumed strong, constant and due to the initial loading on an unloaded surface, and was therefore removed from Figure H.1. Moreover, the reason why in the actual simulation we know that the upward viscous effect due to recent ice changes is weak, is that there the model was already loaded before the year 1972, so the change in ice mass on the surface is negligible compared to the total ice mass. This is proven in Simpson et al. (2011). However, here, the mass goes from 0 to the total ice thickness, which then creates a really strong negative viscous response.

Lastly, to prove one more time that the graphs in Figure 4.1 are a valid way of assessing the differences between the models, we can plot the difference in ice height between the year 1982 and 2019, as done in Figure H.2, and compare the pattern with the graphs in Figure 4.1.

[1]Reminder: the uplift rate at the year 1982, is the one from the step 1972 to 1982.

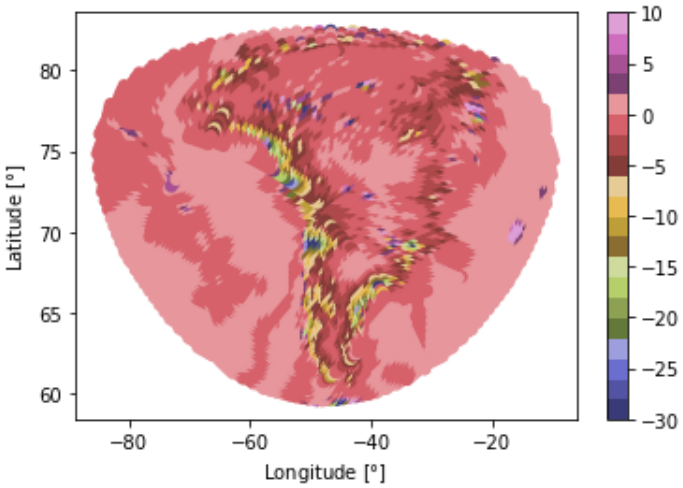

Figure H.2: Change in ice heights [m] input in the parametric study between the years 1982 and 2019.

In Figure H.2, it can clearly be seen, if its compared with the deflection approximation due to modern day changes in ice, that the pattern of ice mass loss presented in Figure H.2 is the same as the deflection pattern in Figure 4.1. The only difference is that it seems that in Figure 4.1, the changes in ice heights also 'pull' upward the surrounding regions too.